Reliability Based Design Including Future Tests and Multi-Agent Approaches

Diane Villanueva

Ecole Nationale Supérieure des Mines
SAINT-ETIENNE

NNT : 2013 EMSE 0687

THÈSE

présentée par

Diane VILLANUEVA

pour obtenir le grade de
Docteur de l'École Nationale Supérieure des Mines de Saint-Étienne
en cotutelle avec l'Université de Floride

Spécialité : Mécanique et Ingénierie

OPTIMISATION FIABILISTE : PRISE EN COMPTE DES TESTS FUTURS ET APPROCHE PAR SYSTÈMES MULTI-AGENT

soutenue à Gainesville, Floride, Etats-Unis, le 13 mai 2013

Membres du jury

Président :	Stan URYASEV	Professor, University of Florida
Rapporteurs :	Natalia ALEXANDROV	Project Scientist, NASA Langely Research Center, Hampton
	Eduardo SOUZA DE CURSI	Professor, INSA Rouen, Rouen
Examinateurs :	Bhavani SANKAR	Newton C. Ebaugh Professor, University of Florida,
	Jean-Pierre GEORGÉ	IRIT Université Paul Sabatiér, Toulouse
Directeurs de thèse :	Rodolphe LE RICHE	CNRS permanent research associate, Saint-Etienne
	Raphael HAFTKA	Distinguished Professor, University of Florida
Co-Encadrant:	Gauthier PICARD	Associate Professor, Ecole des Mines de Saint-Etienne
Invité:	Peter IFJU	Professor, University of Florida

Spécialités doctorales :	Responsables :
SCIENCES ET GENIE DES MATERIAUX	K. Wolski Directeur de recherche
MECANIQUE ET INGENIERIE	S. Drapier, professeur
GENIE DES PROCEDES	F. Gruy, Maître de recherche
SCIENCES DE LA TERRE	B. Guy, Directeur de recherche
SCIENCES ET GENIE DE L'ENVIRONNEMENT	D. Graillot, Directeur de recherche
MATHEMATIQUES APPLIQUEES	O. Roustant, Maître-assistant
INFORMATIQUE	O. Boissier, Professeur
IMAGE, VISION, SIGNAL	JC. Pinoli, Professeur
GENIE INDUSTRIEL	A. Dolgui, Professeur
MICROELECTRONIQUE	Ph. Collot, Professeur

EMSE : Enseignants-chercheurs et chercheurs autorisés à diriger des thèses de doctorat (titulaires d'un doctorat d'État ou d'une HDR)

AVRIL	Stéphane	PR2	Mécanique et ingénierie	CIS
BATTON-HUBERT	Mireille	PR2	Sciences et génie de l'environnement	FAYOL
BENABEN	Patrick	PR1	Sciences et génie des matériaux	CMP
BERNACHE-ASSOLLANT	Didier	PR0	Génie des Procédés	CIS
BIGOT	Jean Pierre	MR(DR2)	Génie des Procédés	SPIN
BILAL	Essaid	DR	Sciences de la Terre	SPIN
BOISSIER	Olivier	PR1	Informatique	FAYOL
BORBELY	Andras	MR(DR2)	Sciences et génie de l'environnement	SMS
BOUCHER	Xavier	PR2	Génie Industriel	FAYOL
BRODHAG	Christian	DR	Sciences et génie de l'environnement	FAYOL
BURLAT	Patrick	PR2	Génie Industriel	FAYOL
COLLOT	Philippe	PR0	Microélectronique	CMP
COURNIL	Michel	PR0	Génie des Procédés	DIR
DARRIEULAT	Michel	IGM	Sciences et génie des matériaux	SMS
DAUZERE-PERES	Stéphane	PR1	Génie Industriel	CMP
DEBAYLE	Johan	CR	Image Vision Signal	CIS
DELAFOSSE	David	PR1	Sciences et génie des matériaux	SMS
DESRAYAUD	Christophe	PR2	Mécanique et ingénierie	SMS
DOLGUI	Alexandre	PR0	Génie Industriel	FAYOL
DRAPIER	Sylvain	PR1	Mécanique et ingénierie	SMS
FEILLET	Dominique	PR2	Génie Industriel	CMP
FOREST	Bernard	PR1	Sciences et génie des matériaux	CIS
FORMISYN	Pascal	PR0	Sciences et génie de l'environnement	DIR
FRACZKIEWICZ	Anna	DR	Sciences et génie des matériaux	SMS
GARCIA	Daniel	MR(DR2)	Génie des Procédés	SPIN
GERINGER	Jean	MA(MDC)	Sciences et génie des matériaux	CIS
GIRARDOT	Jean-jacques	MR(DR2)	Informatique	FAYOL
GOEURIOT	Dominique	DR	Sciences et génie des matériaux	SMS
GRAILLOT	Didier	DR	Sciences et génie de l'environnement	SPIN
GROSSEAU	Philippe	DR	Génie des Procédés	SPIN
GRUY	Frédéric	PR1	Génie des Procédés	SPIN
GUY	Bernard	DR	Sciences de la Terre	SPIN
GUYONNET	René	DR	Génie des Procédés	SPIN
HAN	Woo-Suck	CR	Mécanique et ingénierie	SMS
HERRI	Jean Michel	PR1	Génie des Procédés	SPIN
INAL	Karim	PR2	Microélectronique	CMP
KERMOUCHE	Guillaume	PR2	Mécanique et Ingénierie	SMS
KLOCKER	Helmut	DR	Sciences et génie des matériaux	SMS
LAFOREST	Valérie	MR(DR2)	Sciences et génie de l'environnement	FAYOL
LERICHE	Rodolphe	CR	Mécanique et ingénierie	FAYOL
LI	Jean Michel		Microélectronique	CMP
MALLIARAS	Georges	PR1	Microélectronique	CMP
MOLIMARD	Jérôme	PR2	Mécanique et ingénierie	CIS
MONTHEILLET	Franck	DR	Sciences et génie des matériaux	SMS
PERIER-CAMBY	Laurent	PR2	Génie des Procédés	DFG
PIJOLAT	Christophe	PR0	Génie des Procédés	SPIN
PIJOLAT	Michèle	PR1	Génie des Procédés	SPIN
PINOLI	Jean Charles	PR0	Image Vision Signal	CIS
POURCHEZ	Jérémy	CR	Génie des Procédés	CIS
ROUSTANT	Olivier	MA(MDC)		FAYOL
STOLARZ	Jacques	CR	Sciences et génie des matériaux	SMS
SZAFNICKI	Konrad	MR(DR2)	Sciences et génie de l'environnement	CMP
TRIA	Assia		Microélectronique	CMP
VALDIVIESO	François	MA(MDC)	Sciences et génie des matériaux	SMS
VIRICELLE	Jean Paul	MR(DR2)	Génie des Procédés	SPIN
WOLSKI	Krzystof	DR	Sciences et génie des matériaux	SMS
XIE	Xiaolan	PR1	Informatique	CIS

ENISE : Enseignants-chercheurs et chercheurs autorisés à diriger des thèses de doctorat (titulaires d'un doctorat d'État ou d'une HDR)

BERGHEAU	Jean-Michel	PU	Mécanique et Ingénierie	ENISE
BERTRAND	Philippe	MCF	Génie des procédés	ENISE
DUBUJET	Philippe	PU	Mécanique et Ingénierie	ENISE
FORTUNIER	Roland	PR	Sciences et Génie des matériaux	ENISE
GUSSAROV Andrey	Andrey	Enseignant contractuel	Génie des procédés	ENISE
HAMDI	Hédi	MCF	Mécanique et Ingénierie	ENISE
LYONNET	Patrick	PU	Mécanique et Ingénierie	ENISE
RECH	Joël	MCF	Mécanique et Ingénierie	ENISE
SMUROV	Igor	PU	Mécanique et Ingénierie	ENISE
TOSCANO	Rosario	MCF	Mécanique et Ingénierie	ENISE
ZAHOUANI	Hassan	PU	Mécanique et Ingénierie	ENISE

Mise à jour : 07/01/2013

PR 0	Professeur classe exceptionnelle
PR 1	Professeur 1ère classe
PR 2	Professeur 2ème classe
PU	Professeur des Universités
MA (MDC)	Maître assistant
DR	Directeur de recherche

Ing.	Ingénieur
MCF	Maître de conférences
MR (DR2)	Maître de recherche
CR	Chargé de recherche
EC	Enseignant-chercheur
IGM	Ingénieur général des mines

SMS	Sciences des Matériaux et des Structures
SPIN	Sciences des Processus Industriels et Naturels
FAYOL	Institut Henri Fayol
CMP	Centre de Microélectronique de Provence
CIS	Centre Ingénierie et Santé

To my parents, Lamberto and Diwata, and my sister, Tisha

ACKNOWLEDGMENTS

First and foremost I would like to thank my advisors Dr. Raphael Haftka and Dr. Bhavani Sankar at the University of Florida and Dr. Rodolphe Le Riche and Dr. Gauthier Picard at the École des Mines de Saint-Étienne. All of your insights, guidance, and patience has been greatly appreciated.

I would also like to thank the members of my advisory committee, Dr. Peter Ifju, Dr. Stanislav Uryasev, and Dr. Jean-Pierre Géorgé. Also, thank you to the reviewers of this dissertation, Dr. Natalia Alexandrov and Dr. Eduardo Souza de Cursi. For their hospitality and guidance during my summer visit, I thank Christapher Lang and Kim Bey at NASA Langley Research Center.

Thank you to the many members of the Structural and Multidiscplinary Group for your friendship, support, and thoughtful questions and comments during group meetings. Also, thank you to the members of the Institut Henri Fayol and other departments for your frienship and hospitality, especially with anything that involves speaking, reading, or writing in French.

To my family and friends, I can not express how much your support has meant to me. None of this would be possible without you.

Finally, I would like to express my gratitude to NASA (Award No. NNX08AB40A), the Agence Nationale de la Recherche (French National Research Agency) (Ref. ANR-09-COSI-005), and Air Force Office of Scientific Research (Award FA9550-11-1-0066) for funding this work, and the administrations in Florida and Saint-Étienne that helped make the joint PhD program possible.

TABLE OF CONTENTS

LIST OF TABLES

LIST OF FIGURES

Abstract of Dissertation Presented to the Graduate School
of the University of Florida in Partial Fulfillment of the
Requirements for the Degree of Doctor of Philosophy

RELIABILITY BASED DESIGN INCLUDING FUTURE TESTS
AND MULTI-AGENT APPROACHES

By

Diane Villanueva

August 2013

Chair: Raphael T. Haftka
Cochair: Bhavani V. Sankar
Major: Aerospace Engineering

The initial stages of reliability-based design optimization involve the formulation of objective functions and constraints, and building a model to estimate the reliability of the design with quantified uncertainties. However, even experienced hands often overlook important objective functions and constraints that affect the design. In addition, uncertainty reduction measures, such as tests and redesign, are often not considered in reliability calculations during the initial stages. This research considers two areas that concern the design of engineering systems: 1) the trade-off of the effect of a test and post-test redesign on reliability and cost and 2) the search for multiple candidate designs as insurance against unforeseen faults in some designs.

In this research, a methodology was developed to estimate the effect of a single future test and post-test redesign on reliability and cost. The methodology uses assumed distributions of computational and experimental errors with re-design rules to simulate alternative future test and redesign outcomes to form a probabilistic estimate of the reliability and cost for a given design. Further, it was explored how modeling a future test and redesign provides a company an opportunity to balance development costs versus performance by simultaneously designing the design and the post-test redesign rules during the initial design stage.

The second area of this research considers the use of dynamic local surrogates, or surrogate-based agents, to locate multiple candidate designs. Surrogate-based global optimization algorithms often require search in multiple candidate regions of design space, expending most of the computation needed to define multiple alternate designs. Thus, focusing on solely locating the best design may be wasteful. We extended adaptive sampling surrogate techniques to locate multiple optima by building local surrogates in sub-regions of the design space to identify optima. The efficiency of this method was studied, and the method was compared to other surrogate-based optimization methods that aim to locate the global optimum using two two-dimensional test functions, a six-dimensional test function, and a five-dimensional engineering example.

EXTENDED SUMMARY (FRENCH)

Introduction. Les premières étapes d'une conception fiabiliste impliquent la formulation de critères de performance et de contraintes de fiabilité d'une part, et le choix d'une représentation des incertitudes d'autre part. Force est de constater que, le plus souvent, des aspects de performance ou de fiabilité conditionnant la solution optimale ne seront pas connus ou seront oubliés lors des premières phases de conception. C'est pourquoi des tests et de nouvelles conceptions complènt la conception amont pour mieux garantir que la solution choisie n'est ni dangereuse, ni trop conservatrice. En outre, l'identification de plusieurs solutions possibles apporte une garantie complémentaire contre une solution initiale rendue caduque par de nouvelles informations. Le travail exposé dans ce manuscrit aborde la conception optimale de systèmes sous deux angles : 1) le compromis entre performance et coût généré par les tests supplémentaires et les re-conceptions et, 2) l'identification de solutions optimales multiples en conception comme stratégie contre les erreurs initiales de conception.

Dans la première partie de notre travail, une méhodologie est proposée pour estimer l'effet sur la performance et le coût d'un produit d'un test supplévvvmentaire et d'une éventuelle re-conception. Notre approche se base d'une part sur des hypothèses probabilistes sur les distributions des erreurs de calcul et des erreurs expérimentales et, d'autre part, sur une rêgle de reconception a priori. Ceci permet d'estimer a posteriori la probabilité et le coût d'un produit. Nous montrons comment, à travers le choix de politiques de prochain test et de re-conception, une entreprise est susceptible de contrôler le compromis entre performance et coût de développement.

Dans la seconde partie de notre travail, nous proposons une méthode pour l'estimation de solutions candidates multiples à un problème de conception. Cette méthode d'optimisation est basée sur des agents optimiseurs utilisant des métamodèles et se reconfigurant dynamiquement. Notre algorithme traite le problème de l'optimisation globale. A ce titre, il doit explorer différentes régions de l'espace de recherche, ce qui est coûteux en calculs. Dans le contexte de fonctions coûts et contraintes obtenues à travers des simulateurs numériques

coûteux en calculs qui est le notre, nous utilisons des métamodèles pour remplacer une partie des appels aux simulateurs. Nous proposons de conserver plusieurs candidats optima car conserver simplement la meilleure solution d'une optimisation globale représente une perte d'informations difficiles à recueillir. Nous avons ainsi généralisé les approches d'optimisation globale par métamodèles en leur faisant traiter l'espace de conception par sous-parties pour qu'elles localisent différentes solutions. Notre méthode est testée et comparée à d'autres approches d'optimisation globale par métamodèles sur des exemples analytiques en dimensions 2 à 6, ainsi que sur la conception d'un bouclier thermique en 5 dimensions.

Ces deux contributions sont présentées avec davantage de détails ci-après. Une dernière section décrit les perspectives ouvertes par ce travail.

Conception fiabiliste incluant les effets d'un test futur et d'une re-conception. Il est courant de tester un produit juste après sa conception et de recommencer son optimisation si le test montre une fiabilité trop grande (solution conservatrice non performante) or trop faible. Le test post-conception permet de réduire les incertitudes portant sur le produit, par exemple les incertitudes entachant la probabilité de rupture. Cette réduction d'incertitudes n'est typiquement pas prise en compte dans les calculs de conception fiabiliste. Pourtant, elle peut induire une re-conception, quand il devient clair que le design est trop risqué ou trop conservateur (et non performant).

Une méthodologie est développée pour estimer l'effet d'un test futur lors de la conception d'une structure. Le test affine le calcul de fiabilité et peut être suivi d'une nouvelle conception, ce qui change la fiabilité de la structure finale. Notre approche utilise les distributions des erreurs expérimentales et de simulation, qui doivent être fixées a priori. Elle utilise également une règle de re-conception. Au moyen d'une procédure d'échantillonnage des résultats de tests et de simulation, la fiabilité de la structure après test et re-conception éventuelle peut être estimée.

Plus précisément, l'algorithme de simulation d'un test futur contient les étapes suivantes:

1. Instancier une valeur vraie des erreurs expérimentales et de simulation. Ces valeurs seront considérées comme les valeurs vraies du test et de la simulation.

2. Comparer la prédiction de la simulation (avec erreur) et du test.

3. Mettre à jour le modèle de simulation à partir du test vrai , soit en calibrant un facteur de correction (méthode déterministe) soit par mise à jour bayésienne de l'erreur de simulation (méthode probabiliste).

4. Décider si une re-conception est nécessaire (solution trop risquée ou trop conservatrice),

5. Si re-conception, utiliser le simulateur avec modèle mis à jour. Dans le cas déterministe, le nouveau design restaure la marge de sécurité originale. Dans le cas probabiliste, le nouveau design atteint une probabilité de rupture cible.

6. Mettre à jour les critères de performance (e.g., la masse) et la probabilité de rupture pour ce test futur particulier.

Ces procédures sont répétées pour plusieurs tests futurs, ce qui veut dire que les erreurs vraies des tests et des simulations sont échantillonnées plusieurs fois. Une distribution des critères de performance et des probabilités de rupture est obtenue.

La méthodologie est testée pour la conception d'un bouclier thermique de véhicule spatial réutilisable. De tels boucliers intègrent à la fois des fonctions de tenue structurale et de protection thermique.

Nous observons que la re-conception à la suite d'un test peut réduire la probabilité de rupture de plusieurs ordres de grandeur quand l'objectif de la re-conception est de restaurer les marges de sécurité originales. La re-conception pour une probabilité de rupture cible quant à elle permet des gains de masse.

Nous étudions l'impact de la simulation du test futur et de la re-conception sur le compromis entre le coût de développement du produit et la performance. En particulier, ce compromis est contrlé à travers le critère de re-conception. Ainsi, on peut simultanément optimiser le produit et sa règle de re-conception. Du fait des normes et des traditions de

conception, l'usage de facteurs de sécurité est beaucoup plus commun dans l'industrie que l'usage des probabilités. Ce travail montre qu'il est possible de continuer d'utiliser les facteurs de sécurité en employant les probabilités pour choisir leurs valeurs et choisir les critères de re-conception.

Cette méthode est appliquée à l'optimisation du bouclier thermique avec comme variables d'optimisation de haut niveau les facteurs de sécurité initiaux, les marges déclenchant la re-conception, et les valeurs cibles des marges après re-conception. Les critères de performance sont la masse et la probabilité de re-conception (comme quantification du coût). Nous observons que les marges de sécurité et de re-conception optimales créent d'abord une solution conservatrice dont la masse est ensuite réduite par re-conception, par opposition à un cycle commenant avec un design léger dont la fiabilité est ensuite restaurée. Ce cycle optimal est conforme aux normes et pratiques qui commencent par des solutions à fortes marges de sécurité.

Optimisation par systèmes d'agents pour trouver de multiples optima locaux. La seconde partie de notre recherche s'intéresse au partitionnement adaptatif de l'espace des variables d'optimisation pour trouver les optima locaux de fonctions coûteuses en calculs. Trouver les optima locaux d'un problème est une précaution supplémentaire contre les erreurs de modélisation et de formulation du problème d'optimisation (de conception) initial.

Notre stratégie pour trouver les optima locaux s'appuie sur les principes suivants:

1. L'espace de recherche est partitionné dynamiquement en cellules de Voronoi au sein desquelles ont lieu des optimisations autonomes ce qui constituent autant d'agents. Une cellule de Voronoi est repérée par son centre.

2. Dans chaque partition, les optima locaux sont trouvés par des algorithmes d'optimisation locale utilisant les gradients des fonctions. Les recherches locales sont initialisées en plusieurs points et les meilleures solutions non encore connues sont gardées. Si toutes les recherches locales (dans une partition) produisent le même résultat, le prochain point de recherche est obtenu par remplissage d'espace.

3. Le centre de chaque cellule de Voronoi est localisé sur le meilleur point connu dans la partition. Ainsi à convergence, les partitions se stabilisent sur les optima locaux.

4. Les optimisations locales réalisées par les agents portent sur des approximations des vraies fonctions par métamodèles (de type krigeage). Ces métamodèles peuvent être construits localement dans la partition de chaque agent ou globalement (i.e., un métamodèle est partagé par tous les agents).

5. Les agents se coordonnent par échange de points d'évaluations exactes des fonctions optimisées et en modifiant les partitions.

6. Les agents sont créés et enlevés par les mécanismes suivants:

    - Des agents sont créés lors de l'apparition de plusieurs bassins d'attraction dans une partition (identifiés par clustering) ou pour explorer de nouvelles régions en cas de stagnation.
    - Des agents sont enlevés lorsque leurs centres sont trop proches (cas de convergence vers le même optimum).

Les idées sous-jacentes à cet algorithme sont 1) la résolution collective d'une t¢che par des processus autonomes (système d'agents) et 2) l'utilisation de métamodèles pour résoudre le problème du temps de calcul des fonctions coût et contraintes basées sur des simulateurs numériques. Un agent est donc un processus d'optimisation ayant son propre métamodèle pour résoudre un sous-problème d'optimisation dans sa propre sous-partie de l'espace.

Les agents avec métamodèles locaux sont comparés aux mêmes agents mais avec un métamodèle commun. Il est observé qu'il n'y a pas d'avantage clair à utiliser des métamodèles locaux. La méthode a donc évoluée vers l'emploi d'un métamodèle global.

Ensuite, la méthode a été comparée 1) à un algorithme d'optimisation locale produisant plusieurs solutions par cycle par répétition de recherches locales sur métamodèle en variant les points initiaux 2) à l'algorithme Efficient Global Optimization (EGO) qui est une méthode état de l'art pour l'optimisation globale à partir d'un métamodèle de krigeage. EGO produit des points qui réalisent un compromis entre zones à haute performance et zones mal connues. EGO réalise un compromis entre exploration et intensification. Notons que notre méthode d'agents, contrairement à EGO, intensifie d'abord à travers les recherches locales sur métamodèles, et n'explore que quand c'est nécessaire. L'exploration de la méthode d'agent est stratifiée par les partitions du domaine de recherche.

En moyenne sur plusieurs fonctions tests, nous n'observons pas de différence de performance entre la méthode multi-agents et l'algorithme avec métamodèle unique ajoutant plusieurs points par itération. Par performance, nous entendons ici l'aptitude et l'efficacité à trouver tous les optima locaux. Nous observons que le partitionnement de l'espace de recherche créé une distribution des recherches locales non uniforme (contrairement à l'algorithme sans partition), stratifiée autour des candidats optima locaux déjà trouvés.

Nos tests montrent qu'EGO permet de localiser tous les optima locaux quand ceux ci sont de fonctions coûts équivalentes. Par contre, EGO n'a pas de mécanisme lui permettant de trouver avec une probabilité suffisante les optima locaux non compétitifs.

Les expériences réalisées montrent bien que les recherches locales sont la clé pour déterminer avec précision les optima locaux. La plupart des algorithmes d'optimisation globale, comme EGO, sont lents à converger vers les optima locaux car une fois que les bons bassins d'attraction sont approximativement localisés, les phases d'exploration de nouvelles régions ralentissent la convergence. Au contraire, notre méthode d'agents qui repose sur des recherches locales multiples trouve les optima locaux avec précision.

Perspectives. Les travaux présentés dans ce manuscrit sont un premier pas qui mérite d'être prolongé dans trois directions:

1. l'identification efficace des optima locaux,
2. l'estimation de la gamme des solutions acceptables à partir de la vulnérabilité de la meilleure solution connue,
3. les algorithmes d'optimisation distribués.

Pour les deux premières directions de recherche, il s'agit d'isoler les bassins d'attraction et d'allouer plus ou moins de ressources de calcul à leur exploration en fonction de leur potentiel et de la vulnérabilité de la meilleure solution connue. Nos travaux sur les tests futurs et la re-conception fournissent un indicateur de vulnérabilité de solutions établies.

La troisième direction de recherche peut se baser sur les partitions et leurs gestion dynamiques (nos agents) pour distribuer l'optimisation sur des noeuds de calcul indépendants

et asynchrones. Quand le nombre de noeuds croît, la plupart des algorithmes d'optimisation peuvent distribuer les évaluations de points (fonctions coût et contraintes) mais la vitesse de génération de nouveaux points (l'optimiseur) devient bloquante. L'optimisation avec système d'agents ne connait pas ce goulot de parallélisation.

CHAPTER 1
INTRODUCTION

Designers in the aerospace industry have typically used a safety factor approach in order to compensate for uncertainties. This practice of using safety factors in design, along with safety margins and knockdown factors, is known as deterministic design. It is common to use safety factors that are based on tradition and experience without consideration of uncertainties. Therefore, the deterministically optimized design may not lead to a minimum cost design. For example, a failure mode with too high of a safety factor will be over-designed and unnecessarily costly. In reliability based design optimization (RBDO), the design is optimized in consideration of the uncertainties and their effect on the probability of failure of the design taking into account each failure mode and the system as a whole. In probabilistic design, the designer can optimally allocate risk amongst the failure modes such that most risk is allocated to the most difficult failure mode to protect against. Less risk is then allocated to the cheaper, easier-to-protect-against modes.

An important step in probabilistic design is the identification and quantification of uncertainties in the design or the tools used in the design process. A broad and often used classification of uncertainties categorizes uncertainty as either aleatory (or intrinsic) or epistemic [1, 2]. The terms “aleatory” and “epistemic” are often used interchangeably with “variability” and “error”, respectively. Aleatory uncertainty generally refers to inherent uncertainties, such as those associated with physical properties of materials or the environment [3]. Some examples include the variations in the yield strength of a material, applied loads, or geometric dimensions of a structure. Epistemic uncertainty, or error, arises due to lack of knowledge. It is often associated with the inability to adequately characterize a phenomenon by use of models, such as finite element models, or through experiments.

These uncertainties are considered when calculating the reliability of the structure, and, in RBDO, the structure is optimized with constraints on the reliability. However, after design, it is customary for the component to undergo various uncertainty reduction measures

(URMs) followed by possible remediation, such as redesign or repair, if necessary. Examples of URMs in the aerospace field include thermal and structural testing, inspection, health monitoring, maintenance, and improved analysis and failure modeling. These URMs are generally not considered at the initial design stage, and the effect of future remediation are not reflected in the reliability calculations or design optimization.

In recent years, there has been a movement to quantify the effect of URMs and associated remediation on the safety of the product over its life cycle. Much work has been completed in the areas of inspection and maintenance for structures under fatigue loading [4–7]. Studies by Acar et al. [2] investigated the effects of future tests and redesign on the final distribution of failure stress and structural design with varying numbers of tests at the coupon, element, and certification levels. Sankararaman et al. [8] proposed an optimization algorithm of test resource allocation for multi-level and coupled systems.

RBDO can become quite costly, partly due to the need for numerous reliability assessments. Though cheaper analytical approaches exist (e.g., first order reliability method), computationally expensive simulation methods, such as Monte Carlo simulation (MCS), are attractive because they can consider the interaction between failure modes, whereas the analytical approaches can not.

The use of expensive models is another source of cost of an optimization problem. In many engineering applications, it is not uncommon for complex simulations to take up to days or weeks to complete. For instance, consider the cost of using a Monte Carlo simulation in combination with a moderately expensive finite element model to evaluate the probability of failure. Even if the amount of time required to complete one simulation of the finite element model is on the order of one minute, a Monte Carlo simulation with a sample size of 1000 would take nearly a day! Consequently, much research has been devoted to the formulation of problems and development of methodologies that reduce the cost of RBDO.

Surrogates, or metamodels, are frequently used to reduce the computational cost in optimization problems. The purpose of a surrogate is to replace an expensive model by a

simple mathematical model - the surrogate - fitted to a set of data points evaluated using the expensive model. The surrogate can then provide predictions of the expensive model at a lower cost. One of the most well known and cheapest to fit surrogates is the polynomial response surface, but others such as kriging, radial basis neural networks, and support vector regression are becoming increasingly popular though they can be more costly to fit. Surrogate-based optimization generally proceeds in cycles, where in one cycle a new point is found through optimization, the point is added to the surrogate, and the surrogate is updated (refit using the new point). This updated surrogate is used in the next cycle to find a new point.

The recent advances in computer throughput have been followed by an increased interest in parallel and distributed computing. Parallel computation is now regularly used to reduce the time and cost of expensive simulations, such as finite element models. In the area of surrogates, there is a growing interest in combining the predictions obtained with the simultaneous use of multiple surrogates during optimization, rather than a single one [9–12]. The aim is to protect against poor surrogates, possibly while reducing the number of cycles required to find the optimum. Viana and Haftka have developed an algorithm to add several points per optimization cycle, which are found through parallel simulations [13]. They have shown that better results can be found in a fraction of the cycles compared to a traditional implementation.

The increased interest in distributed computing is clearly evident in the area of multi-agent systems for optimization. With its roots in computer science, multi-agent systems have a natural connection with constrained optimization. Multi-agent systems solve complex problems by decomposing them into autonomous sub-tasks. A general definition posits a multi-agent system to be comprised of several autonomous agents with possible different objectives that work toward a common task. Through their own objectives, the agents as a system reach a global solution for the whole constraint-based problem. A multi-agent system can solve decomposed problems such that the agents only know subproblems.

Generally, the optimization framework consists in distributing variables and constraints among several agents that cooperate to set values to variables that optimize a given cost function, like in Distributed Constraint Optimization Problem (DCOP) model [14]. Another approach is to decompose problems or to transform problems in dual problems that can be solved by separate agents [15] (for problems with specific properties, as with linear problems). This cooperative approach as been applied to numerous distributed constraint-based problems, such as preliminary aircraft design [16] and university time-tabling [17].

1.1 Outline of Dissertation

1.1.1 Objectives

The objective of this research is to address the following topics:

1. Future tests and redesign in reliability assessment: Develop a methodology to incorporate the effect of a test that will take place in the future (possible followed by redesign) into the reliability assessment at the design stage. In addition, consider the effect of redesign due to an unacceptable test result. A methodology based on Monte Carlo sampling of uncertainties, particularly the errors, simulates possible results of the future test, and we propose two methods of model calibration and redesign based on the test result. The aim is to explore the reduction in uncertainties, the probability of failure, the uncertainty in the probability of failure, and mass that can occur.

2. Tradeoff of tests vs weight: Compare the cost of performing a test and redesign to building a conservative design at the design stage. The aim of this research is to explore what changes occur in the initial design knowing that a test will occur, while also being able to design the test with redesign.

3. Dynamic design space partitioning use surrogate-based agents to locate multiple candidate designs: The aim is to exploit multi-agent system techniques to reduce the cost of solving problems that require expensive function evaluations. We propose to define agents based on surrogates, with inspiration drawn from multiple surrogate techniques. The goal is to locate multiple local optima as a means of obtaining multiple candidate designs for insurance in the design process.

1.1.2 Outline of Text

The organization of this work is as follows. Chapter 2 presents an overview of reliability-based design optimization and some techniques, such as Monte Carlo simulation and surrogates, that are used in this work. It also describes a test problem, the design of an integrated thermal protection system. Chapter 3 presents a methodology to include the

effect of a future test and redesign on reliability assessments. It shows how performing redesign following a single future test can potentially lead to both a reduction in probability of failure and weight reduction through an example that uses the integrated thermal protection system. Chapter 4 uses the modeling of future redesign to provide a way of balancing development costs (test and redesign costs) and performance (mass) by designing the design and redesign rules. By simultaneously designing safety margins and redesign criterion based on probabilities and costs, we show that a company can balance probabilistic design and the more traditional deterministic approach. Chapter 5 describes a method to dynamically partition the design space and locate multiple candidate designs by surrogate-based optimization. Chapter 6 further investigates the use of surrogates to locate multiple candidate designs. The final chapter concludes with a summary of the major aspects of the work presented and describes some research directions that could be pursued based on this work.

CHAPTER 2
BACKGROUND AND LITERATURE REVIEW

Reliability-based design involves evaluating the safety of the design in terms of the probability of failure, and designing to meet a specified level of reliability. The terms reliability and probability of failure are complementary, in that the more reliable the design, the lower the probability of failure. This section discusses the formulation of reliability-based design optimization problems, the methods used to evaluate the reliability, the methods used in optimization, and various methods that reduce uncertainty and consequently affect the reliability. Since surrogate-based methods are widely used in the optimization methods discussed, this section concludes with a review of surrogates and surrogate-based optimization.

2.1 Reliability-Based Design Optimization

Reliability-based design optimization is a probabilistic approach to optimization that is attractive in its ability to allow the designer to prescribe the required level of reliability. RBDO problems are primarily formulated to minimize a cost function f, such as the mass, while satisfying constraints on the reliability. The optimization occurs over the design variables x, considering the uncertain random variables r. The uncertainty present in the random variables is discussed in the next section, Sec. 2.2.

A basic optimization problem[1] can be formulated over the failure modes to form a component level optimization problem. For a problem with n failure modes, the problem can be formulated as

$$\begin{aligned} \underset{x}{\text{minimize}} \quad & E[f(x,r)] \\ \text{subject to} \quad & P_{f,i}(x) \leq P_{f,i}^{allow} \quad i = 1 \ldots n \end{aligned} \tag{2–1}$$

where $P_{f,allow}$ is the allowable probability of failure.

[1] Here, the objective function is shown as the expectation f. This is only an example; the objective can also be a percentile of f.

System-level failure occurs in parallel, series, or a combination of both. For parallel failure, failure must occur in all modes for system failure to occur. For series series, system failure results from the failure in any mode. If the system-level failure is considered, the problem a basic formulation is

$$\begin{aligned} \underset{x}{\text{minimize}} \quad & E[f(x,r)] \\ \text{subject to} \quad & P_{f,sys}(x) \leq P_{f,sys}^{allow} \end{aligned} \tag{2–2}$$

Though both Eqs.(2–1) and (2–2) show constraints on probability of failure, these constraints can also be formulated in terms of the reliability index β. The reliability index is related to the probability of failure by $P_f = \Phi(-\beta)$, where Φ is the standard normal cumulative density function (CDF). The constraints would then be formulated such that $\beta(x,r) \geq \beta_{target}$, where β_{target} is the minimum allowable reliability index .

2.1.1 Optimization Methods

2.1.1.1 Double-loop (nested) methods

In the double-loop approach to RBDO, the design optimization is carried out in the outer loop and the probability of failure is estimated in the inner loop. This can be quite costly due to the methods used to evaluate the reliability (see Sec. 2.1.2), and, in addition, there can be problems with convergence (as seen in the Reliability Index Approach [18])so techniques have been proposed to reduce the computational costs. Two categories have been identified: (i) techniques to improve the efficiency (e.g. fast probability integration [19], two-point adaptive non-linear approximations [20], (ii) techniques that modify the formulation of probabilistic constraints (e.g. inverse reliability measures such as the performance measure approach [18] or the probabilistic sufficiency factor [21]).

2.1.1.2 Single-loop methods

The basic idea of a single loop method is to formulate the probabilistic constraints as deterministic constraints by two ways: (i) the approximation of the Karush-Kuhn-Tucker

optimality conditions at the most probable point [22], (ii) finding approximations of probabilistic design through deterministic design [23–25]. Du and Chen developed the sequential optimization and reliability assessment method (SORA), which uses the information from the reliability assessment to shift the boundaries of violated constraints to the feasible region [26].

2.1.2 Methods to Evaluate Reliability

Failure is defined by a limit state function g, which is a function of the design variables x and the random variables r. It is often defined as the difference between the response R and capacity C defined for a failure mode. The limit state function can be expressed as

$$g(x, r) = C(x, r) - R(x, r) \tag{2–3}$$

where R and C are both functions of both the design and random variables. Failure occurs when the response exceeds the capacity ($g < 0$). The probability of failure can be expressed as

$$P_f = P(g(R) < 0) = \int \dots \int_{g(R)<0} f_R(R) dX \tag{2–4}$$

where $f_R(R)$ is the joint probability density function for the vector R that contains the random variables r. As Melchers explains, the analytical calculation of this expression is challenging because the joint probability density function $f_R(R)$ is not usually easily obtained, and, for the cases when it is obtained, the integration over the failure domain is not easy. Moment and simulation based methods were developed to calculate the probability of failure.

2.1.2.1 Moment based methods

In moment based methods, the vector of variables is mapped to an independent standard normal space (known as u-space) by a transformation. Different transformations exist (e.g., Nataf transformation), but a common transformation is the Rosenblatt transformation [3, 27]. Moment based methods of calculating the reliability have the advantage of being generally cheaper than other methods. However, they can only evaluate the probability of failure of a single mode.

One of the most common moment based methods is the first-order reliability method (FORM). The variables are mapped to an independent standard normal space (u-space) by a transformation. The limit state function is approximated as linear, and FORM is fairly accurate when the curvature of the limit state function is not too severe. In the standard normal space, the point on the limit state function where $g(u) = 0$ at the minimum distance from the origin is the most probable point (MPP) of failure. The reliability index β is the distance from the origin to the MPP. The MPP is expressed as

$$\begin{aligned} &\underset{u}{\text{minimize}} \quad \beta = \sqrt{u^T u} \\ &\text{subject to} \quad g(u) = 0 \end{aligned} \tag{2–5}$$

where u is the vector of variables in standard normal space.

Second order methods can be used when the curvature of the limit state function is high. The second-order reliability method (SORM) approximates the limit state as a quadratic, and provides a more accurate approximation in such cases.

2.1.2.2 Sampling based methods

Monte Carlo sampling (MCS) is a technique to numerically integrate the probability of failure as expressed in Eq.(2–4). It requires random sampling of the random variables r for design x. The limit state is checked for each realization. Formally, for N trials, this is expressed as

$$P_f = \frac{1}{N} \sum_{i=1}^{N} I[g(C_i, R_i) < 0] \tag{2–6}$$

where I is the indicator function, which equals 1 when $g < 0$ and 0 otherwise. The main advantage of MCS is that it allows the evaluation of the probability of failure considering joint failures between two or more modes.

The accuracy of the probability of failure given by Eq.(2–6) is estimated by the coefficient of variation of the probability of failure given by Eq.(2–7), and approximated as shown when P_f is small [28].

$$CV(P_f) = \sqrt{\frac{(1 - P_f)}{P_f N}} \approx \sqrt{\frac{1}{P_f N}} \tag{2–7}$$

By this approximation, it is seen that, for a probability of failure of 1e-6, 100 million simulations are needed to achieve 10% accuracy for one-sigma level of confidence. Clearly, when the calculation of the limit state involves complex analyses, such as finite element models, the accurate calculation of small probabilities of failure becomes expensive.

Smarslok et al. developed the separable Monte Carlo method (SMC) to reformulate the limit state when the types of uncertainty in the limit state (i.e. response and capacity) are independent [28]. In separable Monte Carlo, the number of simulations of the response and capacity can be different, such that an expensive response can be evaluated a fewer number of times.

$$P_f = \frac{1}{MN} \sum_{i=1}^{N} \sum_{j=1}^{M} I[g(C_j, R_i) < 0] \tag{2–8}$$

2.2 Definition of Types of Uncertainty

Many have attempted to identify and classify different types of uncertainty that should be considered in a reliability assessment. A broad and often used classification of uncertainties categorizes uncertainty as either aleatory (or intrinsic) or epistemic [1, 2]. The terms “aleatory” and “epistemic” are often used interchangeably with “variability” and “error” , respectively.

Aleatory uncertainty generally refers to inherent uncertainties, such as those associated with physical properties of materials or the environment [3]. Some examples include the variations in the yield strength of a material, applied loads, or geometric dimensions of a component. Variability can be reduced with more data (e.g. more tests to reduce the variation of the yield strength of a material), or quality control (e.g. improved quality control to reduce variations in dimensions).

Epistemic uncertainty, or error, arises due to lack of knowledge. It is often associated with the inability to adequately characterize a phenomenon by use of models, such as finite element models, or through experiments. Epistemic uncertainty can often by reduced by

simply adding more knowledge by more research, expert consultation, and tests to calibrate analytical models, for example.

2.3 Uncertainty Reduction Methods in Reliability Based Design

After design, it is customary for the component to undergo various uncertainty reduction measures (URMs) followed by remediation, such as redesign or repair, if necessary. Examples of URMs in the aerospace field include thermal and structural testing, inspection, health monitoring, maintenance, and improved analysis and failure modeling.

In recent years, there has been a movement to quantify the effect of URMs on the safety of the product over its life cycle. Much work has been completed in the areas of inspection and maintenance for structures under fatigue loading. Fujimoto et al. [4], Toyoda-Makino [5], and Garbatov et al. [6] developed methods to optimize inspection schedules for a given structural design to maintain a specific level of reliability. Even further, Kale et al. [7, 29] explored how simultaneous design of the structure and inspection schedule allows the trading of cost of additional structural weight against inspection cost of stiffened panels affected by fatigue crack growth.

There have been few studies that have incorporated the effects of future tests followed by possible redesign on the design of a structure. Studies by Acar et al. [2, 30] investigated the effects of future tests and redesign on the final distribution of failure stress and structural design with varying numbers of tests at the coupon, element, and certification levels. Such studies showed that these tests with possible redesign can greatly reduce the probability of failure of a structure, and estimated the required structural weight to achieve the same reduction without tests. Sankararaman et al. [8] proposed an optimization algorithm of test resource allocation for multi-level and coupled systems.

2.4 The Role of Surrogates

Surrogate models, or meta-models, are often used to reduce the cost associated with expensive function evaluations, such as those from finite element analysis or computational fluid dynamics. Some examples of surrogates include polynomial response surfaces

[31, 32], kriging [33–35], support vector regression [36], and neural networks [37, 38]. In optimization, surrogates are often used to provide approximations of the objective function and/or constraints in optimization. The use of surrogates has been well documented, and for a complete review surrogates and surrogate-based optimization techniques, the reader is referred to references [39–43].

Traditional surrogate-based optimization progresses in iterations, or cycles, until an optimum or suitable solution is found. In one cycle, data from expensive simulations is fit to a surrogate, the surrogate is used to find a candidate optimum, and the optimum is evaluated by the expensive simulator. The optimum is generally added to the surrogate in the next iteration.

In recent years, many have proposed strategies for using multiple surrogates for optimization [9–12]. Viana explains that the use of multiple surrogates over a single surrogate makes sense because "(i) no single surrogate works well for all problems, (ii) the cost of constructing multiple surrogates is often small compared to the cost of simulations, and (iii) use of multiple surrogates reduces the risk associated with poorly fitted models" [39]. In particular, the ability of multiple surrogates to give different interpretations (i.e., predictions and uncertainty estimates) of the same design space is attractive.

Multiple surrogates have been used to simply compare the multiple solutions given by each surrogate. For example, Samad et al. [10] compared polynomial response surface, kriging, radial basis neural network, and a weighted average surrogate in the shape optimization of a compressor blade, and found that the most accurate surrogate did not lead to the best solution. Zerpa et al. [44] showed that the use of multiple surrogates helped to identify alternative optimal solutions corresponding to different regions in the design space.

Multiple surrogate techniques include using an ensemble of surrogates, where the prediction is a weighted result of the surrogate predictions [45–47]. The weights placed on each surrogate prediction are generally based on local or global error metrics. Proposed

methods for choosing the weight factors include error correlation, cross-validation error, prediction variance, and error minimization.

The addition of multiple points per optimization cycle has also been explored [48–50]. Viana and Haftka and later Chaudhuri et al. developed an algorithm for adding several points per optimization cycle based on approximated computation of the probability of improvement (the probability of being below a target value) [13, 51]. Comparing their results with traditional sequential based optimization with kriging, they were able to deliver better results in a fraction of the optimization cycles using this algorithm.

2.5 Integrated Thermal Protection System Test Case Description

This section describes the main test case that is used to illustrate the methodologies presented in this proposal. The integrated thermal protection system was used as an illustrative example in the articles in Refs. [52–57].

2.5.1 Integrated Thermal Protection System

Large portions of the exterior surface of many space vehicles are devoted to providing protection from the severe aerodynamic heating experienced during ascent and atmospheric reentry. Traditionally, thermal protection systems (TPS) do not provide structural support functions, and are added to only to protect the underlying structure, thereby adding to the launch weight. This is the case with the TPS of the Apollo, Space Shuttle Orbiter, and X-33 VentureStar. A proposed integrated thermal protection system (ITPS) provides structural load bearing function in addition to its insulation function, and in so doing provides a chance to reduce launch weight.

One proposed ITPS design is the corrugated core sandwich structure, which is illustrated in Fig. 2-1. This design evolved from studies for reusable launch vehicles (RLV) and evolved towards robust metallic TPS concepts [58–60], which been the subject of several studies [61–63]. These studies have shown that this design should be an adequately robust, weight-efficient, load-bearing structure.

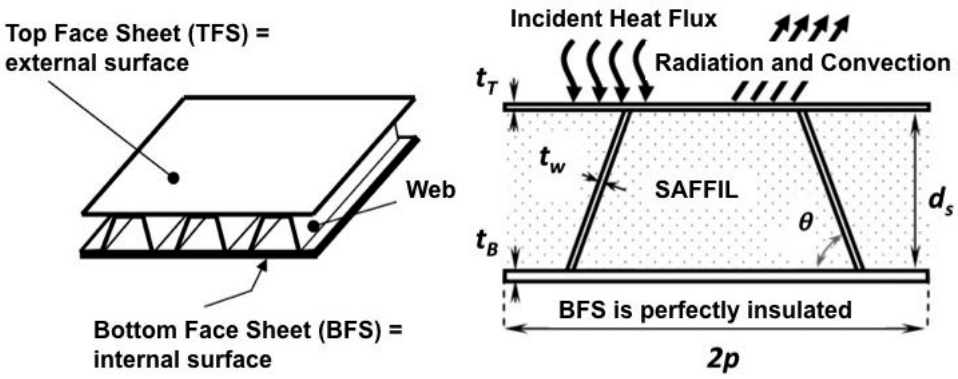

Figure 2-1. Corrugated core sandwich panel ITPS concept

The design consists of a top face sheet and webs made of titanium alloy (Ti-6Al-4V), and a bottom face sheet made of beryllium (grade S200-F, vacuum hot pressed). Saffil® foam is used as insulation between the webs. The material properties are assumed to be normally distributed (with the exception of the density of the insulation foam), with the nominal values and coefficient of variations given in Table 2-1.

Table 2-1. ITPS material properties

Property	Symbol	Nominal	CV(%)
density of titanium[1]	ρ_{Ti}	4429 $\frac{kg}{m^3}$	2.89
density of beryllium[2]	ρ_{Be}	1850 $\frac{kg}{m^3}$	2.89
density of foam	ρ_S	24 $\frac{kg}{m^3}$	0
thermal conductivity of titanium	k_{Ti}	7.6 $\frac{W}{m/K}$	2.89
thermal conductivity of beryllium	k_{Be}	203 $\frac{W}{m/K}$	3.66
thermal conductivity of foam	k_S	0.105 $\frac{W}{m/K}$	2.89
specific heat of titanium	c_{Ti}	564 $\frac{J}{kg/K}$	2.89
specific heat of beryllium	c_{Be}	1875 $\frac{J}{kg/K}$	2.89
specific heat of foam	c_S	1120 $\frac{J}{kg/K}$	2.89

1 Top face sheet and web material
2 Bottom face sheet material

The relevant geometric variables of the ITPS design are also shown on the unit cell in Fig. 2-1. The variables considered are the top face thickness (t_T), bottom face thickness (t_B), thickness of the foam (d_S), web thickness (t_w), corrugation angle (θ), and length of unit cell ($2p$).

The thermal and structural requirements often conflict due to the nature of the mechanisms that protect against the failure in the different modes. Examples of conflicts between thermal and structural requirements include:

- Thin webs allow less heat to flow to the bottom face sheet, but are more susceptible to buckling failure.
- As the depth of the ITPS is reduced, the design resists buckling better but is a poorer insulator.
- A thick bottom face sheet increases stresses in the web, but decreases the bottom face sheet temperature.

2.5.2 Thermal and Structural Analysis

Thermal analysis of the ITPS was performed using 1-D heat transfer equations on a model of the unit cell. The heat flux incident on the top face sheet of the panel is highly dependent on the vehicle shape as well as the vehicle's trajectory. As in previous studies by Bapanapalli [61], incident heat flux on a Space Shuttle-like vehicle was used. A large portion of the heat is radiated out to the ambient by the top face sheet, and the remaining portion is conducted into the ITPS. We consider the worst-case scenario where the bottom face sheet cannot dissipate heat by assuming the bottom face sheet is perfectly insulated. Also, there is no lateral heat flow out of the unit cell, so that heat flux on the unit cell is absorbed by that unit cell only. For an in-depth description of the model and boundary conditions, the reader is referred to the Bapanapalli and Sharma references [61, 63].

The maximum temperature of the bottom face sheet of the ITPS panel is calculated using the quadratic response surface developed by Villanueva et al. [53] by a process similar to that of Gogu et al. [62], using the MATLAB toolbox developed by Viana [64]. It is a function of the previously described geometric variables and the density, thermal conductivity, and specific heat of titanium alloy, beryllium, and Saffil® foam.

The maximum von Mises stress in the web was also found using an analysis in Abaqus, at the time when the temperature difference between the top and bottom face sheets was maximum. A quadratic response surface of the maximum von Mises stress in the web

was developed as a function of the geometry, Young's modulus, Poisson's ratio, and the coefficient of thermal expansion. The overall buckling of the web is assumed to be Euler buckling. It is modeled as a function of the web thickness and width of the foam, along with the coefficient of thermal expansion and Young's modulus of the web material to represent a load due to the temperature difference between the top and bottom.

The mass per unit area m of the ITPS is calculated using Eq.(2–9) where ρ_T, ρ_B, and ρ_w are the densities of the materials that make up the top face sheet, bottom face sheet, and web, respectively.

$$m = \rho_T t_T + \rho_B t_B + \frac{\rho_w t_w d_S}{p \sin\theta} \tag{2–9}$$

CHAPTER 3
INCLUDING THE EFFECT OF FUTURE TESTS AND REDESIGN IN RELIABILITY CALCULATIONS

It is common to test components after they are designed and redesign if necessary. The reduction of the uncertainty in the probability of failure that can occur after a test is usually not incorporated in reliability calculations at the design stage. This reduction in uncertainty is accomplished by additional knowledge provided by the test and by redesign when the test reveals that the component is unsafe or overly conservative. In this chapter, we develop a methodology to estimate the effect of a single future thermal test followed by redesign, and model the effect of the resulting reduction of the uncertainty in the probability of failure. Using assumed distributions of computation and experimental errors and given re-design rules, we obtain possible outcomes of the future test and redesign through Monte Carlo sampling to determine what changes in probability of failure, design, and weight will occur. In addition, Bayesian updating is used to gain accurate estimates of the probability of failure after a test. These methods are demonstrated through a future thermal test on an integrated thermal protection system. We observe that performing redesign following a single future test can reduce the probability of failure by orders of magnitude, on average, when the objective of the redesign is to restore original safety margins. Redesign for a given reduced probability of failure allows additional weight reduction.

3.1 Motivation for Examining Future Tests and Redesign

Traditionally, aerospace structures have been designed deterministically, employing safety margins and safety factors to protect against failure. After the design stage, most components undergo tests, whose purpose is to validate the model and catch unacceptable designs and redesign them. After production, inspection and manufacturing are done to ensure safety throughout the lifecycle. In contrast, probabilistic design considers uncertainties to calculate the reliability, which allows the trade-off of cost and performance.

In recent years, there has been a movement to quantify the effect of uncertainty reduction measures, such as tests, inspection, maintenance, and health monitoring, on

the safety of a product over its life cycle. Much work has been completed in the areas of inspection and maintenance for structures under fatigue [4–7]. Studies by Acar et al. [2] investigated the effects of future tests and redesign on the final distribution of failure stress and structural design with varying numbers of tests at the coupon, element, and certification levels. Golden et al. [65] proposed a method to determine the optimal number of experiments required to reduce the variance of uncertain variables. Sankararaman et al. [8] proposed an optimization algorithm of test resource allocation for multi-level and coupled systems. A method to simultaneously design a structural component and the corresponding proof test considering the probability of failure and the probability of failing the proof test was introduced by Venter and Scotti [66].

Most aerospace components are designed using a computational modeling technique, such as finite element analysis. We expect some error, often labeled as epistemic uncertainty (associated with lack of knowledge), in the modeled behavior. The true value of this error is unknown, and thus we consider this lack of knowledge to lead to an uncertain future. Tests are performed to reduce the error, thus narrowing the range of possible futures through the knowledge gained and the correction of unacceptable futures by redesign.

In this study, we examine the effect of a single future thermal test followed by possible redesign on the reliability and weight of an integrated thermal protection system (ITPS). A description of the integrated thermal protection system is presented in Sec. 2.5.1. An experiment that finds the bottom face sheet temperature of a small ITPS panel is usually conducted in a vacuum chamber with heat applied to the top face sheet by heat lamps. The sides of the panel are typically surrounded by some kind of insulation to prevent lateral heat loss. The temperature of the bottom face sheet is found with thermocouples embedded into or in contact with the lower surface of the bottom face sheet. The thermal test considered in this study measures the maximum temperature of the bottom face sheet, which is critical due to its proximity to the underlying vehicle structure. A design is considered to have failed thermally if it exceeds the maximum allowable temperature.

In previous work on the optimization of the ITPS, Villanueva et al. [53] used probability of failure calculations that considered only the variability in geometric and material parameters and error due to shortcomings in the analytical model. Expanding on those studies, we include the information gained from a test in a temperature estimate, the reduction in uncertainty resulting from the test, and the ability of the test to guide redesign for dangerous or overly conservative designs. Thereby, the objective of this chapter is to:

1. Present a methodology to both predict and include the effect of a future redesign following a test during the design stage
2. Illustrate the ability of a test in combination with redesign to reduce the probability of failure even when a test shows that the design is computationally unconservative
3. Examine the overall changes in mass resulting from redesign based on the future test

The uncertainty model and probability of failure calculations are described in Section 3.2. Section 3.3 continues with the methodology to calibrate the computational model based on a test and includes redesign based on the test. The method to simulate future tests is summarized in Section 3.4. Section 3.5 presents an illustrative example that details the effect of including the test and redesign in probability of failure calculations.

3.2 Uncertainty Modeling

3.2.1 Classification of Uncertainties

Oberkampf et al. [1] provided an analysis of different sources of uncertainty in engineering modeling and simulation, which was simplified by Acar et al. [2]. We use classification similar to Acar's to categorize types of uncertainty as errors (uncertainties that apply equally to every ITPS) or variability (uncertainties that vary in each individual ITPS). We further describe errors as epistemic and variability as aleatory. As described by Rao et al. [67], the separation of the uncertainty into aleatory and epistemic uncertainties allows more understanding of what is needed to reduce the uncertainty. Tests reduce errors by allowing us to calibrate analytical models. For example, testing can be done to reduce the uncertainty in failure predictions due to high stresses. Variability can be reduced by lowering tolerances in

manufacturing. Variability is modeled as random uncertainties that can be modeled probabilistically. In contrast, errors are fixed for a given ITPS and are largely unknown, but here they are modeled probabilistically as well.

Variability in material properties and construction of the ITPS leads to variability in the ITPS thermal response. More specifically, we will have variability in the calculated temperature due to the input variabilities. We simulate this process with a Monte Carlo simulation (MCS) that generates values of the random variables r based on an estimated distribution and calculates the bottom face sheet temperature T_{calc} for each, generating the probability distribution function. The calculated temperature distribution that reflects the random variability is denoted $f_{calc}(T)$. In estimating the probability of failure, we also need to account for the modeling or computational error. We denote this computational error by e_c, where e_c is modeled as a uniformly distributed random variable within confidence limits the in the computational model as defined by the analyst. Unlike the variability, the error has a single value, and the uncertainty is due to our lack of knowledge.

For a given design given by d and r, the possible true temperature T_{Ptrue} can be found by Eq.(3–1) in terms of possible computational errors e_c. The sign in front of e_c is negative so a positive error implies a conservative calculation, meaning it overestimates the temperature.

$$T_{Ptrue}(d, r, e_c) = T_{calc}(d, r)(1 - e_c) \tag{3–1}$$

Since the analyst does not know e_c and it is modeled as a random variable, we can form a distribution of the possible true temperature, denoted as $f_{Ptrue}(T)$. To illustrate the difference between the true distribution of the temperature $f_{true}(T)$ and possible true distribution $f_{Ptrue}(T)$, let us consider a simple example where the calculated temperature of the nominal design is 1, the true temperature is 1.05, and the computational error is uniformly distributed in the range [-0.1,0.1]. The possible true temperature without variability are uniformly distributed in [0.9,1.1] by Eq.(3–1). Now, let us consider an additional variability in the temperature due to manufacturing tolerances in the range [-0.02, 0.01], such that

$T_{calc}(d,r)$ is uniformly distributed in the range [0.98,1.01]. Finally, the true temperature will vary from [1.03,1.06] as $f_{true}(T)$, and the possible true temperature from [0.882, 1.111] as $f_{Ptrue}(T)$.

Figure 3-1 illustrates how we arrive at the distribution $f_{Ptrue}(T)$. The input random variables have initial distributions, denoted as $f_{inp}(r)$, and these random variables, in combination with the design variables, lead to the distribution of the calculated temperature $f_{calc}(T)$. The random computational error is applied, leading to the distribution of the possible true temperature $f_{Ptrue}(T)$, which has a wider distribution than $f_{calc}(T)$.

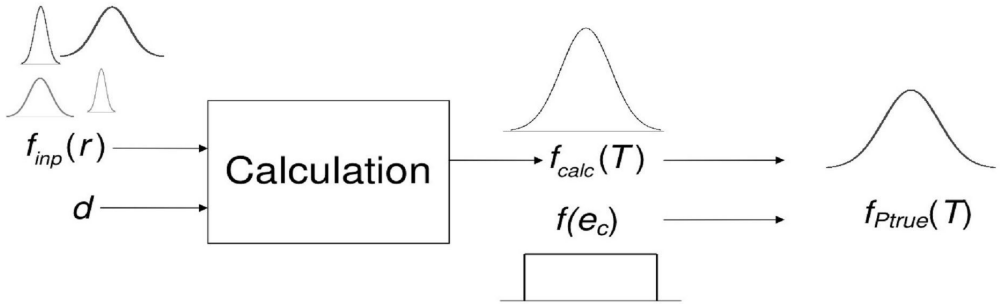

Figure 3-1. Illustration of the variability of the input random variables, calculated value, computational error, and resulting distribution of possible true temperature

As previously noted, e_c is modeled as a random variable not because it is random, but because its value is unknown to the analyst. To emphasize this point, the actual true temperature is known only when we know the actual value of e_c as $e_{c,true}$ as illustrated in Eq.(3–2).

$$T_{true}(d,r) = T_{calc}(d,r)(1 - e_{c,true}) \tag{3–2}$$

Again, these true values are unknown to the analyst. This distinction between true values and analyst-estimated, possible true values is important and will be a point of comparison throughout this chapter.

Figure 3-2 shows an example of the probability distribution of the true temperature $f_{true}(T)$, as well as the probability density functions (pdf) of $f_{calc}(T)$ and $f_{Ptrue}(T)$. For this example, we modeled the variability in the material properties and variability in geometry

with normal distributions, and the computational error with a uniform distribution. The plots of each pdf show the probability of exceeding the allowable temperature T_{allow}, represented by the area where the temperature exceeds the allowable.

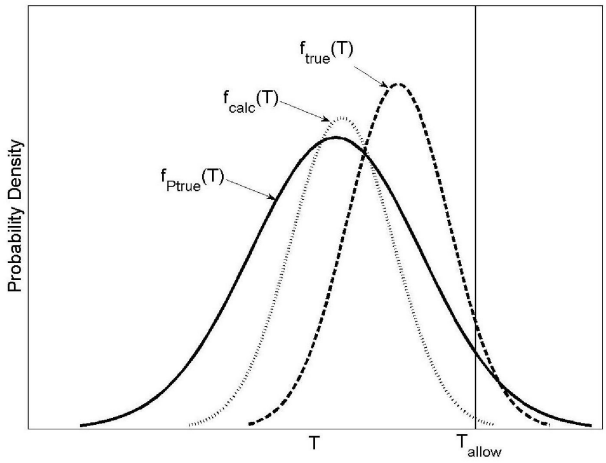

Figure 3-2. Illustration with unconservative calculation of temperature. When including the error in the estimate, the estimate of the probability of failure is improved.

We chose an illustration where the computational error is unconservative so the $f_{calc}(T)$ provides an underestimate of the probability of failure given by $f_{true}(T)$. This computational error between the mean of $f_{calc}(T)$ and the mean of $f_{true}(T)$ is $e_{c,true}$. However, since we include e_c as a random variable, we widened the distribution $f_{calc}(T)$, resulting in $f_{Ptrue}(T)$. This provides a more conservative estimate of the probability that can compensate for the unconservative calculation. Of course, when the error in the calculation is conservative, this wide distribution will grossly overestimate the probability of failure.

3.2.2 True Probability of Failure Calculation

The true probability of failure of a design d with random variables r can be found when the true computational error is known. This is clearly a hypothetical situation because in reality the true computational error is not known by the analyst. Here, Monte Carlo simulation (MCS) is used to calculate the true probability of failure. The limit state equation g is

formulated as the difference between a capacity C and response R as shown in Eq.(3–3).

$$g = T_{allow} - T_{true}(d, r) \equiv C - R \tag{3–3}$$

Since we consider failure to occur when the maximum bottom face sheet temperature exceeds the allowable temperature T_{allow}, the response is T_{true} and the capacity is the allowable temperature. The true probability of failure $p_{f,true}$ is estimated with Eq.(3–4).

$$p_{f,true} = \frac{1}{N} \sum_{i=1}^{N} I[g(C_i, R_i) \leq 0] \tag{3–4}$$

The indicator function I equals 1 if the response exceeds the capacity, and equals 0 for the opposite case. The number of samples is N.

3.2.3 Analyst-Estimated Probability of Failure Calculation

Since the true computational error is unknown, the true probability of failure is unknown as well. Because of this, the best estimate the analyst can obtain uses the calculated temperature T_{calc} and the computational error through the possible true temperature of Eq.(3–1) to determine the estimated probability of failure with the limit state equation formulated as in Eq.(3–5).

$$g = T_{allow} - T_{Ptrue}(d, r, e_c) \equiv C - R \tag{3–5}$$

Since the two types of uncertainty (computational errors and variability in material properties and geometry) in the response are independent, Separable Monte Carlo (SMC) sampling[28] can be used when evaluating the probability of failure. The limit state equation can be reformulated so that the computational error is on the capacity side, and all random variables associated with material properties and geometry lie on the response side.

$$g = \frac{T_{allow}}{1 - e_c} - T_{calc}(d, r) \equiv C' - R' \tag{3–6}$$

This analyst-estimated probability of failure $p_{f,analyst}$ can then be calculated with Eq.(3–7), where M and N are the number of capacity and response samples, respectively.

$$p_{f,analyst} = \frac{1}{MN} \sum_{i=1}^{N} \sum_{j=1}^{M} I[g(C_j, R_i) \leq 0] \tag{3–7}$$

3.3 Including the Effect of a Calibration Test and Redesign

We consider a test, performed for the purpose of validating and calibrating a model, for a selected design d_{test} to determine the temperature of the test article T_{test}. We further assume that the test article is carefully measured for both d_{test} and r_{test} so that both are accurately known, and that the errors in the computed temperatures due to uncertainty in the values of d_{test} and r_{test} are small compared to the measurement errors and can be neglected. If no errors are made in the measurements of d_{test}, r_{test}, and T_{test}, then the experimental result is actually the true temperature of the test article. We denote this error-free test temperature $T_{test,true}$.

$$T_{test,true} = T_{true}(d_{test}, r_{test}) \tag{3–8}$$

However, there is unknown measurement error e_x, which we model as a random variable based on our estimate of the accuracy of the test. The measured temperature T_{meas} then includes the experimental error $e_{x,true}$. The experimental error could also include a component due to the fact that r_{test} is not perfectly known.

$$T_{meas} = \frac{T_{test,true}}{1 - e_{x,true}} \tag{3–9}$$

Using the computational and experimental results, along with the corresponding error estimates for the test article, we are able to refine the calculated value and its error for any design described by the design variables d and random variables r. In this way, the result of the single test can be used to calibrate calculations for other designs. We examine two methods, which take different approaches in using the test as calibration. The first approach introduces a simple correction factor based on the test result. The second uses the Bayesian method to update the uncertainty of the calculated value for d_{test} based on the test result and then transfers this updated uncertainty to other calculations as the means of calibration.

3.3.1 Correction Factor Approach

The correction factor approach is a fairly straightforward method of calibration. Assuming that the test result is more accurate than the calculated result for the test article, we scale T_{calc} for any value of d and r by the ratio of the test result to the calculated result to obtain the corrected calculation $T_{calc,corr}$.

$$T_{calc,corr} = T_{calc}(d, r)\left(\frac{T_{meas}}{T_{calc}(d_{test}, r_{test})}\right) \tag{3–10}$$

3.3.2 Bayesian Updating Approach

Before the test, we have an expectation of the test results based on the computational result of d_{test} and r_{test}. We denote this distribution by $f^{ini}_{test,Ptrue}$, which can be viewed as the distribution of $f_{Ptrue}(T)$ of the test article with fixed random variables r_{test}. Furthermore, it may be viewed as the possible true temperature distribution of the test article just before the test.

In the test, we measure a temperature T_{meas}. Because of experimental error e_x, the true test result $T_{test,true}$ is not equal to T_{meas} (as seen in Eq.(3–9)). The possible true value of the test result is instead given as

$$T^{meas}_{test,Ptrue} = T_{meas}(1 - e_x) \tag{3–11}$$

where $T^{meas}_{test,Ptrue}$ forms the distribution of possible true test results available from the measurements only. We thus have two distributions of possible true test results. One is based on the calculated value and the distribution of the calculation error, and the other is based on the measurement and the distribution of the measurement error.

The Bayesian approach combines these two distributions to obtain a narrower and more informative distribution. In this formulation, the probability distribution of the possible true temperature of the test article $f_{test,Ptrue}(T)$ is updated as

$$f^{upd}_{test,Ptrue}(T) = \frac{l_{test}(T) f^{ini}_{test,Ptrue}(T)}{\int_{-\infty}^{+\infty} l_{test}(T) f^{ini}_{test,Ptrue}(T) dT} \tag{3–12}$$

where the likelihood function $l_{test}(T)$ is the conditional probability density of obtaining the test result T_{meas} when the true temperature of the test article is T. That is, l_{test} is the probability density of $\frac{T}{1-e_x}$ evaluated at $T = T_{meas}$.

The updated estimate $f^{upd}_{test,Ptrue}(T)$ is the distribution of the updated true possible test result $T^{upd}_{test,Ptrue}$. This is used to find the distribution of the Bayesian estimate of the computational error e_{Bayes} with Eq.(3–13).

$$e_{Bayes} = 1 - \frac{T^{upd}_{test,Ptrue}}{T_{calc}(d_{test}, r_{test})} \tag{3–13}$$

We can then replace the possible true temperature given by Eq.(3–1) with a true temperature that uses the Bayesian estimate of the error.

$$T_{Ptrue}(d, r, e_{Bayes}) = T_{calc}(d, r)(1 - e_{Bayes})(1 - e_{extrap}) \tag{3–14}$$

The additional error e_{extrap} is included to account for the error that occurs when applying this Bayesian estimate of the error to some design other than the test design. This extrapolation error is further described in Sec. 3.3.2.2.

Note that it is also possible to perform the Bayesian updating by reversing the roles of the two possible true test temperatures. That is, we could take the distribution based on the measurement error as the initial distribution, and take the computed result as the additional information. However, in this case the likelihood function would require repeated simulations for different possible true temperatures, greatly increasing the computational cost.

3.3.2.1 Illustrative example of calibration by the Bayesian approach

To illustrate how Bayesian updating is used to calibrate calculations based on a single future test, we consider a simple case where both the computational and experimental errors are uniformly distributed. To simplify the problem, we normalize all temperatures by the calculated temperature so that $T_{calc}(d_{test}, r_{test}) = 1$. The error bound of the calculation is $\pm 10\%$ and the error bound of the test is $\pm 7\%$. The normalized test result is $T_{meas} = 1.05$.

In this work, we make the simplifying assumption that the likelihood function is about T_{meas} rather than T. That is, we use conditional probability of obtaining the temperature T given the measured temperature. This allows for a uniform value of the likelihood function where it is nonzero, which thereby results in a uniform distribution of the updated Bayesian estimate of the computational error since the distribution of $f^{upd}_{test,Ptrue}$ will also be uniform. The effect of this approximation of the likelihood function is examined in Appendix A. The initial probability distribution $f^{ini}_{test,Ptrue}(T)$ and the likelihood function l_{test} are described by Eqs. (3–15) and (3–16), respectively.

$$f^{ini}_{test,Ptrue}(T) = \begin{cases} \frac{1}{0.2T_{calc}(d_{test},r_{test})} & \text{if } \left|\frac{T}{T_{calc}(d_{test},r_{test})} - 1\right| \leq 0.1; \\ 0 & \text{otherwise.} \end{cases} \tag{3–15}$$

$$l_{test}(T) = \begin{cases} \frac{1}{0.14T_{meas}} & \text{if } \left|\frac{T-T_{meas}}{T_{meas}}\right| \leq 0.07; \\ 0 & \text{otherwise.} \end{cases} \tag{3–16}$$

Since $T_{calc}(d_{test}) = 1$ and the computation error bounds are $\pm 10\%$, the initial distribution of the true temperature is $f^{ini}_{test,Ptrue}(T) = 5$ on the interval (0.9, 1.1) and zero elsewhere. This is shown in Fig. 3-3. The test result of $T_{meas} = 1.05$ results in a likelihood of $l_{test} = 6.803$ on the interval (0.9765, 1.1235) and zero elsewhere. Equation (3–12) is used to find the updated T_{true} distribution so that $f^{upd}_{test,Ptrue}(T) = 8.1$ on the interval (0.9765, 1.1) and zero elsewhere.

The updated distribution shows that the true temperature is somewhere on the interval (0.9765, 1.1). Using this temperature distribution along with the calculated value $T_{calc}(d_{test})$, the updated error distribution e_{Bayes} can be found. Through Eq.(3–13), we determine that e_{Bayes} is uniformly distributed from -10% to 2.35%.

3.3.2.2 Extrapolation error in calibration

Figure 3-4 illustrates how the Bayesian approach is used to calibrate the calculations for other designs described by d. Here, we consider the case when the calculated temperature

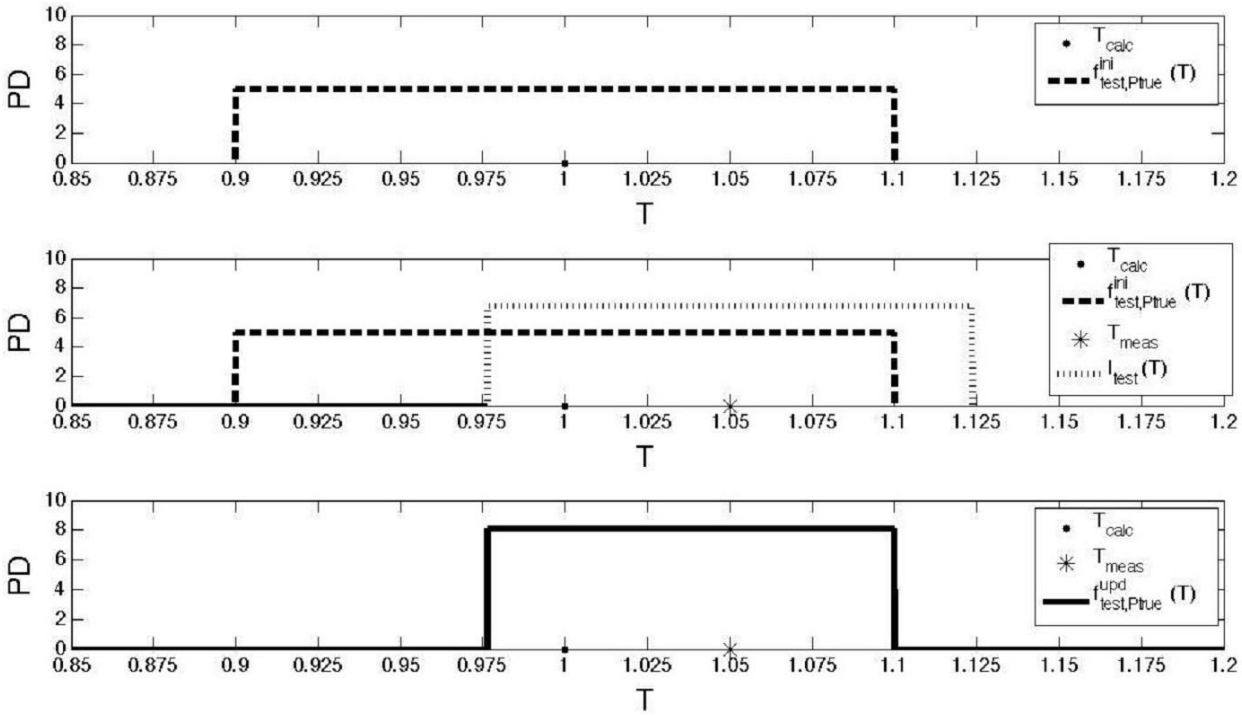

Figure 3-3. Illustrative example of Bayesian updating showing the initial distribution (top), initial distribution and test (middle), and updated distribution (bottom).

is linear in the design variable d, and there is no variability (random variables fixed at nominal values).

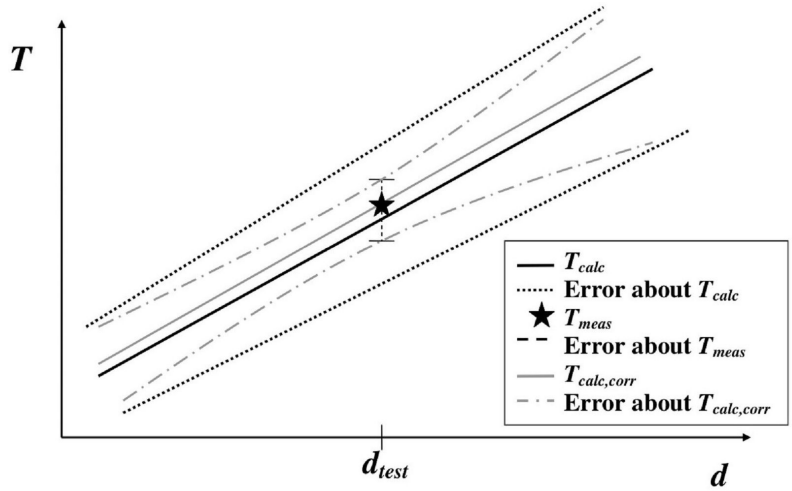

Figure 3-4. Illustration of the calibration using Bayesian updating

At design d_{test}, we have the same error scenario similar to that illustrated in Fig. 3-3. That is, we represent the calculated temperature at d_{test} as a point on the solid black line, and the error bounds about this calculation by the dotted black lines. The star represents the experimentally measured temperature, and the error bars show the uncertainty in this temperature. By the Bayesian approach, we obtain a corrected test temperature as represented by the point on the grey line, as well as updated error bounds represented by the grey dash-dot line.

However, this correction and updated error is most accurate at the test design. Therefore, we apply an additional error, the extrapolation error e_{extrap}, when calibrating designs other than d_{test}. Note that at d_{test} the updated error bounds in Fig. 3-4 coincide with the error bounds of the test. As the design becomes increasingly different from d_{test}, the updated error bounds become wider.

The magnitude of e_{extrap} is assumed to be proportional the distance between d and d_{test}, such that

$$e_{extrap} = (e_{extrap})_{max} \frac{\|d - d_{test}\|}{\Delta d_{lim}} \tag{3–17}$$

This defines the extrapolation error so that it is maximum when the distance between d and d_{test} is at limit of this distance Δd_{lim} and zero at the test design. The extrapolation error is a measure of the variation of the errors in the model away from the test design. In this work, we assume that the magnitude of e_{extrap} is linear with the distance between d and d_{test}, which would be reasonable for small changes in the design. However, we examine the effect of this assumption in Appendix B where we use a quadratic variation.

3.3.3 Test-Corrected Probability of Failure Estimate

The corrected probability of failure $p_{f,analyst-corr}$ after the test can be estimated by the analyst using the updated error obtained from the Bayesian approach. Separable Monte Carlo is used to calculate $p_{f,analyst-corr}$.

$$g = \frac{T_{allow}}{1 - e_{Bayes}} - T_{calc}(d, r)(1 - e_{extrap}) \equiv C - R \tag{3–18}$$

$$p_{f,analyst-corr} = \frac{1}{MN} \sum_{i=1}^{N} \sum_{j=1}^{M} I[g(C_j, R_i) \leq 0] \tag{3–19}$$

3.3.4 Redesign Based on the Test

Two criteria for redesign are considered, each with different perspectives on the purpose of the redesign. The first criterion is based on the agreement between the measured and calculated values for the test article. The second criterion considers the probability of failure estimated by the analyst.

3.3.4.1 Deterministic redesign

In deterministic redesign, redesign occurs when there is a significant difference between the experimentally measured temperature T_{meas} and the expected temperature given by the computational model. It is assumed that the temperature given by the computational model (T_{calc}) is the desired value. Therefore, the component is redesigned to restore this original temperature.

The deterministic redesign criterion is implemented by imposing limits on the acceptable ratio of the measured temperature to the calculated temperature. Redesign occurs when $\frac{T_{meas}}{T_{calc}(d_{test}, r_{test})}$ is less than the lower limit D_L (conservative computational model) or exceeds the upper limit D_U (unconservative computational model).

3.3.4.2 Probabilistic redesign

In probabilistic redesign, the original structure is designed for a specified probability of failure, and redesign is also done to achieve a specified probability of failure. It is reasonable to select the target redesign probability $p_{f,target}$ to be the same as that obtained with probabilistic design. The target redesign probability of failure can also be set to make the design safer after the test. Therefore, redesign occurs when the test-corrected probability of failure estimate, given by Eq.(3–19) is outside the limits of the acceptable range. The lower limit of this range is denoted P_L, and the upper limit P_U.

3.4 Monte Carlo Simulations of a Future Test and Redesign

Monte Carlo simulations are used to simulate the effect of a future test for a design described by design variables d and random variables r with the goal of simulating multiple possible outcomes of this test. To simulate a single outcome of the future test, we first obtain a single sample of the true computational and experimental errors.

Using the calculated value for the test design and the true computational error, we can obtain the true temperature by Eq.(3–2). Next, the experimentally measured temperature is found using Eq.(3–9). The choice can be made to calibrate by the correction factor approach or the Bayesian updating approach, and, further, the choice of deterministic or probabilistic redesign can be made.

The true and corrected analyst-estimated probabilities of failure after the test can then be determined. At this point, the effect of only one possible outcome of the test has been examined. The major steps and equations involved in the simulation of a single outcome of the test are summarized in the pseudocode given in Algorithm 1 [1] .

To determine another possible outcome, the true computational and experimental errors are re-sampled and the process is repeated. Therefore, for n possible outcomes of a future test, we sample n pairs of the errors and true probabilities of failure, n analyst-estimated probabilities of failure after the test, and up to n updated designs. Note that there is a single initial design, but if k of the n cases are re-designed we will end up with up to $k+1$ different designs.

3.5 Illustrative Example

In this example, we compare the probabilities of failure of an ITPS with the dimensions and material properties of probabilistic optimum found in [53]. In that study, the optimum

[1] In the implementation of this algorithm, it is assumed that all analysts performing the test have the same value of r_{test}. Since each analyst accurately measured r_{test},the effect of this assumption is likely to be negligible.

Algorithm 1 Procedure to simulate n possible true computational errors to calculate probability of failure for design d and r, and n possible outcomes of the future test with redesign for a design described by d_{test} and r_{test}. The random variables r_{test} are fixed for the test. The set of samples of r are fixed over the original design and the redesigns.

Sample set of values of random variables r (this set is fixed over the n possible outcomes, and for the original design d and any redesigned d)
Sample n values of e_c and e_x
Calculate $T_{calc}(d, r)$ using computational model and $T_{calc,test}(d_{test}, r_{test})$
Calculate $p_{f,analyst}$ by n samples of e_c and Eqs. (3–6) and (3–7)
for $i = 1 \rightarrow$ n **do**
    Set $e_{c,true} = e_c(i)$ and $e_{x,true} = e_x(i)$
    Calculate $p_{f,true}$ by Eqs. (3–3) and (3–4)
    Calculate $T_{true,test}(d_{test}, r_{test})$ by Eq. (3–2) and T_{meas} by Eq. (3–9)
    if Correction-Factor Calibration **then**
        Calculate $T_{calc,corr}(d, r)$ by Eq. (3–10)
    else if Bayesian Calibration **then**
        Calculate e_{Bayes} by Eqs. (3–12) and (3–13), and e_{extrap} by Eq. (3–17)
        Update $p_{f,analyst-corr}$ by n samples of e_c and Eqs. (3–18) and (3–19)
    end if
    if Deterministic Redesign **then**
        if $\frac{T_{meas}}{T_{calc}(d_{test},r_{test})} < D_L \parallel \frac{T_{meas}}{T_{calc}(d_{test},r_{test})} > D_U$ **then**
            Redesign for $(T_{calc,corr}(d, r))_{redesign} = (T_{calc}(d, r))_{\text{original design}}$
            Update $p_{f,true}$ by Eqs. (3–3) and (3–4)
        end if
    else if Probabilistic Redesign **then**
        if $p_{f,analyst-corr} > p_{f,target} + P_U \parallel p_{f,analyst-corr} < p_{f,target} - P_L$ **then**
            Redesign for $p_{f,analyst-corr} = p_{f,target}$
            Update $p_{f,true}$ by Eqs. (3–3) and (3–4)
            Update $p_{f,analyst-corr}$ by n samples of e_c and Eqs. (3–6) and (3–7)
        end if
    end if
end for

was found with constraints on the maximum bottom face sheet temperature, buckling of the web, and maximum von Mises stress in the webs with the bottom face sheet, web thickness, and foam thickness as the design variables. The failure considered here is exceeding the allowable bottom face sheet temperature T_{allow}. All random variables are normally distributed with the mean and coefficient of variation (CV) shown in Table 3-1.

In this example, we consider uniform distributions of the errors, with the experimental error significantly smaller at $\pm 3\%$ than the computational error at $\pm 10\%$, as shown in Table

Table 3-1. ITPS variables

Variable	Symbol	Nominal	CV(%)
web thickness	t_w	1.77 mm	2.89
bottom face sheet	t_B	7.06 mm	2.89
foam thickness	d_s	71.3 mm	2.89
top face sheet thickness	t_T	1.2 mm	2.89
half unit cell length	p	34.1 mm	2.89
angle of corrugation	θ	80°	2.89
density of titanium[1]	ρ_{Ti}	4429 $\frac{kg}{m^3}$	2.89
density of beryllium[2]	ρ_{Be}	1850 $\frac{kg}{m^3}$	2.89
density of foam	ρ_S	24 $\frac{kg}{m^3}$	0
thermal conductivity of titanium	k_{Ti}	7.6 $\frac{W}{m/K}$	2.89
thermal conductivity of beryllium	k_{Be}	203 $\frac{W}{m/K}$	3.66
thermal conductivity of foam	k_S	0.105 $\frac{W}{m/K}$	2.89
specific heat of titanium	c_{Ti}	564 $\frac{J}{kg/K}$	2.89
specific heat of beryllium	c_{Be}	1875 $\frac{J}{kg/K}$	2.89
specific heat of foam	c_S	1120 $\frac{J}{kg/K}$	2.89

[1] Top face sheet and web material
[2] Bottom face sheet material

3-2. The original estimated probability of failure is 0.12% and the nominal mass per unit area is 35.1 kg/m^2. Since the distributions of the errors are bounded, we remove the possibility of extreme differences between the calculated and experimentally measured values in the simulated the future test. With these values of the errors, in the most extreme case, the temperatures differ by approximately 13%, which occurs when the errors are sampled at opposing bounds of the distribution (e.g. $e_{c,true} = 0.1$ and $e_{x,true} = -0.03$). If normal distributions of the errors were used, this difference can become infinite.

Table 3-2. Distribution of errors

Error	Distribution	Bounds
e_c	Uniform	$\pm 10\%$
e_x	Uniform	$\pm 3\%$

The extrapolation error e_{extrap} is estimated to be 2% when d is changed by $\pm 10\%$ from d_{test}, and varies linearly with change in d.

$$e_{extrap} = 0.02\frac{||d - d_{test}||}{0.1||d_{test}||} \tag{3–20}$$

It is possible to assume other relationships between of the extrapolation error and the distance of d from d_{test}. In Appendix B, we examine the effect of assuming the magnitude of e_{extrap} is quadratic with the change in d.

In this example, we examine the benefits of including a future test by examining several cases that include future tests, one without redesign and one with redesign based on the future test by the process described in Section 3.4. We will examine 10,000 possible future test outcomes (10,000 samples of the errors), and use 10,000 samples of the random variables. Therefore, the true probability of failure is calculated with 10,000 samples each of the response and capacity, whereas the analyst-estimated probability of failure is calculated with 10,000 samples of the capacity and 10,000 of the response by separable Monte Carlo. To reduce the effect of noise, the set of 10,000 random variables was held constant through each of the 10,000 possible future test outcomes.

3.5.1 Future Test without Redesign

Using the 10,000 possible outcomes of the single future test, we can estimate the effectiveness of the Bayesian approach by comparing three cases. In the first case, the analyst accepts T_{calc} as the best estimate of the test article temperature. In the second, the analyst accepts T_{meas}. In the third, the analyst accepts T_{Bayes} where T_{Bayes} is the temperature with the maximum likelihood in the updated distribution . Since this example simplifies the likelihood function (see Section 3.3.2.1) so that the updated distribution is uniform, we take the mean the distribution as T_{Bayes}. We compare the absolute error of each from the true temperature in Table 3-3.

Table 3-3. Comparing absolute true error when using T_{calc}, T_{meas} and T_{Bayes} as the test article temperature

T compared	Mean error (%)	Standard deviation of error (%)
T_{calc}	5.0	2.9
T_{meas}	1.5	0.8
T_{Bayes}	1.3	0.8

These results show that the Bayesian approach provides the analyst with the most accurate estimate of T_{true} for the test article. Accepting T_{meas} results in a slightly increased

error and accepting only the original T_{calc} has the worst error with a mean value of 5%. Table 3-4 shows the in which number of occurrences the comparison temperature is closer to the true temperature compared to another temperature out of the 10,000 possible outcomes It

Table 3-4. Number of occurrences in which the comparison temperature is closer to the true temperature compared to another temperature out of 10,000 possible outcomes

	Comparison Temperature		
	T_{Bayes}	T_{meas}	T_{calc}
	(# of occurrences)		
Better than T_{calc}	8490	8490	–
Better than T_{meas}	1964	–	1507
Better than T_{Bayes}	–	998	1507
Better than all temperatures	1962	997	1507
Equal to T_{calc}	2	2	–
Equal to T_{meas}	7038	–	2
Equal to T_{Bayes}	–	7038	2

was observed that accepting either T_{Bayes} or T_{meas} instead of T_{calc} was better in 8490 cases. Of these cases, T_{Bayes} and T_{meas} were equal in 5531. In the remainder of the 7038 times T_{Bayes} and T_{meas} were equal (1507 cases), accepting T_{calc} was better.

In addition, we can compare the analyst-estimate probability of failure to the true probability of failure. These results are given in Table 3-5. We observe that the mean true probability of failure is equal to that of the original estimated probability of failure before the test. This result is not unexpected as we did not allow redesign, thus preventing any changes in design and thus the probability of failure.

Table 3-5. Probabilities of Failure without Redesign (using Bayesian Correction)

Parameter	Mean	Standard Deviation	Minimum	Maximum
$p_{f,true}$ (%)	0.12	0.39	0	2.00
$p_{f,analyst-corr}$ (%)	0.12	0.27	0	1.93

It is important to note that 8884 out of the 10000 possible outcomes show that the true probability of failure is less than the original estimate of the probability of failure. In fact, the median true probability of failure is zero, and is zero up to the 85th percentile. A summary of the percentiles is shown in Table 3-6.

Table 3-6. Summary of the percentiles of the true probability of failure without redesign

	Percentiles						
	25%	50%	75%	88.8%	90%	95%	97.5%
$p_{f,true}$ (%)	0	0	0	0.15	0.20	1.10	1.80

Based on the large number of true probability of failures that are zero, it would be expected that if redesign were implemented to restore the original estimated probability of failure, most redesigns would increase the probability of failure.

3.5.2 Redesign Based on Test

In this section, we examine the effect of deterministic and probabilistic redesign for the example. These two redesign methodologies are described in Sec. 3.3.4.

3.5.2.1 Deterministic redesign

We chose deterministic redesign to occur when the ratio $\frac{T_{meas}}{T_{calc}(d_{test},r_{test})}$ is greater than 1.05 (unconservative computational model) or less than 0.95 (conservative computational model). We consider one design variable, the foam thickness d_s. This variable was chosen since it has a large impact on the bottom face sheet temperature. The results including deterministic redesign are given in Table 3-7.

Table 3-7. Calibration by the correction factor approach with deterministic redesign.

Parameter	Original	Mean	Standard Deviation	Minimum	Maximum
d_S (mm)	71.3	71.5	1.2	44.8	99.4
mass (kg/m^2)	35.1	35.1	2.8	28.9	41.6
$p_{f,true}$ (%)	0.12	0.0007[12]	0.009	0	0.20

[1] Of the 10000 possible outcomes of the future test, 4964 required redesign. Conservative cases account for 2425 of the redesigns, and unconservative cases account for 2539.

[2] 99.3% of true probability failures are below the mean.

These results show that the true probability of failure is greatly reduced when redesign is allowed. In addition, the standard deviation is also reduced. Since the redesign is symmetric, it does not cause much change in the average mass. The reason for this drastic reduction in probability of failure is the substantial reduction in error that allowed us to redesign all the designs that had a probability of failure above 0.12%. So while the system was

designed for a probability of failure of 0.12%, it ended up with a mean probability of failure of 0.0007%.

However, we note a large standard deviation in d_s, with the minimum and maximum values quite different from the design value of 71.3 mm. In practice, the redesign may not be allowed to be this drastic. Therefore, we also examine the case where the bounds of the redesigned d_s are restricted to $\pm 10\%$ of the original nominal d_S. These results are given in Table 3-8.

Table 3-8. Calibration by correction factor with deterministic redesign, bounds of redesigned d_s restricted to $\pm 10\%$ of original d_s

Parameter	Original	Mean	Standard Deviation	Minimum	Maximum
d_S (mm)	71.3	71.4	0.5	64.1	78.4
mass (kg/m^2)	35.1	35.1	1.2	33.4	36.7
$p_{f,true}$ (%)	0.12	0.0007	0.009	0	0.20

We observe that restricting the bounds of d_S does not change the true probability of failure, and does not cause a significant change in the average mass.

3.5.2.2 Probabilistic redesign

The initial design does not necessarily meet the reliability requirements of the designer. It can be, for example, a candidate design in a process of design optimization. When it comes to probabilistic redesign, one may examine re-design to the mean probability without redesign or to a target probability. Here we assume the latter, and we examine cases where the target redesign probability is $p_{f,target} = 0.01\%$ with and without bounds on d_s. Here, we require redesign to occur when the estimated probability of failure is not within $\pm 50\%$ of the target. We require that all unconservative (dangerous) designs above the 50% threshold be redesign but reject the redesign of overly conservative cases if its mass does not decrease by at least 4.5%. Since only one design variable, the foam thickness, is considered, a decrease in mass can only result from a decrease in foam thickness, which causes an increase in temperature. The results are shown in Table 3-9.

Without bounds on the redesigned d_s, we observe that the analyst-estimated target probability of failure is close to the target of 0.01%. It is also observed that there is a significant reduction in mass (4% reduction) and a reduction in the original mean true probability of failure from 0.12% to 0.003%. The analyst is able to estimate this true probability of failure with reasonable accuracy.

When we include the bounds on d_s, the true probability of failure is unable to converge to the target probability of failure, but there is better agreement between the analyst-estimated probabilities of failure and the true value. This is due to the inclusion of the extrapolation error in the probability of failure in the redesign process. We also observe a 1.7% reduction in mean mass from the original value.

On a final note, we recognize that the large percentage of redesigns is undesirable. This percentage can be greatly reduced by less stringent redesign rules while still having very low probabilities of failure.

3.6 Summary and Concluding Remarks

This study presented a methodology to include the effect of a single future test followed by redesign on the probability of failure of an integrated thermal protection system. Two methods of calibration and redesign based on the test were presented. We observed that the deterministic approach, which represents current design/redesign practices, leads to a greatly reduced probability of failure after the test and redesign, a reduction that usually is not quantified.

The probabilistic approach includes the Bayesian technique for calibrating the temperature calculation and re-design to a target probability of failure. It provides a way to more accurately estimate the true probability of failure after the test. In addition, it allows us to trade weight against performing additional tests.

Though the methodology is presented in the context of a future thermal test and redesign on the ITPS, the methodology is applicable for estimating the reliability of almost any component that will undergo a test followed by possible redesign. Given a computational

model, uncertainties, errors, and redesign procedures, along with the statistical distributions, the procedure of simulating the future test result by Monte Carlo sampling, calibration, and redesign can be readily applied.

This study brought to light many tunable parameters in the test, such as the bounds on the design variables, the target probability of failure for redesign, and the redesign criterion itself. By including these parameters into the optimization, we will not only optimize the design but optimize the test as well. This work is the focus of Ch. 4.

Table 3-9. Calibration by the Bayesian updating approach with probability of failure based redesign ($p_{f,target} = 0.01\%$)

Restriction on redesigned d_s	Parameter	Original	Mean	Standard Deviation	Minimum	Maximum
No bounds	d_S (mm)	71.3	65.3	8.9	47.5	77.7
	mass (kg/m^2)	35.1	33.7	2.1	29.5	36.5
	$p_{f,true}$ (%)	0.12	0.003[12]	0.016	0	0.100
	$p_{f,analyst-corr}$ (%)	0.12	0.007	0.004	0	0.015
Within $\pm 10\%$ of d_{test}	d_S (mm)	71.3	68.8	5.1	64.1	77.7
	mass (kg/m^2)	35.1	34.5	1.2	33.4	36.5
	$p_{f,true}$ (%)	0.12	0.003	0.016	0	0.100
	$p_{f,analyst-corr}$ (%)	0.12	0.003	0.005	0	0.015

[1] Of the 10,000 possible outcomes of the future test, 7835 are redesigned. With the requirement of a 4.5% decrease in mass, 5126 of the 7001 conservative models ($p_{f,analyst} < p_{f,target}$) are redesigned. For unconservative designs, 2709 are redesigned.

[2] 97.4% of true probabilities of failure are below the mean.

CHAPTER 4
ACCOUNTING FOR FUTURE REDESIGN TO BALANCE PERFORMANCE AND DEVELOPMENT COSTS

As seen in the previous chapter, most components undergo tests after they are designed and are redesigned if necessary. Tests help designers find unsafe and overly conservative designs, and redesign can restore safety or increase performance. In general, the expected changes to the performance and reliability of the design after the test and redesign are not considered. In this chapter, we explore how modeling a future test and redesign provides a company an opportunity to balance development costs versus performance by simultaneously designing the design and the post-test redesign rules during the initial design stage. Due to regulations and tradition, safety margin and safety factor based design is common practice in industry as opposed to probabilistic design. In this chapter, we show that it is possible to continue to use safety margin based design, and employ probability solely to select safety margins and redesign criteria. In this study, we find the optimum safety margins and redesign criterion for an integrated thermal protection system. These are optimized in order to find a minimum mass design with minimal redesign costs. We observed that the optimum safety margin and redesign criterion call for an initially conservative design and use the redesign process to trim excess weight rather than restore safety. This would fit well with regulatory constraints, since regulations usually impose minimum safety margins.

4.1 Motivation for Accounting for Future Redesign

The previous chapter described a method to simulate these possible futures including test and redesign, and studied the effect of a single future thermal test followed by redesign on the initial reliability estimates of an integrated thermal protection system (ITPS). Monte Carlo sampling of the assumed computational and experimental errors was used to sample future test alternatives, or the possible outcomes of the future test. Using the future alternatives, the methodology included two methods of calibration and redesign. It was observed that the deterministic approach to calibration and redesign, which acted to restore the original (designed) safety margin, led to a greatly reduced probability of failure after the test

and redesign, a reduction that usually is not quantified. A probabilistic approach was also presented, which provided a way to more accurately estimate the probability of failure after the test, while trading off weight against performing additional tests. Matsumura et al. [68] extended the methodology to include additional failure modes of the ITPS.

In this chapter, we show that modeling future redesign provides a company with the opportunity to trade off development costs (test and redesign) and performance (mass) by designing the initial design criteria and the redesign rules. As regulations and tradition drive companies to use traditional deterministic design with safety margins and safety factors, we limit ourselves to deterministic design and redesign processes. The probabilistic approach can be limited to select safety margins and redesign criteria. This is a two-stage stochastic optimization problem [69], a type of problem which has been studied extensively in the area of process planning under uncertainty [70, 71]. Here, in the first stage, a decision is made about the initial design before the test (i.e., an initial optimum design is found) and then decisions are taken based on the updated information from the test result (i.e., to redesign or not) in the second stage.

The following section of the chapter will provide a brief description of the test problem, the integrated thermal protection system. In Sec. 4.3, the process of test and redesign is described in detail. Section 4.4 provides a detailed description of the uncertainties considered in this study, and Sec. 4.5 describes how these uncertainties are used to obtain a distribution of the probability of failure. In Sec. 4.6, the process of simulating the future test and redesign for a single candidate design is described. An illustrative example is provided in Sec. 4.7.

4.2 Integrated Thermal Protection Shield Description

Figure 4-1 shows the ITPS panel that is studied, which is a corrugated core sandwich panel concept. The design consists of a top face sheet and webs made of titanium alloy (Ti-6Al-4V), and a bottom face sheet made of beryllium. Saffil® foam is used as insulation between the webs. The relevant geometric variables of the ITPS design are also shown

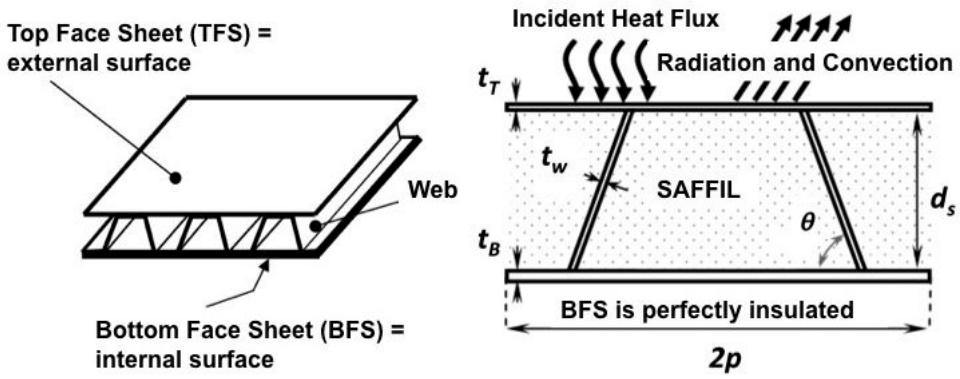

Figure 4-1. Corrugated core sandwich panel ITPS concept

on the unit cell in Figure 4-1. These variables are the top face thickness (t_T), bottom face thickness (t_B), thickness of the foam (d_S), web thickness (t_w), corrugation angle (θ), and length of unit cell ($2p$). The mass per unit area is calculated using Eq.(2–9).

$$m = \rho_T t_T + \rho_B t_B + \frac{\rho_w t_w d_S}{p \sin\theta} \tag{2–9}$$

where ρ_T, ρ_B, and ρ_w are the densities of the materials that make up the top face sheet, bottom face sheet, and web, respectively. In this chapter, the material properties used are the same as listed in Table 3-1, but the density and the thermal conductivity values of the materials are correlated as shown in Table 4-1.

Table 4-1. Correlated random variables

Variable	Correlation Coefficient
density of titanium thermal conductivity of titanium	0.95
density of beryllium thermal conductivity of beryllium	0.95
density of foam thermal conductivity of foam	0.95

In this study, we again consider thermal failure to occur when the temperature of the bottom face sheet exceeds an allowable temperature, and assume that tests of the structure will be conducted to verify the design. Observed data from the test is used to calibrate errors in analytical calculations.

4.3 Analysis and Post-Design Test with Redesign

It is assumed that an analyst has a computational model by which to calculate the change in the temperature of the bottom face sheet of the ITPS, ΔT_{calc}, for a design described by design variables d and random variables r. The randomness is due to variabilities in material properties, manufacturing, and environmental effects. Using ΔT_{calc}, the calculated temperature is defined as

$$T_{calc}(d, r, v_0) = T_0(1 - v_0) + \Delta T_{calc}(d, r) \tag{4–1}$$

where T_0 is the initial temperature of the bottom face sheet, which also has variability represented by v_0.

The design is obtained via a deterministic optimization problem which requires that the calculated temperature be less than or equal to some deterministic allowable temperature T^{det}_{allow} by some a safety margin S_{ini} as shown in Eq.(4–2). Traditionally, the value of this safety margin is determined by regulations and past experience.

$$\begin{aligned} \min_{d=\{t_w, t_B, d_S\}} \quad & m(d) \\ \text{subject to} \quad & T_0 + \Delta T_{calc}(d, r_{nom}) + S_{ini} \leq T^{det}_{allow} \\ & t_{w,L} \leq t_w \leq t_{w,U} \\ & t_{B,L} \leq t_B \leq t_{B,U} \\ & d_{S,L} \leq d_S \leq d_{S,U} \end{aligned} \tag{4–2}$$

Note that for the deterministic design, the random variables are held at the nominal value r_{nom} and the variability in the initial temperature is zero. The subscripts L and U on the design variables represent the lower and upper bounds, respectively. The solution of the optimization problem is denoted as d^*_{ini}.

After the design stage, a test is conducted to verify the chosen design. The test is performed on a test article described by d_{test} (possibly slightly different than d^*_{ini} due to manufacturing tolerances) and r_{test}[1] , and an experimentally measured change in temperature, ΔT_{meas}, is found. For this test design, $\Delta T_{calc}(d_{test}, r_{test})$ and $T_{calc}(d_{test}, r_{test})$ are also calculated.

As a means of calibration, the experimentally measured and calculated temperatures can be used in the form of a correction factor θ for the computational model. That is, the corrected calculated temperature is given as

$$\begin{gathered} T_{calc,corr}(d, r, v_0) = T_0(1 - v_0) + \theta \Delta T_{calc}(d, r) \\ \text{where } \theta = \frac{\Delta T_{meas}}{\Delta T_{calc(d_{test}, r_{test})}} \end{gathered} \tag{4–3}$$

Note that this results in an updated distribution of the corrected-calculated temperature.

Should the test result show that a design is unacceptable, redesign occurs. The criterion for redesign is based on the safety margin of the corrected calculated temperature of the original design. The lower and upper limits of the safety margin of the corrected temperature are represented with S_L and S_U, respectively. This is expressed as

$$\begin{gathered} \text{Redesign if: } S_{corr} = T^{det}_{allow} - (T_0 + \theta \Delta T_{calc}(d^*_{ini}, r_{nom})) < S_L \\ \text{or } S_{corr} = T^{det}_{allow} - (T_0 + \theta \Delta T_{calc}(d^*_{ini}, r_{nom})) > S_U \end{gathered} \tag{4–4}$$

Deterministic redesign is performed so that the corrected calculated temperature of the redesign (with the correction factor) is less than or equal to the allowable temperature by a safety margin S_{re}. This safety margin S_{re} does not necessarily need to be equal to the initial safety margin S_{ini}. Since more information is gained from the test, the designer may choose to design to save weight by reducing the safety margin. This can be formulated into an optimization problem to minimize the mass given a constraint on the corrected calculated

[1] It is assumed that the test article design is accurately measured such that both d_{test} and r_{test} are known, and there is no variability in the initial temperature.

temperature of the new redesign, where the design variables are the geometry.

$$\begin{aligned} \min_{d=\{t_w,t_B,d_S\}} \quad & m(d) \\ \text{subject to} \quad & T_0 + \theta\Delta T_{calc}(d, r_{nom})_{re} + S_{re} \leq T^{det}_{allow} \\ & t_{w,L} \leq t_w \leq t_{w,U} \\ & t_{B,L} \leq t_B \leq t_{B,U} \\ & d_{S,L} \leq d_S \leq d_{S,U} \end{aligned} \tag{4–5}$$

The optimum updated design is denoted d^*_{upd}.

4.4 Uncertainty Definition

As described in Ch. 3 and summarized again here, this study requires the classification of uncertainties. Oberkampf et al. [1] provided an analysis of different sources of uncertainty in engineering modeling and simulation, which was simplified by Acar et al. [2]. We use classification similar to Acar's to categorize types of uncertainty as errors (uncertainties that apply equally to every ITPS) or variability (uncertainties that vary in each individual ITPS). We further describe errors as epistemic and variability as aleatory. As described by Rao et al. [67], the separation of the uncertainty into aleatory and epistemic uncertainties allows more understanding of what is needed to reduce the uncertainty (i.e., using tests to gain more knowledge thereby reducing the error), and trade off the value of the information needed to reduce the uncertainty against the cost of the reduction of the uncertainty.

Variability is modeled as random uncertainties that can be modeled probabilistically. We simulate the variability through a Monte Carlo simulation (MCS) that generates values of the random variables r based on an estimated distribution and calculates the change in bottom face sheet temperature ΔT_{calc}. In addition, we sample the variability v_0 in the initial temperature. This forms the temperature T_{calc} for each sample, generating the probability distribution function. The calculated temperature distribution that reflects the random variability is denoted $f_{calc}(T)$. Additionally, we have variability in the allowable temperature T_{allow}. Note that in Ch. 3, the variability in T_{allow} and v_0 were not included, and we considered

the bottom face temperature rather that that change in temperature. The effect of this different formulation and the additional uncertainties is discussed in Appendix D.

In contrast to variability, errors are fixed for a given ITPS and the true values are largely unknown, so they can be modeled probabilistically as well. We have classified two sources of error, which are described in Table 4-2.

Table 4-2. Description of Errors

Symbol	Description
e_c	computational error due to modeling of the temperature change ΔT_{calc}
e_x	experimental error in measuring ΔT_{meas}

In estimating the temperature of a design, the error must also be considered. As previously described, the calculated temperature distribution $f_{calc}(T)$ of the design reflects random variability. If the true value of the computational error is known, then the true temperature distribution, $f_{true}(T)$, associated with $f_{calc}(T)$ is known, as shown in Fig. 4-2(a). The true temperature still has randomness due to the variabilities.

Since the error is unknown and modeled probabilistically, we instead sample the computational error to create several possible distributions of the true temperature distributions,$f^i_{Ptrue}(T)$ corresponding to the ith sample of e_c. This sampling is illustrated in Fig. 4-2(b) for four samples of e_c. Using the allowable temperature distribution, the probability of failure can be calculated for each sample of the computational error. This forms a distribution of the probability of failure, which is further described in the next section.

4.5 Distribution of the Probability of Failure

The true temperature for a design described by geometric design variables d and random variables r can be defined as

$$T_{true}(d, r, v_0) = T_0(1 - v_0) + (1 - e_{c,true})\Delta T_{calc}(d, r) \tag{4–6}$$

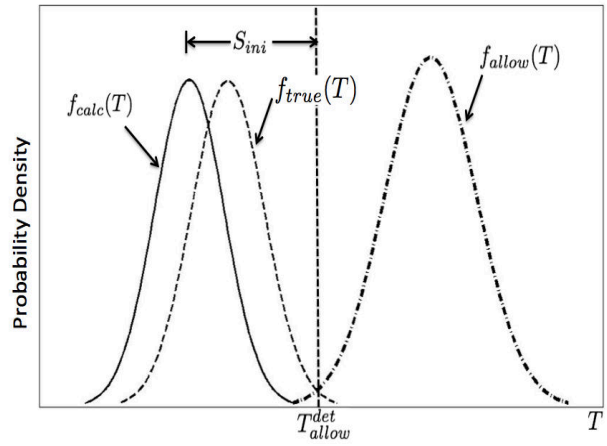

(a) Calculated, true, and allowable temperature distributions

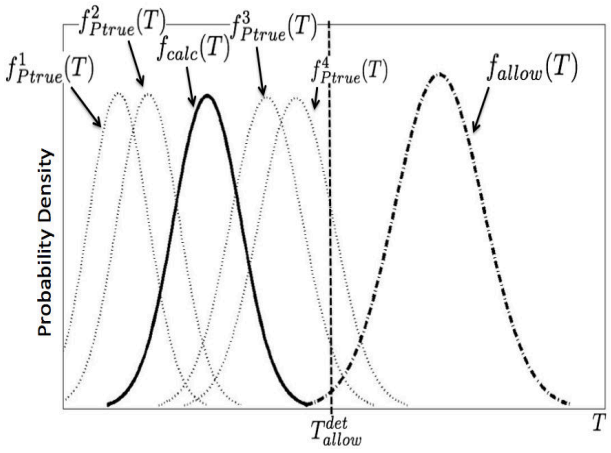

(b) Calculated, allowable, and sampled possible true temperature distributions

Figure 4-2. Example illustrating (a) known calculated and allowable temperature distributions and unknown true distribution, (b) 4 possible true temperature distributions obtained by sampling of 4 values of e_c

The limit state for the probability of failure takes into account the variability in the allowable temperature[2] along with the distribution of the true temperature. The limit state equation g is formulated as the difference between a capacity C and response R as shown in Eq.(4–7).

[2] The absence of the superscript “det” for T_{allow} denotes the allowable temperature with variability to distinguish it from the deterministic allowable temperature T^{det}_{allow}.

$$g_{true} = T_{allow} - T_{true}(d, r, v_0) = C - R \tag{4–7}$$

Using the limit state equation, the probability of failure is calculated using Separable Monte Carlo [28]. The probability of failure p_f is calculated with Eq.(4–8), where M and N are the number of capacity and response samples, respectively. The indicator function I is 1 if the g is less than zero and 0 otherwise.

$$p_f = \frac{1}{MN} \sum_{i=1}^{N} \sum_{j=1}^{M} I[g_{true}(C_j, R_i) < 0] \tag{4–8}$$

As described in the previous section, a distribution of the probability of failure can be formed by sampling the computational error for $e_{c,true}$ and calculating the probability of failure for each sample. Therefore, for n samples of $e_{c,true}$ there are n probability distributions $f_{true}(T)$ from which we can calculate n p_f values. Recall that each sample represents a possible future for the design. From these n values, we can calculate the mean and 95th percentile of the probability of failure. The following section will describe this process of sampling the errors to simulate the future alternatives.

4.6 Simulating Future Processes at the Design Stage

Monte Carlo sampling of the true values of the computational and experimental errors from the assumed error distributions is used to simulate the future test and redesign alternatives for the initial optimum design d^*_{ini}. The steps to simulate a single alternative of the future test with possible redesign, which has been simplified and adapted from Algorithm 1 to fit the work in this chapter, are listed below:

1. Sample set of errors e_c and e_x from assumed distributions (from this, the “before redesign” probability of failure using the e_c sample can be calculated)
2. Use the true e_c and e_x samples to simulate a test result and correction factor θ (Eq.(4–3) with further details in Appendix C)
3. Apply the correction factor based on the test result to ΔT_{calc} (Eq.(4–3))

4. Calculate the safety margin with the corrected temperature and evaluate if redesign is necessary based on S_L and S_U (Eq.(4–4)), then redesign, if necessary (Eq.(4–5))

5. If redesign took place, calculate the mass and probability of failure for this alternative

To simulate another alternative future, the true errors are re-sampled and the process is repeated. For n possible future alternatives, we sample n sets of the errors, and obtain n true probabilities of failure and up to n updated designs (with n mass values). With these n values, we can calculate the mean and 95th percentile of the probability of failure and mass. In how many futures we will need to redesign is determined by the the window defined by S_L, S_U. If a redesign is needed, the updated design will be determined by the choice of safety margin S_{re} required in redesign. Figure 4-3 illustrates how the distribution of $T_{calc,corr}$, probability of failure, and mass changes with redesign for a given S_{ini}, S_{re}, S_L, and S_U for n alternative futures.

If the choice of the safety margin and redesign window lead to k redesigns, the probability of redesign p_{re} is

$$p_{re} = \frac{k}{n} \times 100\% \tag{4–9}$$

Figure 4-4 displays the above process, and the calculation of the mean mass, mean probability of failure, and 95th percentile of the probability of failure of a candidate design, for n alternative futures In this figure, a test is performed from which the correction factor θ is obtained. The corrected safety margin is then used to determine if redesign should be performed based on the redesign criterion. If redesign is required, then the design given the redesign safety margin is found, and the mass and probability of failure are calculated. Otherwise, the original mass of the design and probability of failure is calculated. After this is repeated for the n alternatives (i.e., n θ values), the mean mass, mean probability of failure, and 95th percentile of the probability of failure can be calculated.

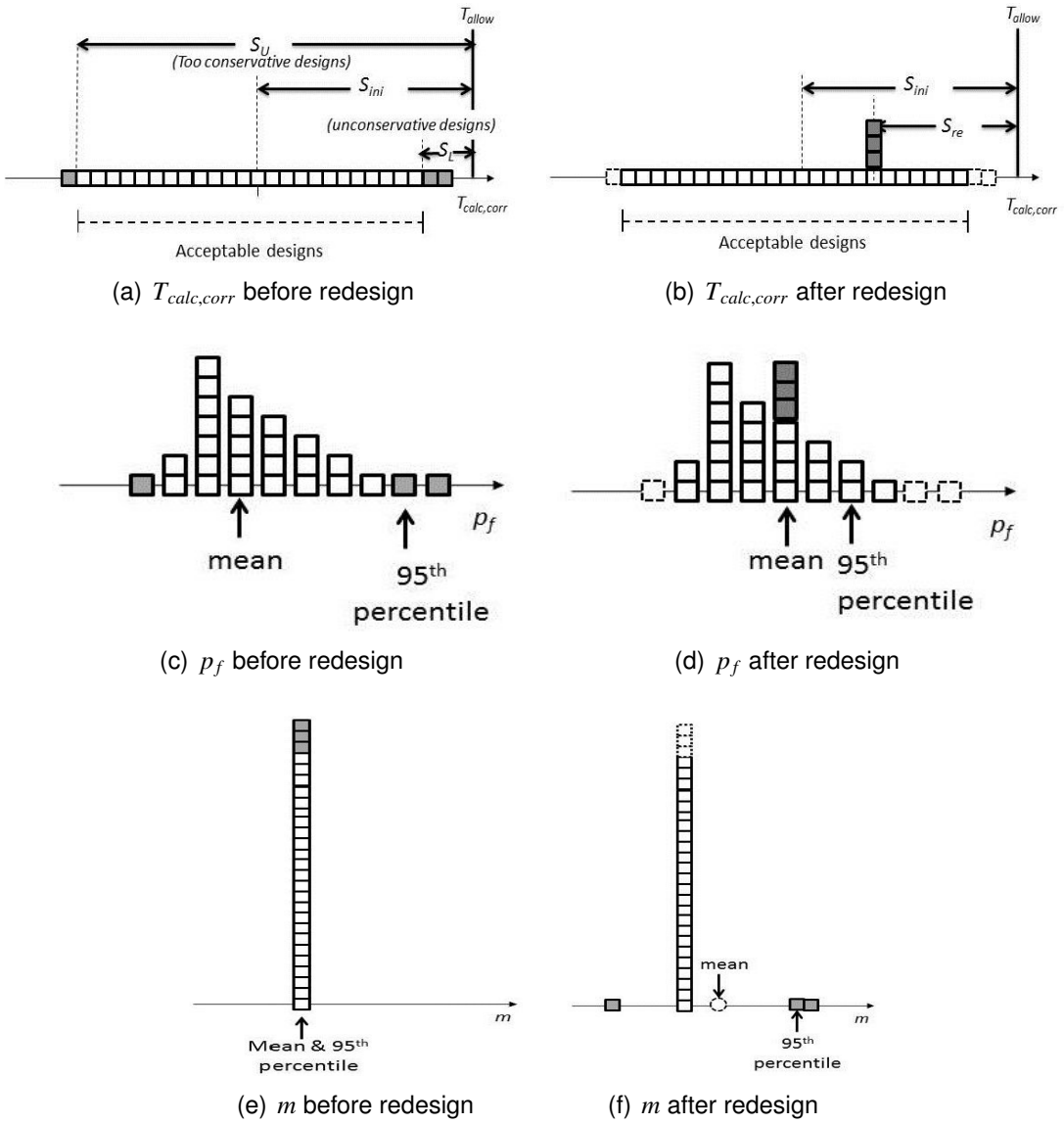

(a) $T_{calc,corr}$ before redesign

(b) $T_{calc,corr}$ after redesign

(c) p_f before redesign

(d) p_f after redesign

(e) m before redesign

(f) m after redesign

Figure 4-3. Illustrative example of before and after redesign distributions of (a)-(b) $T_{calc,corr}$, (c)-(d) probability of failure, and (e)-(f) mass for n alternative futures for a given S_{ini}, S_{re}, S_L, and S_U

4.7 Optimization of the Safety Margins and Redesign Criterion

4.7.1 Problem Description

The process shown in Fig. 4-4 can be thought of as the process that is used by a designer in the design of an ITPS with a given set of safety margins (S_{ini} and S_{re}) and redesign criterion (S_L and S_U), leading to a distribution of the future mass and probability of failure. In this section, we explore how a company may use the probability of failure with

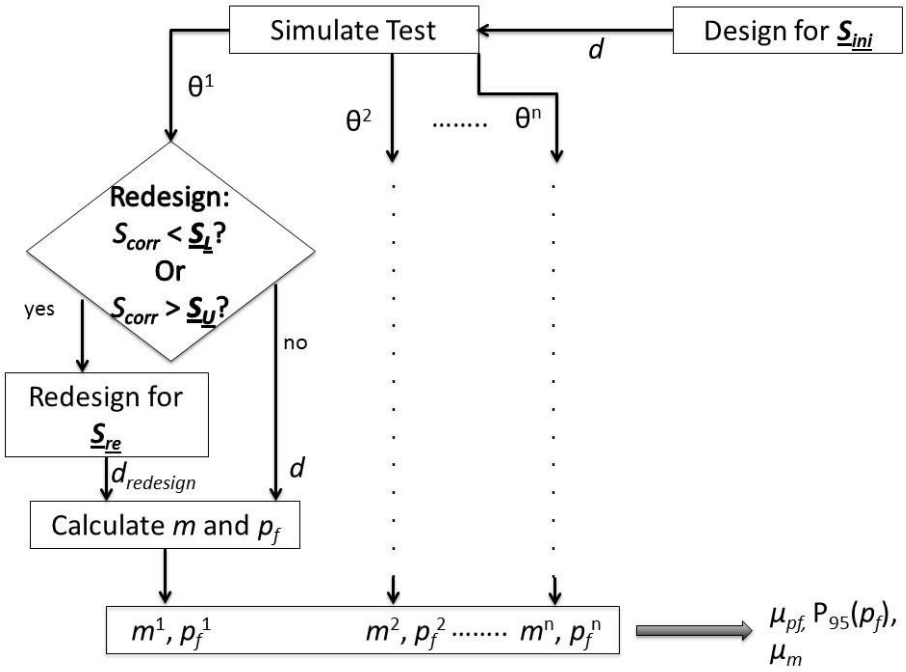

Figure 4-4. Flowchart of the process to calculate the mean mass, mean probability of failure, and 95th percentile of the probability of failure for a candidate design that satisfies the problem in Eq.(4–10) for n future alternatives. Note that the design variables are underlined to show their position in the process.

future redesign to choose the safety margins and redesign criterion to minimize mass and probability of redesign. To do this, we formulate an optimization problem that minimizes the mean mass μ_m and probability of redesign p_{re} subject to constraints on the future mean probability of failure μ_{p_f}, and the 95th percentile of the probability of failure $P_{95}(p_f)$. The design variables are the safety margins and redesign criterion. The formulation is shown in

Eq.(4–10).

$$
\begin{aligned}
\min_{S_{ini},S_L,S_U,S_{re}} \quad & \mu_m, p_{re} \\
\text{subject to} \quad & (\mu_{p_f})_{BeforeRedesign} \leq 0.1\% \\
& (P_{95}(p_f))_{BeforeRedesign} \leq 0.5\% \\
& (\mu_{p_f})_{AfterRedesign} \leq 0.01\% \\
& (P_{95}(p_f))_{AfterRedesign} \leq 0.05\% \\
& 35 \leq S_{ini}, S_{re} \leq 65 \\
& S_{ini} - 35 \leq S_L \leq S_{ini} \\
& S_{ini} \leq S_U \leq S_{ini} + 35 \\
& 1.24mm \leq t_w \leq 1.77mm \\
& 4.94mm \leq t_B \leq 7.06mm \\
& 49.9mm \leq d_S \leq 71.3mm
\end{aligned}
\tag{4–10}
$$

The constraints on S_{ini} and S_{re} restrict the two values to be within the window of 35 to 65 K, and they are not constrained to have equal values. The lower limit is intended to reflect a regulatory mandate, but, just in case, bounds on the before redesign probability of failure are present to prevent designs that are largely unsafe before redesign. The constraints on S_L and S_U restrict the acceptable values of the safety margin after correction to within 35 K of S_{ini}. Note that in this chapter the design and redesign policy is optimized on the basis of a single panel. If an optimization like that is carried out in practice, we assume that compromise values will be used based on similar optimization for several cases.

For this problem, the computational and experimental errors were distributed as described in Table 4-3. Given these distributions, the correction factor θ ranged from 0.85 to 1.15. The distributions of the variables with uncertainty due to variability are provided in Appendix D.

To reduce the computational cost of simulating a future test, surrogates of the mass and reliability index were developed. The reliability index β is related to the probability of failure

Table 4-3. Bounds of computational and experimental errors

Error	Distribution	Bounds
e_c	Uniform	± 0.12
e_x	Uniform	± 0.03

by $p_f = \Phi(-\beta)$, where Φ is the standard normal cumulative density function. For example, for a probability of failure of 0.1%, the reliability index is 3.72. The development of these surrogates is described in Appendix C.

The problem in Eq.(4–10) was solved by forming a cloud of 10,000 points using Latin Hypercube sampling of the design variables S_{ini}, S_L, S_U, and S_{re}. For each set of design variables, 10,000 alternative futures were sampled to obtain the distributions of the mass and probability of failure, and the probability of redesign. The set of points that satisfied the constraints on the probability of failure was found, and, from this set of feasible points, we formed the Pareto front for minimum probability of redesign and mean mass after redesign.

4.7.2 Results

As a point of comparison, we first found the optimum design for minimum mass that satisfied the "before redesign" constraints on the probability of failure. Since redesign was not performed, the only value of interest is S_{ini}. The minimum value of $S_{ini} = 48.9$ K which satisfied the probability constraints of a mean of 0.1% and 95th percentile of 0.5% led to a mass of 24.7 kg/m^2. In addition, we found the minimum S_{ini} design that satisfied the "after redesign" probability of failure constraints without actually performing redesign (i.e., the minimum S_{ini} that satisfied $\mu_{p_f} \leq 0.01\%$ and $P_{95}(p_f) \leq 0.05\%$ without any redesign). In this case, the minimum S_{ini} was 62.5 K for a mass of 25.3 kg/m^3 for $\mu_{p_f} = 0.01\%$ and $P_{95}(p_f) = 0.05\%$. Plots of the probability density of the safety margin after correction (i.e., $S_{corr} = T_{allow} - T_{calc,corr}$) for the $S_{ini} = 48.9$ K and $S_{ini} = 62.5$ K cases are shown in Fig. 4-5.

Figure 4-5 shows the distribution of the corrected safety margins with the two values of S_{ini}. The figure also shows the value of S needed to achieve the desired probabilities of failure ($S_{ini} = 29.7$ K for $\mu_{p_f} = 0.1\%$ in Fig. 4-5(a) and $S_{ini} = 41.3$ K for $\mu_{p_f} = 0.01\%$ in Fig. 4-5(b)) in the absence of epistemic uncertainty. We observed that 79% of S_{corr} values were

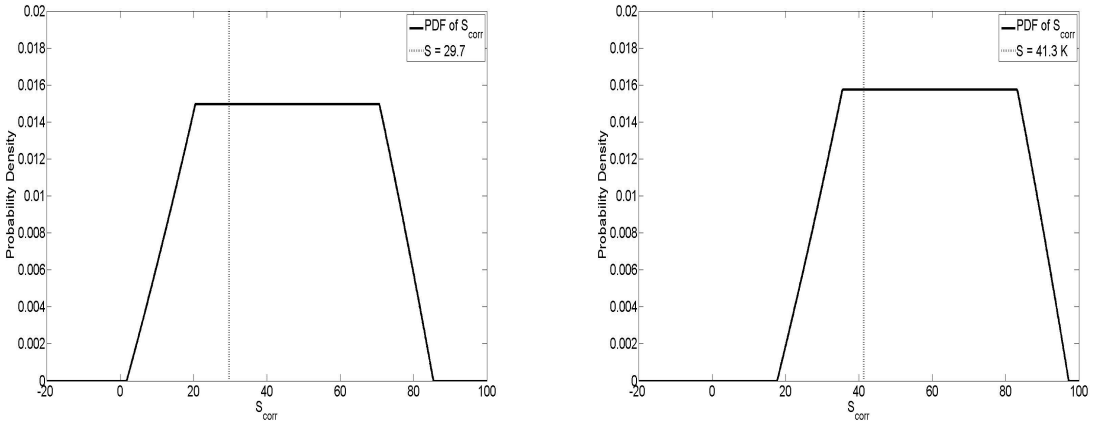

(a) $S_{ini} = 48.9K$ (b) $S_{ini} = 62.5K$

Figure 4-5. Probability density function of the safety margin after correction for (a) $S_{ini} = 48.9K$ which also displays the S_{ini} required in the absence of epistemic uncertainty for a mass of $23.9kg/m^2$ and (b) $S_{ini} = 62.5K$ which also displays the S_{ini} required in the absence of epistemic uncertainty for a mass of $24.3kg/m^2$

greater than 29.7 K for $S_{ini} = 48.9$ K and 84% greater than 62.5 K for for $S_{ini} = 41.3$ K. This was because the mean probability of failure was influenced disproportionally by a few large values as the median probability of failure before redesign was 7.3e-4% for $S_{ini} = 48.9$ K and 3.2e-6% for $S_{ini} = 62.5$ K. The figure caption also notes that the mass required to achieve the desired probability of failure in the absence of epistemic uncertainties was $23.9kg/m^2$ for 0.1% and $24.3kg/m^2$ for 0.01%. With the epistemic uncertainty, we required $25.3kg/m^2$ to compensate for the computational error, and this 1 kg/m^2 or 4% penalty was what can be reduced by more accurate computation or tests.

Allowing redesign, the Pareto front for minimum probability of redesign and mean mass after redesign is displayed in Fig. 4-6 that satisfies the constraints of the problem in Eq.(4–10). We observed reductions in mean mass with increasing probabilities of redesign. The mean mass values after redesign at these points were less than the minimum mass of 25.3 kg/m^3 obtained when redesign was not allowed. At 40% probability of redesign, the mean mass was even less than 24.7 kg/m^3, the mass of the optimum design that

satisfied the relaxed “before redesign” constraints on probability of failure ($\mu_{p_f} \leq 0.1\%$ and $P_{95}(p_f) \leq 0.5\%$).

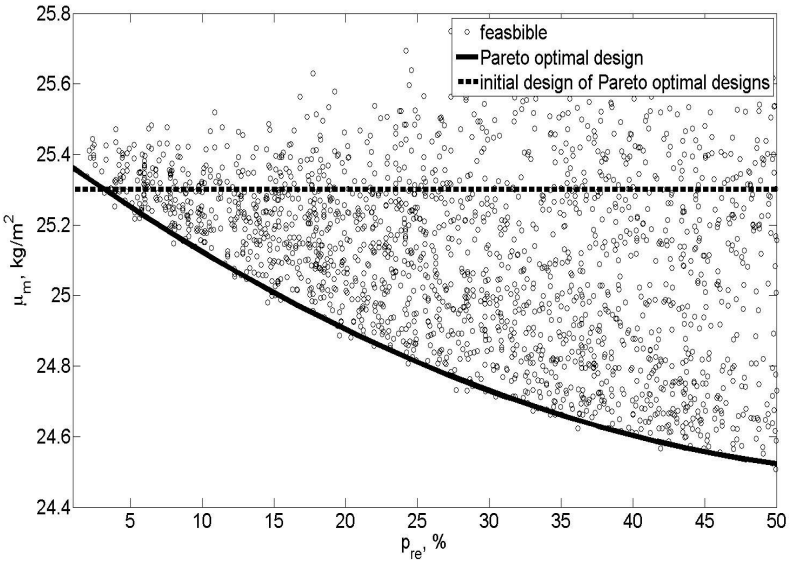

Figure 4-6. Pareto front for minimum probability of redesign and mean mass after redesign. Feasible points in the design space are shown, along with the before-redesign mass of the points on the Pareto front

The values of the safety margins for the designs on the Pareto front are displayed in Fig. 4-7. We observed that the initial safety margin S_{ini} was nearly constant at approximately 63 K. The lower bound of the acceptable safety margin with correction S_L remained between 28 to 32 K, for which the difference from S_{ini} is near the upper bound of 35 K (i.e., the constraint on the lower bound of S_L is active or nearly active). This resulted in the small probability of redesign of unconservative designs. In Fig. 4-8, which shows the percentage of the total probability of redesign that is conservative and unconservative, we observed that this was indeed the case, and that less than 5% of the total probability of redesign was attributed to unconservative redesign for all points on the Pareto front.

For the upper bound on acceptable safety margin with correction S_U, we observed that the values were large (nearly 100 K) but gradually reduced to values near S_{ini} at 65 K. This led to the gradual increase in probability of conservative redesign as the probability of unconservative redesign remained at low values. Thus, the probability of conservative

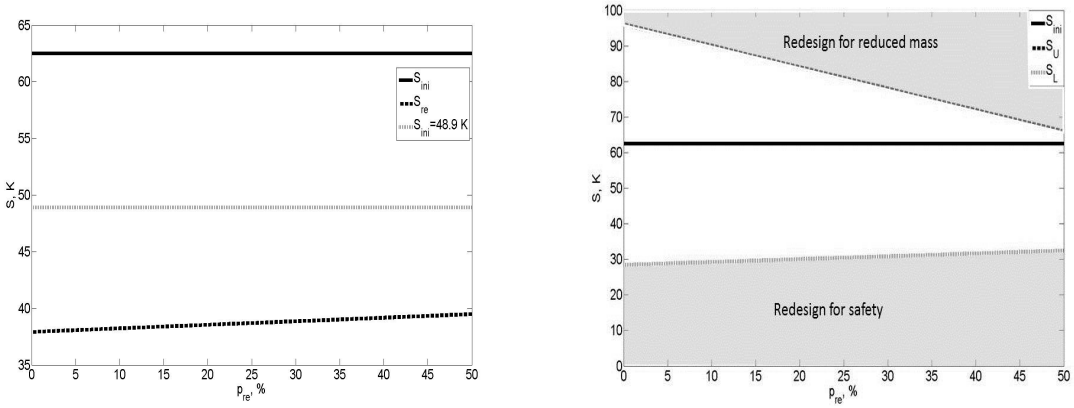

(a) Initial and redesign safety margins (b) Bounds of corrected safety margin

Figure 4-7. For Pareto front for minimum probability of redesign and mean mass after redesign, (a) initial and redesign safety margins versus total probability of redesign and (b) bounds of the acceptable corrected safety margins versus total probability of redesign

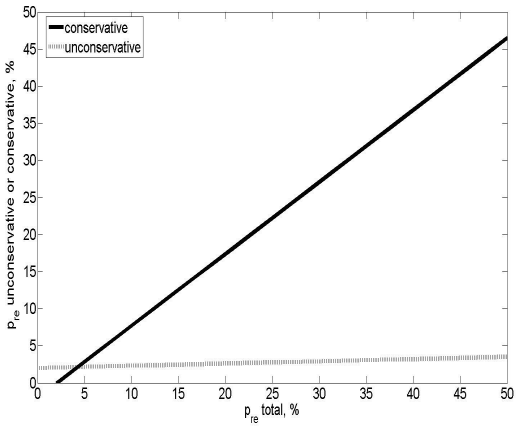

Figure 4-8. Percentage of conservative and unconservative redesigns of the points on the Pareto front

redesign comprised the majority of the total probability of redesign for the designs on the Pareto front. At the same time, we observed that the safety margin S_{re} of the redesign was set to values below S_{ini} and at values less than the minimum value without tests and redesign of 63.5 K. That is, after the test, the redesign has a smaller safety margin than possible for the original design. This value is even less that the safety margin required to satisfy the relaxed before redesign constraints of $S_{ini} = 48.9$ K. The combined effect of

redesigning conservative designs for a reduced safety margin was a reduction in the mean mass while satisfying more stringent constraints on the probability of failure.

The results show that the optimal choice safety margins and redesign criterion can be chosen based on the probability of failure that accounts for future redesign. We observe that companies can benefit by having designers consider conservative safety margins for the initial design, which correspond to the safety margin required to satisfy the probabilistic constraints. The redesign criterion should then mostly result in the redesign of overly conservative designs to trim mass by allowing a smaller safety margin for redesign (because of additional knowledge due to the test in the correction factor), with a few unsafe designs redesigned for safety.

4.7.3 Unconservative Initial Design Approach

While the Pareto optimal designs showed that the initial design should be conservative with redesign performed to trim mass, we examined the trade-off in probability of redesign and mass when starting with an initially unconservative design (i.e., an initial design that does not satisfy the constraints of p_f). In this approach, the designer uses a smaller safety margin to achieve a minimal weight design, relying on the test and redesign to correct any dangerous designs. In this problem, the initial safety margin was fixed at 48.9 K (corresponding to a mass of 24.7 kg/m^2) and the remaining safety margins (S_{re}, S_L, and S_U) were the design variables. The same constraints as in Eq.(4–10) were used. Figure 4-9 displays the Pareto front found with the unconservative approach, and compares the result to the previously found results that used a conservative-first approach found in Sec. 4.7.2.

It was observed that to meet the probability of failure requirements, the probability of redesign was at least 27% for the unconservative approach with $S_{ini} = 48.9$ K. That is, the designer must accept at least a 27% probability of redesign, which would lead to a mean mass of approximately 25.2 kg/m^2. This value of the mass is only 0.4% smaller than the initial mass required to satisfy the probability constraints without redesign with the initially conservative design.

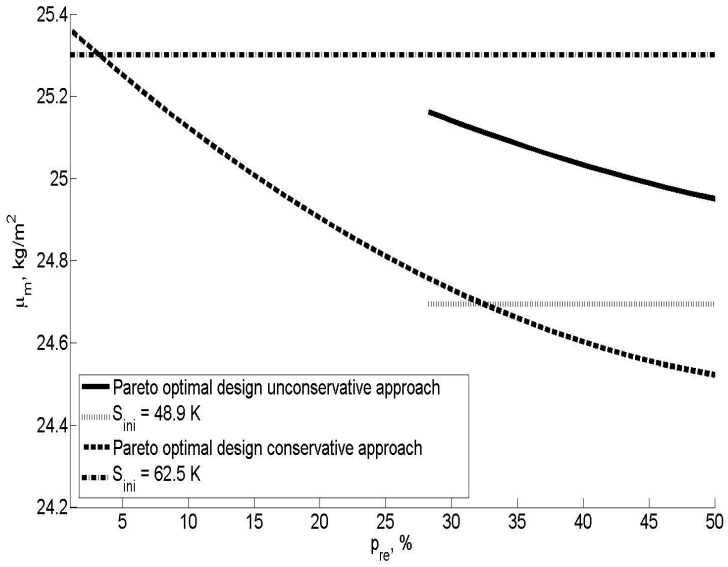

Figure 4-9. Pareto front showing the Pareto front found for the unconservative approach (with $S_{ini} = 48.9$ K) in comparison to the Pareto front with the conservative approach (with $S_{ini} = 62.5$ K)

.

Figure 4-10 displays the values of the design variables of the Pareto optimal solutions, and Fig. 4-11 displays the breakdown of the total probability of redesign due to conservative and unconservative designs. It was observed that redesign was primarily performed to increase safety at the smallest probabilities of redesign (27%), increasing the redesign of conservative designs with increasing probability of redesign.

The histogram of the mass for 10,000 alternative futures after redesign is displayed in Fig. 4-12(a). The approximately 2% increase in the mean mass after redesign is attributed to the large probabilities of failure associated with redesign of unconservative designs. A breakdown of the alternative futures that resulted in the mean mass is shown in Table 4-4. It was observed that the redesign of unconservative designs resulted in a increase of 8% in the mean mass.

In contrast, the same mean mass of 25.2 kg/m^2 after redesign can be achieved with the conservative-first approach with a probability of redesign around 8%, and for a probability of redesign of 27%, the mean mass is nearly 24.7 kg/m^2. In this case, the reduction in mean

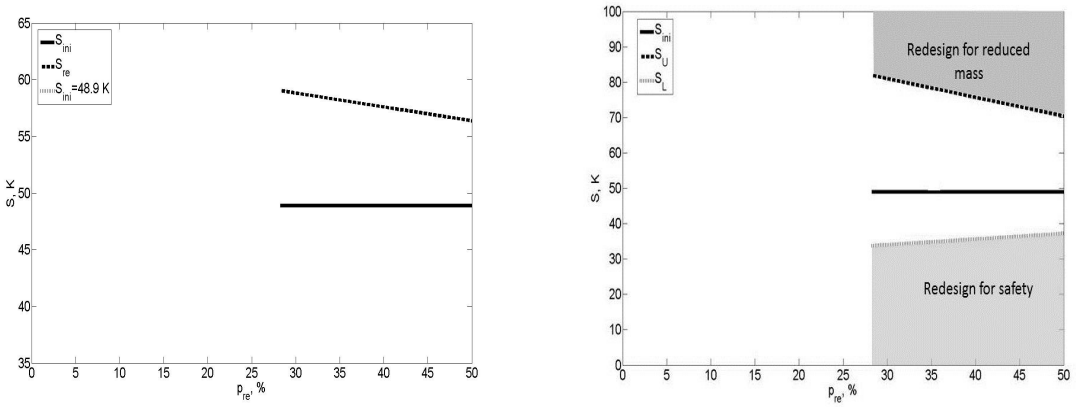

(a) Initial and redesign safety margins

(b) Bounds of corrected safety margin

Figure 4-10. For Pareto front for minimum probability of redesign and mean mass after redesign with the unconservative-first approach, (a) initial and redesign safety margins versus total probability of redesign and (b) bounds of the acceptable corrected safety margins versus total probability of redesign

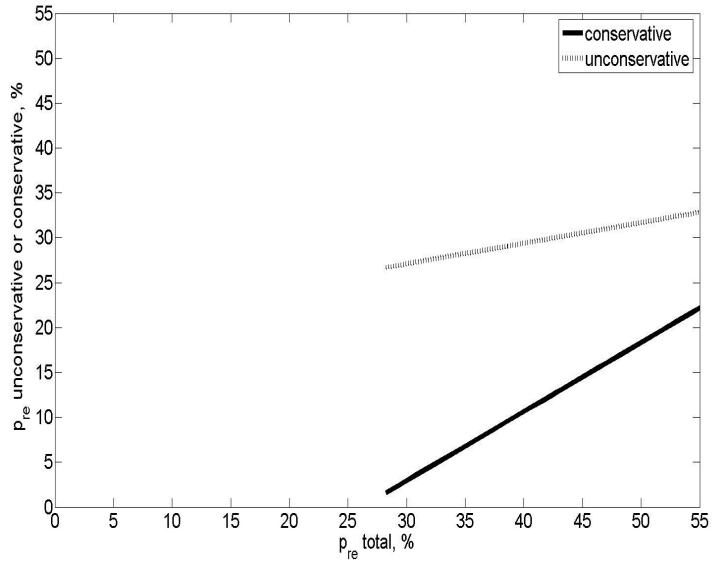

Figure 4-11. Percentage of conservative and unconservative redesigns of the points on the Pareto front with the unconservative-first approach

mass is due to large reductions in mass in the cases that required redesign of conservative designs. The histogram of the mass for 10,000 alternative futures is shown in Fig. 4-12(b) and the mass and probability of redesign is detailed in Table 4-4. It was observed that the redesign of overly conservative designs resulted in a 10% reduction in the mean mass.

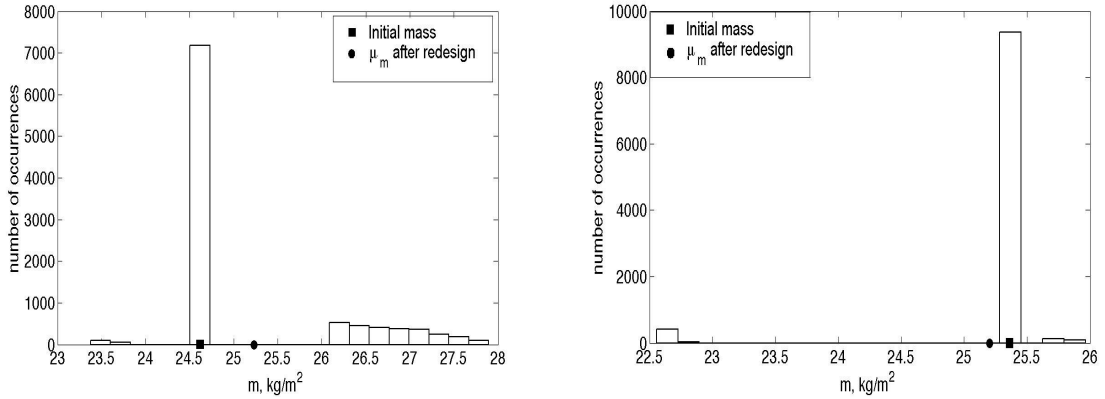

(a) Initially Unconservative (b) Initially Conservative

Figure 4-12. Histograms of mass after redesign for 10,000 alternative futures for (a) initially unconservative design with 27% probability of redesign and (b) initially conservative design with 8% probability of redesign.

Table 4-4. Breakdown of alternative futures for the unconservative initial design with 27% probability of redesign and conservative initial design with 8% probability of redesign

Outcome	p_{re} (%)	Mean Mass (kg/m^2)
Initially Unconservative		
No redesign	73	24.7
Unconservative	25.5	26.8
Conservative	1.5	23.5
Total		25.2[1]
Initially Conservative		
No redesign	93.5	25.3
Unconservative	2.1	25.8
Conservative	4.4	22.7
Total		25.2[1]

1 Calculated as $p_{noredesign}m_0+(p_{re}\mu_m)_{conservative}+(p_{re}\mu_m)_{unconservative}$

Comparing this value along with the 8% increase in mass seen in the initially unconservative case, we observed that the change in mass due to redesign is much larger than the 2% difference in mass of the two initial designs. However, with the initially conservative design most redesigns act to reduce the mass, whereas the mass is mostly increased in the initially unconservative redesign cases. Therefore, the designer has a choice:

1. use a smaller initial safety margin for an initially small mass and accept a 27% probability of redesign that will increase the mass, or

2. use a larger initial safety margin for an initially larger mass that can achieve less than or equal to the same mass with probabilities of redesign greater than 8%.

If the test shows the component does not have to be redesigned, there would be a nearly 2% mass penalty in using the conservative safety margin.

4.7.4 Discussion

Using the minimal safety margin for the initial design can be thought of as using safety margins given by regulatory agencies, which provide minimum values of safety margins and safety factors. For example, the Federal Aviation Administration has recommended minimum design and test factors for structures on reusable launch vehicles [72]. In this work, the values of S_{ini} (and S_{re}) of 35 K may be the minimum value imposed by an agency, and the value of 48.9 K may be the current minimum value imposed by a company based on history or experience. The results presented in the chapter show that a company may have an incentive to impose their own safety margins, and set the design and redesign rules to balance development costs. The results in Sec. 4.7.2 showed that probabilistic constraints can be satisfied by first using a conservative safety margin and accepting a risk of increased development cost through increased redesign to trim excess mass. This directly contrasts the approach of using minimal safety margin values and redesigning based on the test result to increase safety. Considering the possible future redesign and its cost allows the company to make better decisions at the design stage.

4.8 Summary and Discussion on Possible Future Research Directions

In this chapter, we used the modeling of future redesign to provide a way of balancing development costs (test and redesign costs) and performance (mass) by designing the design and redesign rules. We observed that the presence of epistemic uncertainty led to a mass penalty, which could be reduced by a test and redesign. Since deterministic design employing safety margins and safety factors is common practice in industry, we showed that safety margins and redesign criteria can be chosen using the probability of failure with

future redesign. A study on an integrated thermal protection system showed that a minimum mass design that satisfied probabilistic constraints can be achieved by having an initially conservative design and a redesign criterion such that redesign is mainly performed on overly conservative designs to trim excess mass. In contrast, we examined the trade-off in starting with an initially small safety margin, which may be a minimum value recommended by a regulatory agency, and using the test and redesign to correct dangerous designs. Therefore, in this example, a company would have an incentive to use conservative safety margins at the initial design stage, while increasing performance by implementing a redesign criterion aimed at discovering overly conservative designs. This also provides a balance between probabilistic design and the more traditional deterministic approach.

Possible future research includes considering the uncertainty reduction methods that often take place after a component is designed but before a component is tested. For example, lower fidelity methods may be used to find a starting point for the initial design. Before a design is tested, it may be better characterized through higher fidelity modeling or optimization in a smaller design space about this design. Both the higher fidelity modeling and re-optimization can reduce the uncertainty in the design before a test is even performed. Therefore, a study that models these actions and considers the subsequent uncertainty reduction would be useful in finding the optimal balance in design and development costs and performance.

CHAPTER 5
DYNAMIC DESIGN SPACE PARTITIONING FOR LOCATING MULTIPLE OPTIMA: AN AGENT-INSPIRED APPROACH

In this chapter, we explore the use of design space partitioning to tackle optimization problems in which each point is expensive to evaluate and there are multiple local optima. The overarching goal of the method presented is to locate all local optima rather than just the global one. Locating multiple designs provides insurance against discovering that late in the design process a design is poor due to modeling errors or overlooked objectives or constraints. The proposed strategy to locate multiple candidate designs dynamically partitions the search space among several “agents” that approximate their sub-region landscape using surrogates. Agents coordinate by exchanging points to form an approximation of the objective function or constraints in the sub-region and by modifying the boundaries of their sub-regions. Through a self-organized process of creation and deletion, agents adapt the partition as to exploit potential local optima and explore unknown regions. This idea is demonstrated on a six-dimensional analytical function, and a practical engineering example, the design of an integrated thermal protection system.

As part of a history on this research, the idea of working in partitioned designs spaces was born out of an idea to decompose the problem among several agents, which act to solve their own sub-problems and coordinate to solve the global problem. Combined with the idea of solving these sub-problems cheaply, we then turned to the use of surrogates to approximate expensive objective functions or constraints. Thus, we developed a methodology, presented in this chapter, in which an agent uses its own local surrogate to solve the sub-problem in its sub-region. The goal was to limit the amount of information shared between the agents, where each agent would find the best solution in its region. Later on, as presented in the next chapter, we explored the effectiveness of using local surrogates rather than global surrogates and also the use of partitions rather than starting optimization runs from different points of the design space.

5.1 Motivation and Background on Locating Multiple Optima

Many contemporary applications can be modeled as distributed optimization problems (ambient intelligence, machine-to-machine infrastructures, collective robotics, complex product design, etc.). Optimization processes iteratively choose new points in the search space and evaluate their performances until a solution is found. However, a practical and common difficulty in optimization problems is that the evaluations of new points require expensive computations. For instance, if one wants to compute a property of a complex object (e.g. large deflections of an aircraft wing under some loading), a high fidelity computation (e.g. finite element analysis) may be required. Therefore, many researchers in the field of optimization have focused on the development of optimization methods adapted to expensive computations. The main ideas underlying such methods are often the use of surrogates, problem decomposition, and parallel computation. The use of surrogates to replace expensive computations and experiments in optimization has been well documented [40–43]. Moreover, in optimization, a common way to decompose problems is to partition the search space [73, 74]. Furthermore, to take advantage of parallel computing, many have proposed strategies for using multiple surrogates in optimization [9–12]. The goal of most of these algorithms is to locate the global optimum, while trying to minimize the number of calls to the expensive functions. Like these algorithms, we try to reduce the number the number of calls to the expensive functions, but our main goal is to locate multiple optima as multiple candidate designs. For real-world problems, the ability to locate many optima in a limited computational budget is desirable as the global optimum may be too expensive to find, and because it provides the user with a diverse set of acceptable solutions as insurance against late formulation changes (e.g., new constraints) in the design process.

Besides the aforementioned techniques for distributing the solving process, multi-agent optimization is an active research field proposing solutions for distinct agents to cooperatively find solutions to distributed problems [75]. They mainly rely on the distribution (and decomposition) of the formulation of the problem. Generally, the optimization framework

consists of distributing variables and constraints among several agents that cooperate to set values to variables that optimize a given cost function, like in the DCOP model [14]. Another approach is to decompose or transform problems into dual forms that can be solved by separate agents [15] (for problems with specific properties, such as linearity).

Here, we describe a multi-agent method in which the search space is dynamically partitioned (and not the problem formulation) into sub-regions in which each agent evolves and performs a surrogate-based continuous optimization. The novelty of this approach comes from the joint use of (*i*) surrogate-based optimization techniques for expensive computation and (*ii*) self-organization techniques for partitioning the search space and finding all the local optima. Coordination between agents, through exchange of points and self-organized evolution of the sub-region boundaries allows the agents to stabilize around local optima. Like some nature-inspired niching methods [76, 77], such as particle swarm [78–80] and genetic algorithms [81, 82], or clustering global optimization algorithms [83], our goal is to locate multiple optima, but unlike these algorithms, our approach aims to sparingly call the true objective function and constraints. Our multi-agent approach further (i) uses the creation of agents for exploring the search space and, (ii) merges or deletes agents to increase efficiency.

Additionally, the use of surrogates combined with partitioning of the design space allows us to take advantage of local search methods by aiming to optimize using the surrogate predictions rather than the true functions. Here, we propose a methodology that aims to first exploit the surrogate prediction (i.e., by seeking first to minimize the function) and only explore when no points that lead to further improvements can be found. Thus, in this method we do not aim to explicitly balance exploitation versus exploration iterations as with most global optimization algorithms, but instead primarily exploit, and explore through design space partitioning and the occasional addition of space filling points.

In the following section, we discuss more deeply the motivation for multiple candidate designs. Next, we provide some background on surrogate-based optimization. In Sec. 5.4,

we describe the autonomous agents that perform the cooperative optimization process. In Sec. 5.5, we present the methods of space partitioning and point allocation that are intended to distribute local optima among the partitions while maximizing the accuracy of the surrogate in a self-organized way – through agent creation and deletion. In Sec. 5.6 a six-dimensional problem is tackled using our multi-agent optimizer, and in Sec. 5.7 a practical engineering example, the design of an integrated thermal protection system, is presented.

5.2 Motivation for Multiple Candidate Designs

In optimization courses, we often tell students that defining an optimization problem properly is the most important step for obtaining a good design. However, even experienced hands often overlook important objective functions and constraints. There are also epistemic uncertainties, such as modeling errors, in the objective functions and constraints definitions that will typically perturb their relative values throughout the design space. In one case, Nagendra et al. [81] used a genetic algorithm to find several structural designs with comparable weight and identical load carrying capacity. However, when three of these designs were built and tested, their load carrying capacity was found to differ by 10%. For such reasons, alternative local optima may be better practical solutions to a given optimization problem than a single idealized global optimum. As advances in computer power have made it possible to move from settling on local optima to finding the global optimum, when designing engineering systems. This usually requires search in multiple regions of design space, expending most of the computation needed to define multiple alternate designs. Thus, focusing solely on locating the best design may be wasteful.

In engineering design, the simulated behavior of objective functions and constraints usually has modeling error, or epistemic uncertainty, due to the inability to perfectly model phenomena. Modeling errors can degrade local optima or even cause them to disappear.

Let us now turn to a practical engineering design example to demonstrate the presence, diversity, and fragility of candidate designs. Large portions of the exterior surface of many space vehicles are devoted to providing protection from the severe aerodynamic heating

experienced during ascent and atmospheric reentry. A proposed integrated thermal protection system (ITPS) provides structural load bearing function in addition to its insulation function and in doing so provides a chance to reduce launch weight. Figure 5-1 displays the corrugated-core sandwich panel concept of an ITPS, which consists of top and bottom face sheets, webs, and insulation foam between the webs and face sheets.

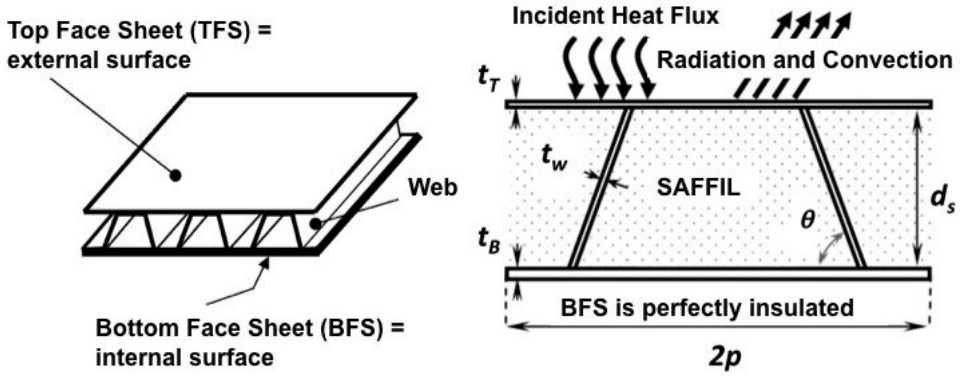

Figure 5-1. Integrated thermal protection system provides both insulation and load carrying capacity, and consequently can lead to alternative optima of similar mass but different way of addressing the thermal and structural requirements.

The thermal and structural requirements often conflict due to the nature of the mechanisms that protect against the failure in the different modes. For example, thin webs prevent the flow of heat to the bottom face but are more susceptible to buckling and strength failure. A reduction in foam thickness (panel depth) improves resistance against buckling of the webs but increases heat flow. A thick bottom face sheet acts as a heat sink and reduces the temperature at the bottom face but increases stress in the web.

These conflicts may be resolved by candidate designs in different ways. Figure 5-2 displays the infeasible and feasible regions with constraints on the temperature of the bottom face sheet and stress in the web for the three-dimensional example, in which the web, bottom face, and foam thicknesses were the design variables.

Three islands of feasibility are observed, in which the design is driven to protect against different failure modes. The two minimum mass designs are in Regions 1 and 2. In Region 1, the failure is primarily from stress, because the webs are thin. This is compensated by

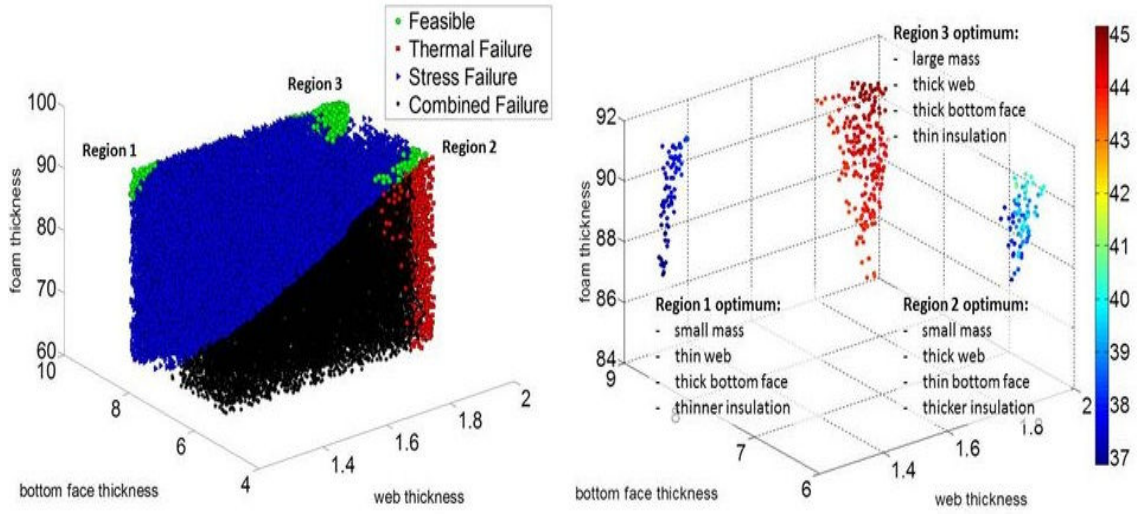

Figure 5-2. Feasible regions 1-3 and infeasible regions (left) and mass objective function represented by color (right). The two competitive optima in Regions 1 and 2 rely on different concepts. In Region 1 the thermal function is satisfied by a thick bottom face sheet acting as heat sink, while in Region 2 it is satisfied by thick insulation.

reducing the length of the web by reducing the foam thickness, and to compensate for the increase heat flow, the bottom face sheet is increased to provide a larger heat sink. In Region 2, both failure modes are present, so that the insulation is thicker to prevent thermal failure and the bottom face is thinner to reduce stress in the web. With both feasible regions being rather narrow, modeling errors can easily wipe out one of these regions, so that having both designs provides valuable insurance. Furthermore, even if modeling errors do not wipe out Region 2 but only narrow it, this can result in substantial increase in mass, while Region 1 is more robust.

This example demonstrates the benefit of multiple candidate designs due to the fragility designs from errors. In the following sections, the dynamic design space partitioning algorithm is described, and a six dimensional analytical example is presented before returning to the ITPS example in Sec. 5.7.

5.3 Surrogate-Based Optimization

A surrogate is a mathematical function that (i) approximates outputs of a studied model (e.g. the mass or the strength or the range of an aircraft as a function of its dimensions), (ii) is of low computation cost and (iii) aims at predicting new outputs [84]. The set of initial candidate solutions, or points, used to fit the surrogate is called the design of experiments (DOE). Known examples of surrogates are polynomial response surface, splines, neural networks or kriging.

Let us consider the general formulation of a constrained optimization problem,

$$\begin{aligned} \underset{x \in \mathcal{S} \subset \mathcal{R}^n}{\text{minimize}} \quad & f(x) \\ \text{subject to} \quad & g(x) \leq 0 \end{aligned} \tag{5–1}$$

In surrogate-based optimization, a surrogate is built from a DOE, denoted by $\mathbb{X}$ that consists of sets of the design variables x. For the design of experiments, there are the calculated values of the objective function f and constraints g that are associated with the DOE, which we denote as $\mathbb{F}$ and $\mathbb{G}$, respectively. We will refer to $\mathbb{X}$ and its associated values of $\mathbb{F}$ and $\mathbb{G}$ as a database.

The database is used to construct the surrogate approximation of the objective function $\hat{f}$ and the approximation of the constraint $\hat{g}$. We can approximate the problem in Eq.(5–1) using the surrogates and formulate the problem as

$$\begin{aligned} \underset{x \in \mathcal{S} \subset \mathcal{R}^n}{\text{minimize}} \quad & \hat{f}(x) \\ \text{subject to} \quad & \hat{g}(x) \leq 0 \end{aligned} \tag{5–2}$$

The solution to this approximate problem is denoted $\hat{x}^*$.

Surrogate-based optimization calls for more iterations to find the true optimum, and is therefore dependent on some iteration time t. That is, after the optimum of the problem in Eq.(5–2) is found, the true values $f(\hat{x}^*)$ and $g(\hat{x}^*)$ are calculated and included in the DOE along with $\hat{x}^*$. At the next iteration, the surrogate is updated, and the optimization is

performed again. Therefore, we denote the DOE at a time t as $\mathbb{X}^t$ and the associated set of objective function values and constraint values as $\mathbb{F}^t$ and $\mathbb{G}^t$, respectively. The surrogate-based optimization procedure is summarized in Algorithm 2 (which also refers to a global optimization procedure in Algorithm 3).

Algorithm 2 Overall surrogate-based optimization

t = 1 (initial state)
while $t \leq t^{max}$ **do**
    Build surrogates $\hat{f}$ and $\hat{g}$ from $(\mathbb{X}^t, \mathbb{F}^t, \mathbb{G}^t)$
    Optimization to find $\hat{x}^*$ (see Algorithm 3)
    Calculate $f(\hat{x}^*)$ and $g(\hat{x}^*)$
    Update database $(\mathbb{X}^t, \mathbb{F}^t, \mathbb{G}^t) \cup (\hat{x}^*, f(\hat{x}^*), g(\hat{x}^*))$
    $t = t + 1$
end while

Algorithm 3 Constrained optimization procedure

Input: $\hat{f}, \hat{g}, \mathbb{X}^t, \mathcal{L}$
Output: $\hat{x}^*$
$\hat{x}^* \leftarrow \underset{x \in \mathcal{L}}{\text{argmin}} \hat{f}(x)$ subject to $\hat{g}(x) \leq 0$
if $\hat{x}^*$ is near $\mathbb{X}^t$ or out of the search domain $\mathcal{L}$ **then**
    $\hat{x}^* \leftarrow \underset{x \in \mathcal{S}}{\text{argmax}}$ distance$(\mathbb{X}^t)$
end if

5.4 Agent Optimization Behavior

As stated in the introduction, our approach consists in splitting the space in sub-regions and assigning agents to each of these sub-regions as presented in Fig. 5-3. Therefore, Algorithm 6 can be thought of as the procedure followed by a single agent to find one point, that will be repeating until termination. However, in the multi-agent approach we describe here, each agent is restricted to only a sub-region of the design space, i.e., $\mathcal{S}$ is replaced by a part of $\mathcal{S}$. The rationale behind this idea is that each agent has an easier optimization subproblem to solve because it searches a smaller space, which we denote as $\mathcal{P}_i$ for the ith agent, and considers a simpler function. Each agent must consider only the points in its sub-region, which are available in its internal database $(\mathbb{X}^t, \mathbb{F}^t, \mathbb{G}^t)_i$. The sub-region of an agent is defined by the position of its center c. A point in the space belongs to the sub-region with

the nearest center, where the distance is the Euclidean distance. This creates sub-regions that are Voronoi cells [85]. The choice of where to place the center is discussed in the next section. Figure 5-3 illustrates the partition of a two-dimensional space into four sub-regions for four agents, which requires four centers. In this example, we place the centers randomly. space partitions will be discussed in Section 5.5.

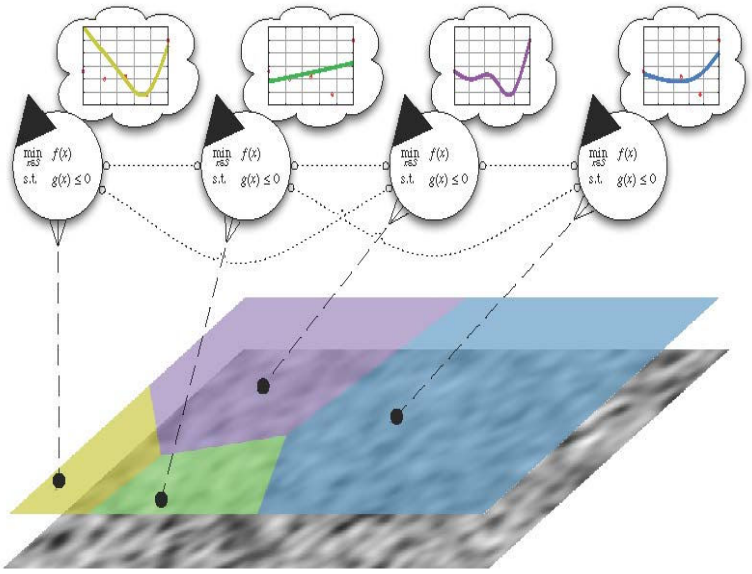

Figure 5-3. Multi-agent System overview: agents perform surrogate-based optimization in different sub-regions of the partitioned search space based on personal surrogates (dashed l.) and exchange points with their direct neighbors (dotted l.)

The procedure of a single agent is given in Algorithm 4. Assuming that sub-regions are defined, each agent fits several surrogates it knows (as many different ways to approximate) and chooses the one that maximizes the accuracy in its sub-region (line 5-9). To avoid ill-conditioning, if more points are needed than are available to an agent, the agent asks neighboring agents for points. The neighboring agents then communicate the information associated with these points (lines 6–8). We define the best surrogate as the one with the minimum cross-validation error, the partial prediction error sum of squares $PRESS_{RMS}$. This is found by leaving out a point, refitting the surrogate, and measuring the error at that point. The operation is repeated for p points in the agent's sub-region (disregarding any points received from other agents) to form a vector of the cross-validation errors e_{XV}. The value of

$PRESS_{RMS}$ is then calculated by

$$PRESS_{RMS} = \sqrt{\frac{1}{p} e_{XV}^T e_{XV}} \tag{5–3}$$

Algorithm 4 Agent i optimization in its sub-region.

1: t = 1 (initial state)
2: **while** $t \leq t^{max}$ **do**
3: Update $\mathcal{P}_i = \{x \in \mathcal{S} \text{ s.t.} \|x - c_i\|^2 \leq \|x - c_j\|^2 \ , \ j \neq i\}$
4: Update internal database from the new space partition
5: Build surrogates $\hat{f}$ and $\hat{g}$ from $(\mathbb{X}^t, \mathbb{F}^t, \mathbb{G}^t)_i$
6: **if** Not sufficient number of points in internal database to build a surrogate **then**
7: Get points from other agents closest to c_i
8: Build surrogates
9: **end if**
10: Choose best surrogate based on partial $PRESS_{RMS}$ error
11: Optimization to find $\hat{x}^*$ [with Algorithm 3 $(\hat{f}, \hat{g}, \mathbb{X}^t, \mathcal{P}_i)$]
12: Calculate $f(\hat{x}^*)$ and $g(\hat{x}^*)$
13: $(\mathbb{X}^{t+1}, \mathbb{F}^{t+1}, \mathbb{G}^{t+1})_i \leftarrow (\mathbb{X}^t, \mathbb{F}^t, \mathbb{G}^t)_i \cup (\hat{x}^*, f(\hat{x}^*), g(\hat{x}^*))$
14: Update center c_i (see Section 5.5.1)
15: Check for merge, split or create (see Section 5.5.2)
16: $t = t + 1$
17: **end while**

Once the agents have chosen surrogates (line 10), the optimization is performed to solve the problem in Eq.(5–2) inside the sub-region (line 11). If the optimizer gives an infeasible point (i.e., the point does not satisfy the constraint in Eq.(5–2) or is out of the sub-region) or repeats an existing point, the agent then explores to find an alternate point in the sub-region. To explore, the agent adds a point to the database that maximizes the minimum distance from the points already in its internal database (see Algorithm 3). The true values f and g of the iterate are then calculated (line 12), and $(\hat{x}^*, f(\hat{x}^*), g(\hat{x}^*))$ is added to the internal database (lines 12–13).

5.5 Dynamic Design Space Partitioning

The previous section expounds the cooperative optimization process performed by agents in a pre-partitioned space. The goal of this method is to have each agent locate a single optimum, such that the partitioning strongly depends on the topology of the space.

Therefore, as a part of the cooperative optimization process, we propose a self-organizing mechanism to dynamically partition the space which adapts to the search space. By self-organizing, we mean that agents (and therefore sub-regions) will be created and deleted depending on the cooperative optimization process. Agents will split when points are clustered inside a single region (*creation*), and will be merged when local optima converge (*deletion*).

5.5.1 Moving the Sub-regions' Centers

The method of space partitioning we propose focuses on moving the sub-regions' centers to different local optima. As a result, each agent can choose a surrogate that is accurate around the local optimum, and the agent can also explore the sub-region around the local optimum. At the beginning of the process, only one agent exists and is assigned to the whole search space. Then it begins optimization by choosing a surrogate, fitting it and optimizing on this surrogate. As a result the agent computes a new point $\hat{x}^{*t-1}$. Then, the center of the sub-region is moved to the "best" point in the sub-region in terms of feasibility and objective function value (line 14). This is done by comparing the center at the last iteration c^{t-1} to the last point added by the agent $\hat{x}^{*t-1}$. The center is moved to the last point added by the agent if it is better than the current center. Otherwise, the center remains at the previous center. For convenience, in comparing two points x_m and x_n, we use the notation $x_m \succ x_n$ to represent x_m "is better than" x_n. For two centers, instead of points x we would consider the centers c. The conditions to determine the better of two points are given in Algorithm 5.

5.5.2 Merge, Split and Create Sub-regions

Once an agent has added a new point in its database (line 13) and moved its center to the best point (line 14), it will check whether to split, or to merge with other ones (line 15). Merging agents (and their sub-regions) prevents agents from crowding the same area, allowing one agent to capture the behavior in a region. Splitting an agent is a way to explore the space as it refines the partitioning of the space in addition to the search that each agent

Algorithm 5 Algorithm to determining if, for two points x_m and x_n, x_m "is better than" x_n ($x_m \succ x_n$) and vice versa. Note that for the algorithm below, the time (superscript t) is omitted as the algorithm is valid for the comparison of any two points at any time.

1: Given $f(x_m), f(x_n), max(g(x_m)), max(g(x_n))$
2: **if** $max(g(x_m)) \leq 0$ & $max(g(x_n)) \leq 0$ **then**
3: *// both points are feasible*
4: **if** $f(x_m) \leq f(x_n)$ **then**
5: $x_m \succ x_n$
6: **else**
7: $x_n \succ x_m$
8: **end if**
9: **else if** $max(g(x_m)) \leq 0$ & $max(g(x_n)) > 0$ **then**
10: *// only x_m is feasible*
11: $x_m \succ x_n$
12: **else if** $max(g(x_m)) > 0$ & $max(g(x_n)) \leq 0$ **then**
13: *// only x_n is feasible*
14: $x_n \succ x_m$
15: **else if** $max(g(x_m)) > 0$ & $max(g(x_n)) > 0$ **then**
16: *// both are infeasible*
17: **if** $max(g(x_m)) \leq max(g(x_n))$ **then**
18: *// maximum constraint violation of x_m is less thanx_n*
19: $x_m \succ x_n$
20: **else**
21: $x_n \succ x_m$
22: **end if**
23: **end if**

can perform in its sub-region. Split and merge occurs at the end of each iteration (line 15): agents are first merged (if necessary), the points belonging to the merged agent(s) are distributed to the remaining agents based on distance from the center of the remaining agents' sub-regions, and then each remaining agents examines to determine whether to split or not.

5.5.2.1 Merge converging agents

Agents are merged (deleted) if the centers of the agents' sub-regions are too close as measured by the Euclidean distance between the centers. We measure the minimum Euclidean distance between two centers as a percentage of the maximum possible Euclidean distance between points in the design space. When examining the agents, the agent with the

center with the lowest performance is deleted. For example, for agents 1 and 2, if $c_1 \succ c_2$, agent 2 is deleted. Before deletion, the deleted agent distributes its internal database points to closest neighbors.

5.5.2.2 Split clustered sub-regions

It is desirable to create an agent if it is found that points are clustered in two separate areas of a single agent's sub-region, as illustrated in Fig.5-4(a). Such a situation can occur if there are two optima in a subregion.

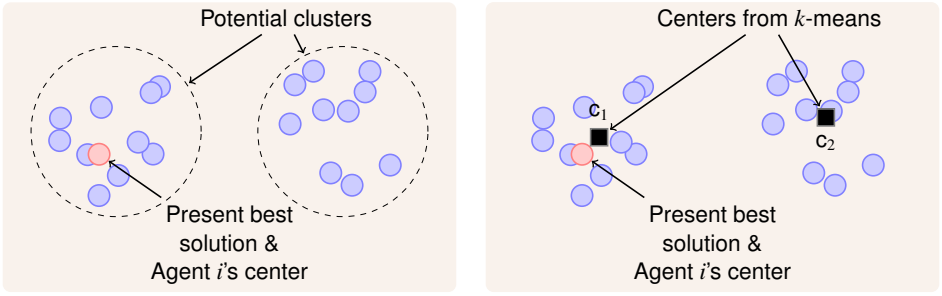

(a) Potential clusters within a sub-region

(b) Clusters from k-means

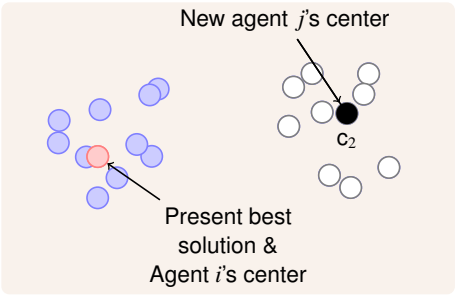

(c) Final clusters after moving centers to present best solution and nearest data point

Figure 5-4. Illustration of process used to create an agent j given points in a single agent i's sub-region.

Agents are created by using k-means clustering [86] for two clusters (k = 2) given the points in the sub-region, where the initial guesses of the centers are the present best solution (the current center) and the mean of the dataset. Since k-means clustering gives centers that are not current data points as illustrated in Fig.5-4(b), we move the centers to available data points to avoid more calls to evaluate the expensive functions. This is done by first

measuring the distance of the centers from k-means to the present best solution, and moving the closest center to the present best solution, as we want to preserve this solution. For the other center, we measure the distance of the current data points to the other center, and make the closest data point the other center. The final clustering is illustrated in Fig.5-4(c). The result is a new agent with a center at an already existing data point, where the creating agent retains its center at its present best solution.

This final clustering is validated using the mean silhouette value of the points in the sub-region. The silhouette, introduced by Rousseeuw [87], is used to validate the number of clusters, by providing a measure of the within-cluster tightness and separation from other clusters for each data point i for a set of points. The silhouette value for each point is given as

$$s(i) = \frac{b(i) - a(i)}{max\{a(i), b(i)\}} \tag{5–4}$$

where a_i is the average distance between point i and all other points in the cluster to which point i belongs, and b_i is the minimum of the average distances between point i and the points in the other clusters. The values of s_i range from -1 to 1. For s_i near zero, the point could be assigned to another cluster. If s_i is near -1, the point is misclassified, and, if all values are close to 1, the data set is well-clustered. The average silhouette of the data points is often used to characterize a clustering. In this work, we accept the clustering if all s_i are greater than 0 and the average value of the silhouette is greater than some value.

5.5.2.3 Create new agents

The agents may reach a point where there is no improvement made by the overall system in several iterations (i.e., the centers of all agents have remained at the same points). For example, this can occur when each agent has located the best point in its sub-region, the area around each best point is populated by points, each agent is driven to explore for several iterations, and no other potential local optima are located. This can also occur at early iterations in which the surrogates are not well-trained in the sub-region. In order to improve exploration, a new agent is created in the design space when there is

no improvement for n iterations (i.e., the centers of the sub-regions have not moved for n iterations). We call this parameter the *stagnation threshold*. To create a new agent, a new center is created at an already existing data point that maximizes the minimum distance from the already existing centers, thus forming a new agent. The design space is then repartitioned.

5.6 Six-Dimensional Analytical Example

In this section, we examine the six-dimensional Hartman function (Hartman 6) that is often used to test global optimization algorithms.

$$\begin{aligned} \underset{x}{\text{minimize}} \quad & f_{hart}(x) = -\sum_{i=1}^{q} a_i exp\left(-\sum_{j=1}^{m} b_{ij}(x_j - d_{ij})^2\right) \\ \text{subject to} \quad & 0 \le x_j \le 1, j = 1, 2, \ldots, m = 6 \end{aligned} \tag{5–5}$$

In this instance of Hartman 6, $q = 4$ and $a = \begin{bmatrix} 1.0 & 1.2 & 3.0 & 3.2 \end{bmatrix}$ where

$$B = \begin{bmatrix} 10.0 & 3.0 & 17.0 & 3.5 & 1.7 & 8.0 \\ 0.05 & 10.0 & 17.0 & 0.1 & 8.0 & 14.0 \\ 3.0 & 3.5 & 1.7 & 10.0 & 17.0 & 8.0 \\ 17.0 & 8.0 & 0.05 & 10.0 & 1.0 & 14.0 \end{bmatrix}$$

$$D = \begin{bmatrix} 0.1312 & 0.1696 & 0.5569 & 0.0124 & 0.8283 & 0.5886 \\ 0.2329 & 0.4135 & 0.8307 & 0.3736 & 0.1004 & 0.9991 \\ 0.2348 & 0.1451 & 0.3522 & 0.2883 & 0.3047 & 0.3047 \\ 0.4047 & 0.8828 & 0.8732 & 0.5743 & 0.1091 & 0.0381 \end{bmatrix}$$

As we wish to locate multiple optima, we modified Hartman 6 to contain 4 distinct local optima by "drilling" two additional Gaussian holes at two locations to form two local optima, in addition to the global optimum and one local optimum provided in the literature [39]. The modified Hartman 6 function is

$$f(x) = f_{hart}(x) - 0.52\phi_1(x) - 0.18\phi_2(x) \tag{5–6}$$

where the mean and standard deviation associated with ϕ_1 and $\mu_1 = \left[0.66\ 0.07\ 0.27\ 0.95\ 0.48\ 0.13\right]$ and $\sigma = 0.3$ (all directions), respectively. The mean and standard deviation associated with ϕ_2 and $\mu_2 = \left[0.87\ 0.52\ 0.91\ 0.04\ 0.95\ 0.55\right]$ and $\sigma_2 = 0.25$ (all directions), respectively. The optima are displayed in Table 5-1. To obtain an approximate measure of the size of the basins of attraction that contain the optima, we measured the percentage of local optimization runs that converged to each optimum. To do this, twenty-thousand points were sampled using Latin Hypercube sampling and a local optimization was performed starting at each one of these points using a SQP algorithm.

Table 5-1. Modified Hartman6 optima and the percentage of runs that found each optimum with multiple starts and a SQP optimizer

Optimum	f	x	percentage of runs
Global	-3.33	(0.20 0.15 0.48 0.28 0.31 0.66)	50
Local 1	-3.21	(0.40 0.88 0.79 0.57 0.16 0.04)	21
Local 2	-3.00	(0.87 0.52 0.91 0.04 0.95 0.55)	9
Local 3	-2.90	(0.64 0.07 0.27 0.95 0.48 0.13)	20

The percentage of starts that converged to an optimum is also a measure of the volume of its basin of attraction in comparison to other basins. Since Local 2 has the smallest percentage of runs, it was expected that it would be the most difficult optimum to locate by the agents. Note, however, that in six-dimensional space a ratio of $\frac{9\%}{50\%}$ in volume would be produced by a ratio of 0.75 in characteristic dimension.

5.6.1 Experimental Setup

Since there are no nonlinear constraints, only the objective function is approximated by surrogates.. The three possible surrogates, which are kriging surrogates with different trend functions, are described in Table 5-2. From this set, each agent chose the best surrogate based on $PRESS_{RMS}$. The set of surrogates and the minimum number of points used to fit each surrogate are provided in Table 5-2. If the minimum number of points are not available, points are borrowed from neighboring sub-regions in the order of increasing distance to the agent center, and, if the requirement is still not met, then all available points are used.

Table 5-2. Surrogates considered in this study

ID	Description	minimum # of pts for fit
1	Kriging (quadratic trend)	
2	Kriging (linear trend)	1.5 * # coefficients for quadratic response surface
3	Kriging (constant trend)	

The parameters in Table 5-3 were used for all results. These parameters include maximum number of agents (e.g., the maximum number of computing nodes available), parameters that dictate how close points and centers can be, and parameters that define if a new agent should be created. Since we are simulating expensive function evaluations, we also fixed a computational budget to 400 function evaluations. Beyond this number, the system stops: this is our only termination criterion. Finally, we start the multi-agent system with a single agent able to split and merge with time.

Table 5-3. Multi-Agent Parameters for modified Hartman 6

Parameter	Value
Max # of function evaluations	400
Max # of agents	8
Initial/Min # of agents	1
Min distance between agent centers	10% of max possible distance in space
Minimum distance between points	1e-3 (absolute for each dimension)
Min average silhouette	0.25
Min # of points in each agent after creation	4
Stagnation threshold	3

The success and efficiency of the multi-agent approach is compared to a single agent system which performs a classical surrogate-based optimization procedure as described in Algorithm 6. However, this *single agent* is unable to perform dynamic partitioning and optimizes over the whole space. This single agent has also a computation budget of 400 calls to the expensive function. The single agent configuration is a standard to which we compare our multi-agent optimizer.

In each case, (multi- or single agent), as to evaluate the capability of the algorithms to explore the search space, we also ran several experiments for different initial DOE sizes

(35[1] , 56, and 100) that still account for the number of function evaluations. Therefore, for a larger initial DOE, the system executes fewer steps. For each of the cases that were studied, the results shown are the median of 50 repetitions (i.e, 50 different initial DOEs). The local optimization problems were solved with a sequential quadratic programming (SQP) algorithm [88]. DOEs are obtained using Latin Hypercube sampling and the *maximin* criterion for five iterations.

5.6.2 Successes to Locate Optima

For 50 repetitions, the percentage of repetitions that successfully located a solution a 1% distance from the optimum with a single agent and a multi-agent system is shown in Fig. 5-5. This distance is the Euclidean distance normalized by the maximum possible distance between points in the design space (here, $\sqrt{6}$). It was observed that the single agent had fewer successes with an equivalent number of function evaluations compared to the multi-agent case. In both the single and multi-agent cases, Local 2 was the optimum that was the most difficult to locate with less than 10 successes with a single agent and 32 successes with a multi-agent system. Based on the small percentage of runs that located Local 2 with multiple starts and the true function values with the SQP optimizer (c.f. Table 5-1), this was not unexpected.

5.6.3 Agent Efficiency and Dynamics

The median objective function value of the solution closest to each optimum is shown in Fig. 5-6. For the global optimum and Local 1, it was observed that the efficiency is nearly equal in the single and multi-agent cases. It was also observed that the smaller DOEs required fewer function evaluations to find these optima. For Local 2 and Local 3, the multi-agent system has a clear advantage in finding solutions with the objective function near the

[1] This does not satisfy the minimum required number of points for the fit, so all points are used (a single surrogate spans the entire design space) until a sufficient number of points are obtained.

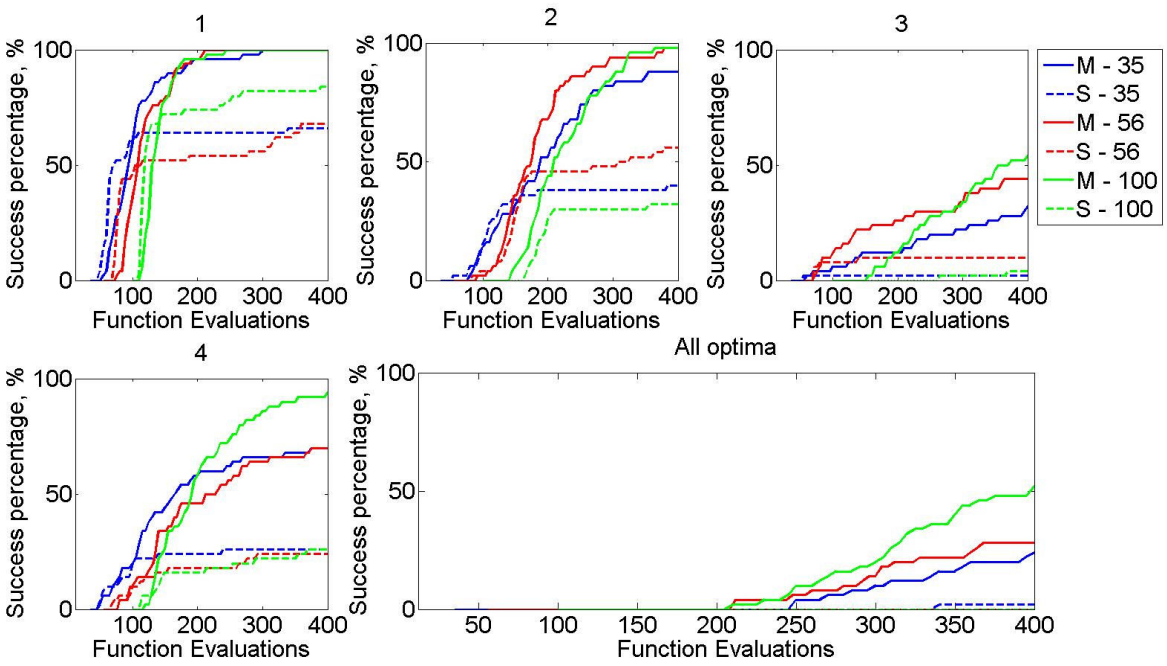

Figure 5-5. For the modified Hartman 6 example, the percentage of repetitions that located a solution within 1% distance from each optimum.

true optimum value. While it is clear for the global optimum and Local 1 that smaller DOEs are more efficient, there is no clear relationship between DOE size and efficiency (consider Local 2). Recall that Local 2 was expected to be the most difficult optimum to find judging by the small percentage of runs of multiple starts with the SQP optimizer that were successful. These results confirm that exploration is required to locate Local 2, and the multi-agent system, in which exploration is an inherent feature, is more capable of finding this optimum.

Exploration by the multi-agent system was measured by the percentage of calls to the true objective function in which exploitation or exploration occurred as shown in Fig. 5-7. We define an exploitation call as when the agent adds a point that minimizes the objective function. Note that we constrained the minimum distance a new point should be from an already existing data point so that multiple local optima could be located. Exploration is when a random point is added by an agent. Exploration generally occurs when exploitation has failed, meaning all starts in the sub-region resulted in points that were not far enough from existing data points or were outside of the sub-region.

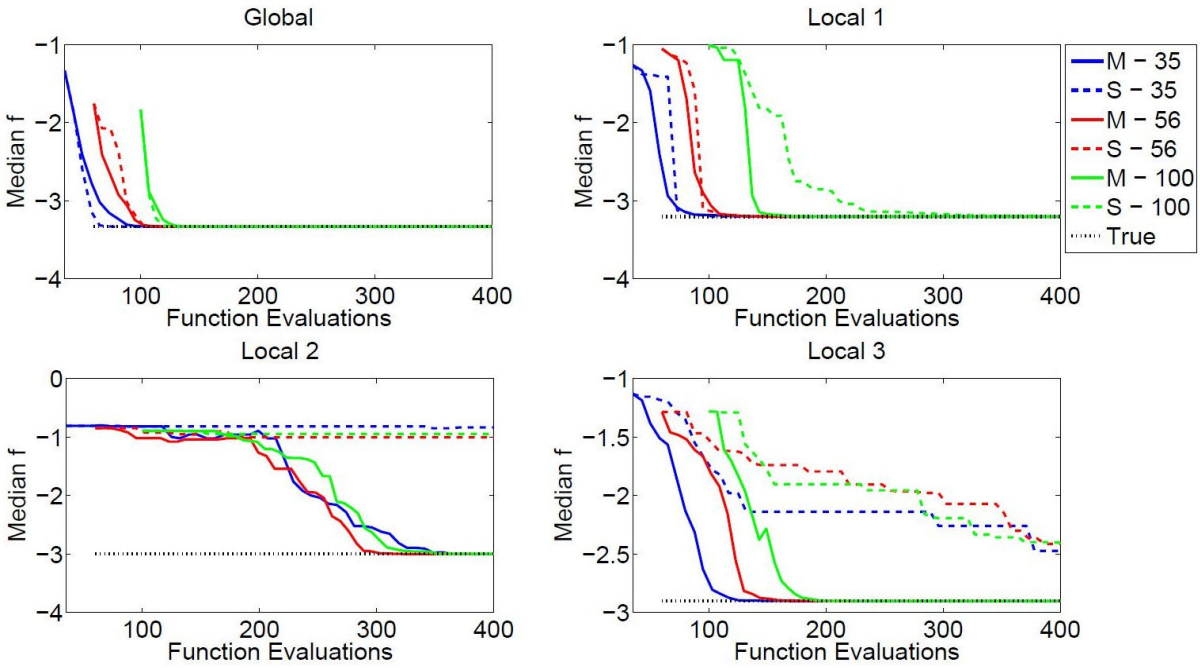

Figure 5-6. Median objective function value of solution closest to each optimum with number of function evaluations. The single agent case is denoted by “S” and the multi-agent case by “M”, with the initial DOE size represented by the number.

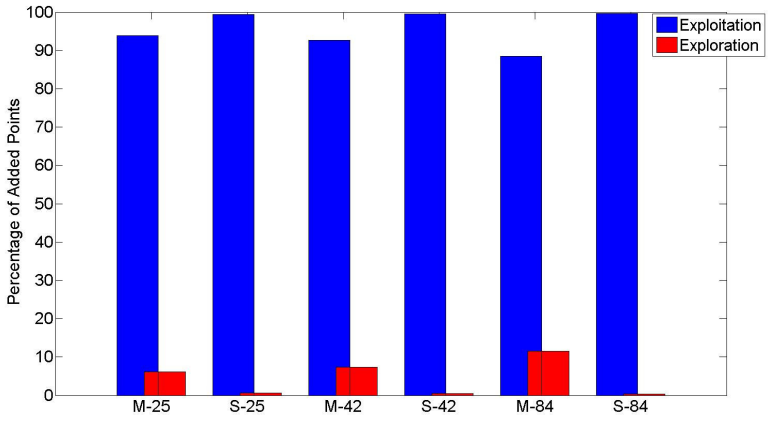

Figure 5-7. For the modified Hartman 6 example, the percentage of points that were added in exploitation or exploration.

We observed that the multi-agent case mostly performed exploitation with a few explorations, whereas the single agent performed exploration only 1% of the time. This could be due to the single agent seeking to tune around the global optimum and Local 1, which it locates with the fewest function evaluations. The number of times in which the an

agent puts point to tune around the optimum can be reduced by increasing the minimum distance between points. In addition, it was observed that the single agent was slowly adding exploitation points in the vicinity of Local 3 as shown in Fig. 5-6.

Figure 5-8 shows the median number of agents. While up to 8 agents could be created, it was observed that the median number of agents stabilized around 4, the number of local optima. This is because once all the local optima are located, new agents are created but are soon deleted as they converge to the basins of attraction of the already found optima.

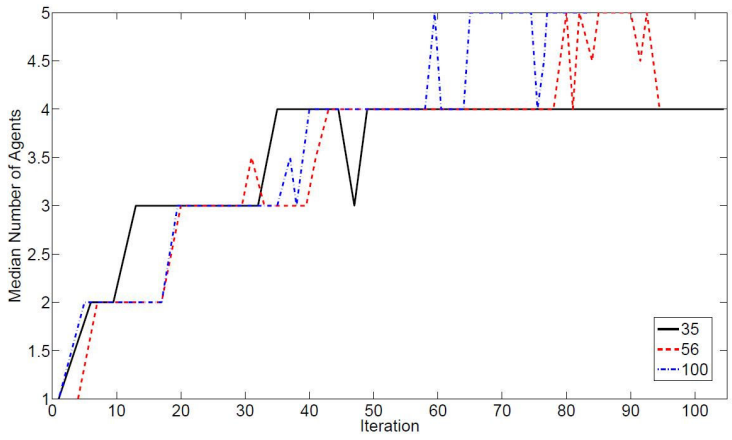

Figure 5-8. For a multi-agent system, the median number of agents

The accuracy of the surrogates was measured by the partial $PRESS_{RMS}$ and the error at 1000 test points by the e_{rms}. $PRESS_{RMS}$ is a leave-one-out cross-validation error. In the single agent case the calculation of PRESS is straightforward, but for the multi-agent case it is taken by calculating $PRESS_{RMS}$ in each sub-region and taking the mean of the values. The values of $PRESS_{RMS}$ and e_{RMS} are displayed in Fig. 5-9. The $PRESS_{RMS}$ indicated that the error was decreasing for both the single and multi-agent cases, with the single agent case slightly more accurate. However, the e_{RMS} provided a more global indication of the accuracy of the surrogate and showed that the approximation made by the multiple agents improved with function evaluations more than the approximation of the single agent did. This is due to the single agent putting many points near the global optimum and Local 1, making the surrogate accurate in these locations but less accurate globally. The slow location of Local 3

by the single agent can also be partially explained by the poor accuracy of the single agent's surrogate.

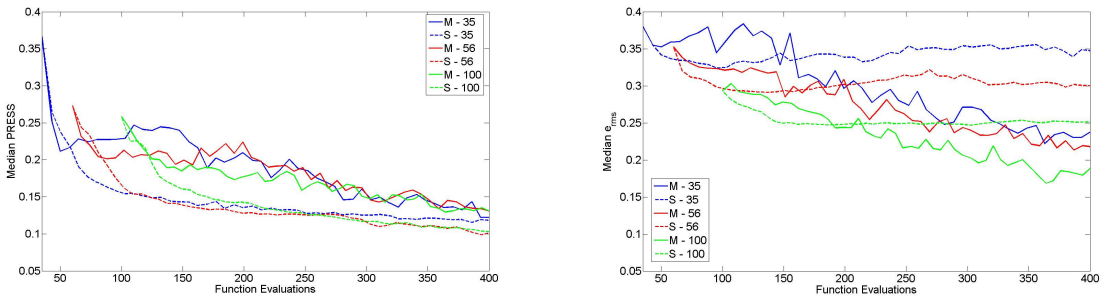

(a) $PRESS$ (b) e_{rms}

Figure 5-9. For the modified Hartman 6 example, (a) the $PRESS_{RMS}$ and (b) error at 1000 test points.

5.7 Engineering Example: Integrated Thermal Protection System

In this section, we illustrate the multi-agent method and the importance of locating multiple candidate designs on an integrated thermal protection system (ITPS). Figure 2-1 shows the ITPS panel that is studied, which is a corrugated core sandwich panel concept. The design consists of a top face sheet and webs made of titanium alloy (Ti-6Al-4V), and a bottom face sheet made of beryllium. Saffil® foam is used as insulation between the webs. The relevant geometric variables of the ITPS design are also shown on the unit cell in Figure 5-10. These variables are the top face thickness (t_T), bottom face thickness (t_B), thickness of the insulation foam (d_S), web thickness (t_w), and corrugation angle (θ). The mass per unit area is calculated using Eq.(2–9)

$$f = \rho_T t_T + \rho_B t_B + \frac{\rho_w t_w d_S}{p \sin\theta} \tag{2–9}$$

where ρ_T, ρ_B, and ρ_w are the densities of the materials that make up the top face sheet, bottom face sheet, and web, respectively.

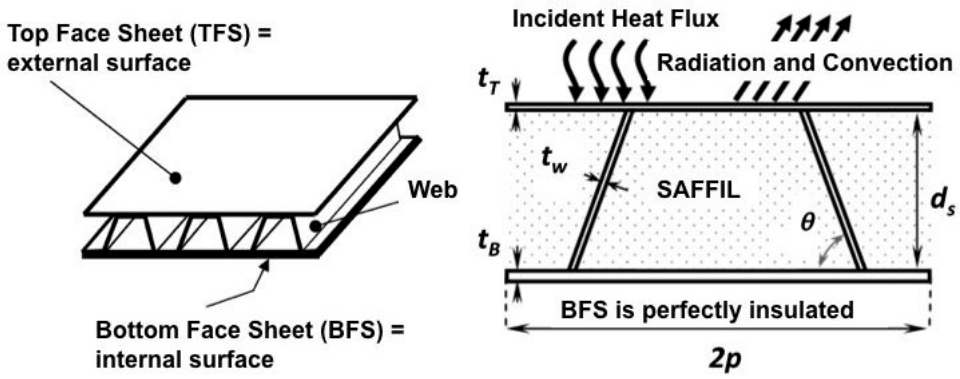

Figure 5-10. Corrugated core sandwich panel ITPS concept

The optimization problem to minimize the mass subject to constraints on the maximum bottom face sheet temperature T_B and maximum stress in the web σ_w is shown in Eq.(5–7).

$$\begin{aligned} \underset{x=\{t_w,t_B,d_S,t_T,\theta\}}{\text{minimize}} \quad & f(x) \\ \text{subject to} \quad & T_B(x) - T_B^{allow} \leq 0 \\ & \sigma_w(x) - \sigma_w^{allow} \leq 0 \\ & x_{L,i} \leq x_i \leq x_{U,i} \text{ for } i = 1 \ldots 5 \\ & \text{where } x_L = \left[1.31\ 6.00\ 60.6\ 1.13\ 75.3\right] \\ & \text{and } x_U = \left[1.96\ 9.00\ 60.6\ 1.27\ 84.8\right] \end{aligned} \tag{5–7}$$

The bottom face sheet temperature and the maximum stress, which are both functions of the design variables all five design variables, are constrained to by their maximum allowable values. As described in Sec. 5.2, the 3-D problem, where the bottom face, web, and foam thicknesses were the design variables, had three distinct feasible regions containing three local optima. For the 5-D problem, we found the true optima by solving the true optimization problem with 1000 random initial points with the SQP optimizer. Table 5-4 lists the optima that were found and gives the percentage of the runs that located each optimum. As the percentage of runs that converge to each optimum is a measure of the difficulty to locate the optimum, we observed that optimum 3 would be the most difficult to locate by the agents.

Table 5-4. 5-D ITPS example optima and the percentage of runs that found each optimum with multiple starts and a SQP optimizer

Optimum	f	x	percentage of runs
1	29.27	(1.31 6.00 76.8 1.13 81.5)	50
2	29.29	(1.31 6.00 75.6 1.13 76.5)	30
3	29.30	(1.31 6.00 77.5 1.13 84.8)	4
4	31.30	(1.31 8.29 60.6 1.27 84.8)	8
5	34.65	(1.31 9.00 74.0 1.13 75.3)	6
6	38.06	(1.84 9.00 65.9 1.25 84.8)	1
Other (points that were not true local optima)			1

5.7.1 Experimental Setup

In this example, we follow the same experimental setup as for the modified Hartman6 example, with the parameters provided in Table 5-3. However, the computational budget is fixed at 120 evaluations of the expensive functions and the maximum number of agents is raised to 10. As the objective function, the mass, calculated by the simple expression in Eq.(2–9) the agents only approximate the two limit states g_1 and g_2 with surrogates. The initial DOE size was varied at 25, 42, and 84 points.

5.7.2 Successes to Locate Optima

For 50 repetitions, the percentage of repetitions that were successful at locating a **feasible** solution within 1% distance from each optimum is provided in Fig. 5-11. The differences in the number of successes between the single and multi-agent cases for all optima were small partitcularly for optima 1 and 2, while the single agent was clearly more efficient and successful in locating optimum 3. It was observed that the multi-agent system was less successful at locating optimum 3, particularly with the initial DOE size of 84. In comparing the success of locating all optima in a single repetition, it was clear that the success in locating all optima was dictated by the success in locating optimum 3.

5.7.3 Agents Efficiency and Dynamics

The median objective function value of the closest solution to each optimum is shown in Fig. 5-12. It should be noted that all solutions were feasible and that in all cases the smallest initial DOE size of 25 was the most efficient. For optima 1, 2, and 4, it was observed that the

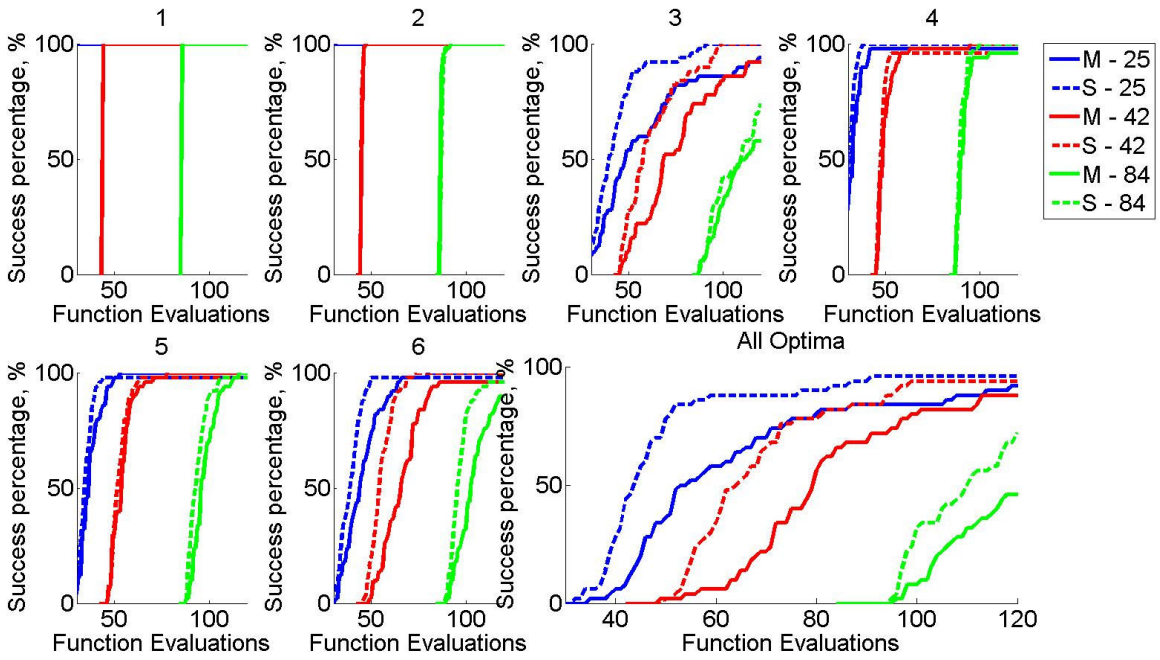

Figure 5-11. For the 5-D ITPS example, the percentage of repetitions that located a solution within 1% distance from each optimum.

differences between the single and multi-agent cases with varying initial DOEs were small. Within 30 function evaluations, both the single and multi-agent cases were able to locate each optimum. For optima 5 and 6, it is clear that the single agent is more efficient that the multi-agent, locating the optimum with 5-10 fewer function evaluations. For optimum 3, which both agents had difficulty locating, we observed that the single agent is clearly much more efficient than the multiple agents. Note that for all initial DOE sizes, the closest solution to optimum 3 is at optimum 1 ($f = 29.27$), which is not unexpected as the two optima are only a distance of 0.16 (in the normalized design space and normalized by $\sqrt{5}$) apart making these the closest pair of all the optima.

Figure 5-13 displays the median number of agents. Though up to 10 agents could be created, the median number of agents stabilized around 3. Figure 5-14 compares the number of exploitations and explorations for the single and multi-agent cases for different initial DOE sizes. We observed that, although the number of agents stabilizes at 3, exploitation is still performed more by the multiple agents considering the constraint on the minimum

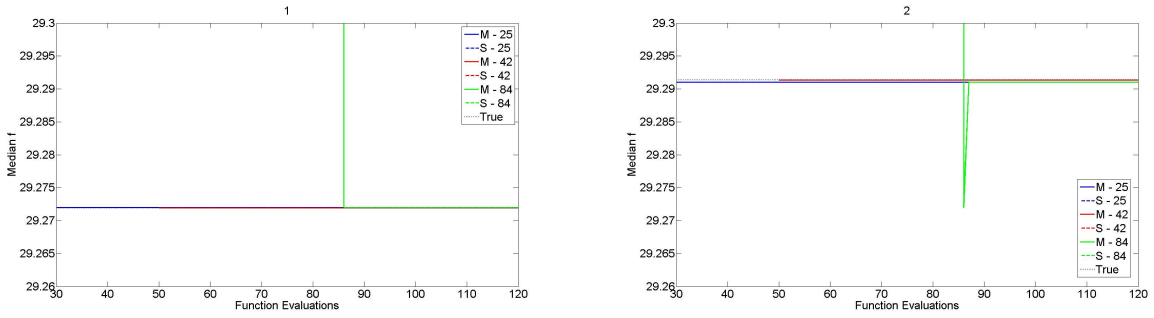

(a) Opt 1

(b) Opt 2

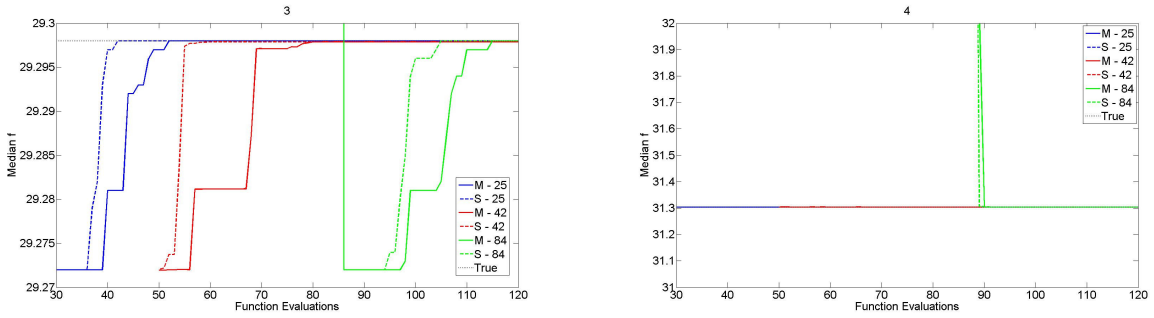

(c) Opt 3

(d) Opt 4

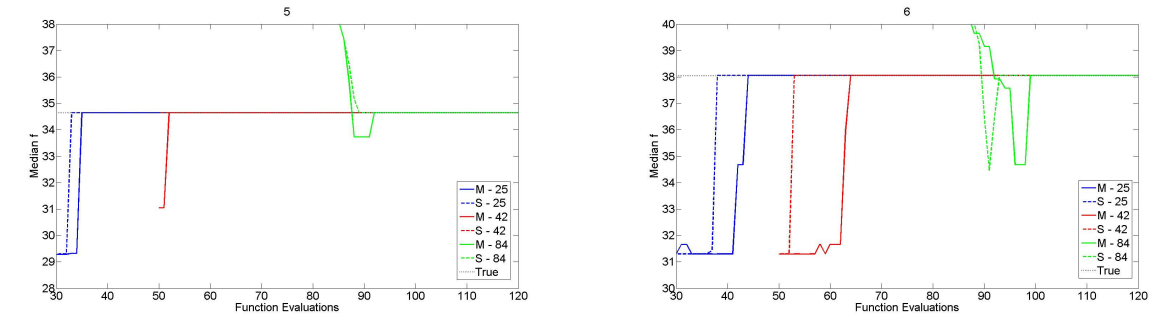

(e) Opt 5

(f) Opt 6

Figure 5-12. For the 5-D ITPS example, the median f of the solution nearest to each optimum. The single agent case is denoted by "S" and the multi-agent case by "M", with the initial DOE size represented by the number.

distance between points. In all multi-agent cases, there was more exploitation than exploration. For the single agent, there was more exploration, except for the initial DOE of 84 points. This was due to the ability of the single agent to locate the multiple optima quickly with exploitation iterations due the constraint on the minimum distance between points. After this occurred, the single agent performed more exploration, which aided in the location of the

most difficult optimum to locate, optimum 3. For the initial DOE of 84, the single agent had fewer evaluations in which to locate all optima, so exploitation was dominant.

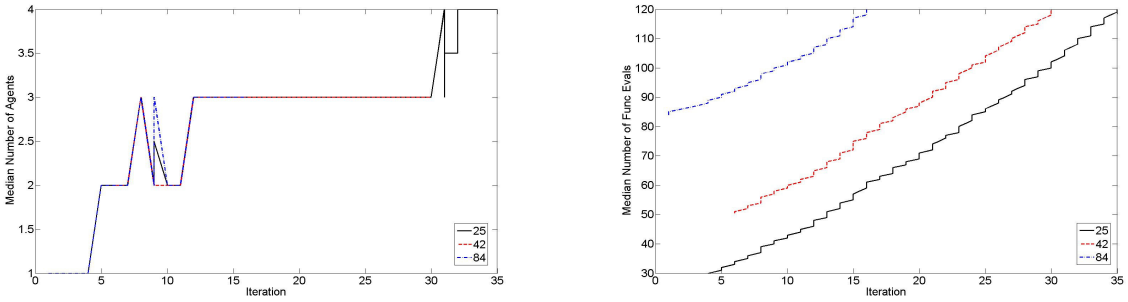

(a) Number of active agents (b) Number of iterations vs function evaluations

Figure 5-13. For the 5-D ITPS example, the number of active agents and the number of iterations.

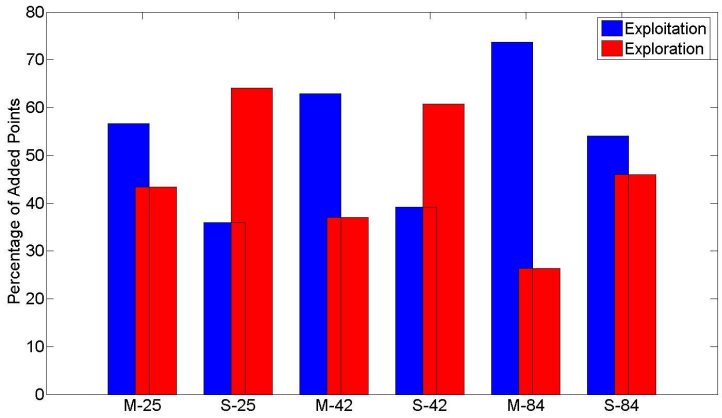

Figure 5-14. For the 5-D ITPS example, the percentage of points that were added in exploitation or exploration.

The superior performance by the single agent was also attributed to the accuracy of its surrogate approximations. Fig. 5-15 compares the $PRESS_{RMS}$ of each surrogate for the single and multi-agent cases. The $PRESS_{RMS}$ decreased with increasing number of function evaluations after it initially increased. This was due to the placement of points around the optima, which made the surrogate less accurate further from the optima. This led to large errors when a point that was far away from other points was left out in calculating the

cross-validation error. As more exploration points were added, the $PRESS_{RMS}$ was reduced. For the multi-agent case, we observed that the $PRESS_{RMS}$ increased through the function evaluations. This was due to the large number of points put around the optima in exploitation iterations, which outnumbered the exploration iterations.

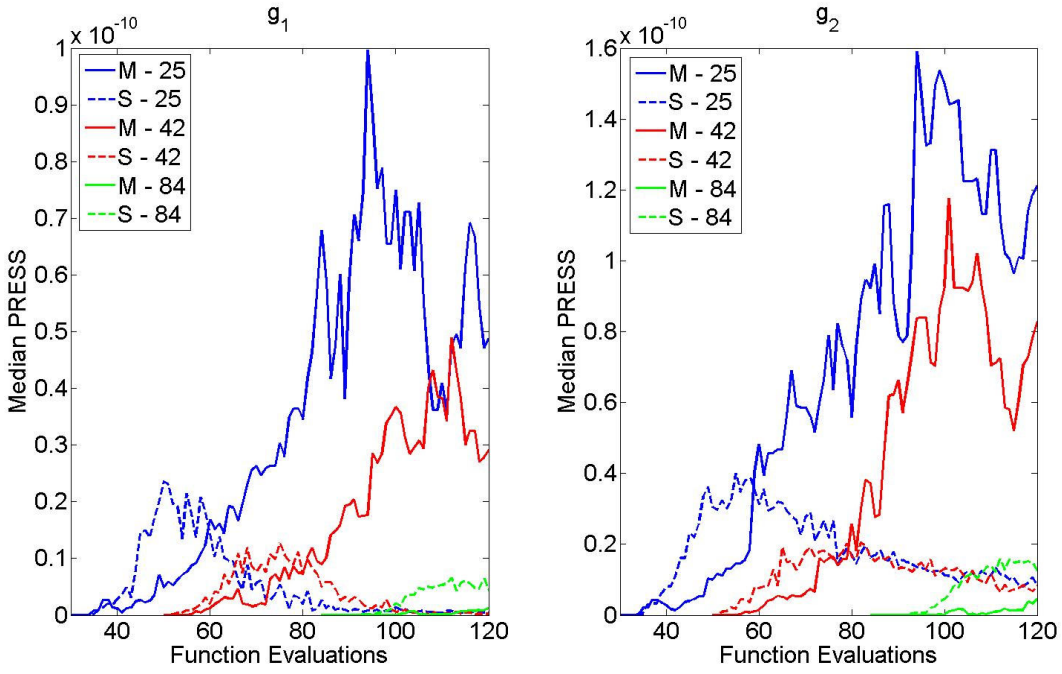

Figure 5-15. Median $PRESS_{RMS}$ of the surrogates of the limit states for the 5-D ITPS example

Figure 5-16 displays the error at 1000 test points e_{RMS}. We observed much of the same trends as with $PRESS_{RMS}$, with the surrogates in the multi-agent case decreasing in accuracy while the surrogates of the single agent cases increased accuracy.

5.8 Discussion

The single agent approach showed a clear advantage over the multi-agent method in the ITPS example in Sec. 5.7. The single agent approach is simple : a global surrogate is used and a constraint on the minimum distance between points is the only way to instigate exploration of the design space. It is advantageous in its simplicity and ease of implementation, but its success depends on how well a single surrogate can approximate the global behavior. The accuracy measures of the limit states for the ITPS example in Fig. 5-16 show

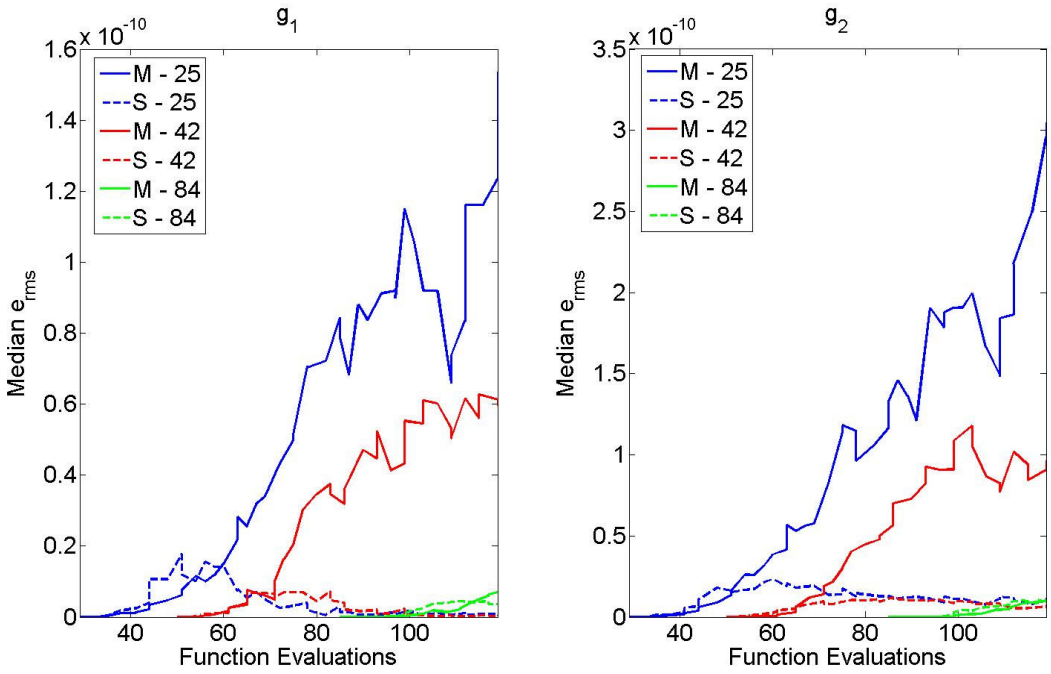

Figure 5-16. Median error at 1000 test points e_{RMS} of the surrogates of the limit states for the 5-D ITPS example

that the global surrogate of the single agent is indeed more accurate than several local surrogates. Upon further investigation of the temperature and stress trends in the design space, it was found that simple quadratic response surfaces over the design space were sufficient approximations.

On the contrary, the modified Hartman 6 function presented in Sec. 5.6, for which the unmodified version is often used as a benchmark function for surrogate-based global optimization algorithms, is thought to be more complex compared to the ITPS example. The error at test points (c.f. Fig. 5-9(b)) shows that the accuracy of the local surrogates is slightly better than that of the single agent's global surrogate. In this example, we observed that the multi-agent method can be successful and efficient.

With that said, the comparisons made here in terms of efficiency are based on the number of function evaluations. Ideally, the multi-agent partitioning method would be parallelized such that a single iteration would involve simulatenous optimization in each sub-region. That is, a single iteration could account for four function evaluations if there

are four agents working in four sub-regions. Therefore, in terms of efficiency the iterations, which give an idea of wall clock time, should also be compared. For the ITPS example, the single agent was shown to be more efficient at locating some optima by five to ten function evaluations, but in terms of iterations the multiple agents are more efficient if the number of function evaluations is translated into iterations by Fig. 5-13(b).

Otherwise, what does this say about this multi-agent algorithm? Based on these two examples, the success rate and efficiency of the multi-agent method may be dependent on having higher accuracy local surrogates compared to a global surrogate. Otherwise, simpler algorithms may be more efficient. Further investigation on the need for local surrogates is required, and a study that uses a global surrogate with the agent-based dynamic design space partitioning is planned. It will allow us to study separately two ingredients that make up the method investigated here: local versus global surrogate and space partitioning to increase chances of visiting many basins of attraction leading to different local optima. Additionally, the efficiency gains from parallelization should be investigated.

5.9 Summary and Discussion on Possible Future Research Directions

This chapter introduced a multi-agent methodology for optimization that dynamically partitions the design space as to find multiple optima. Multiple designs provide insurance against discovering that late in the design process a design is poor due to modeling errors or overlooked objectives or constraints. The method used surrogates to approximate expensive functions and agents optimized using the surrogates in the sub-regions. The centers of the agents subregions moved to stabilize around optima, and agents were created and deleted at run-time as a means of exploration and efficiency, respectively.

The method was applied to two examples, an analytical test function and a practical engineering example. It was observed that for problems in which the behavior is simple to approximate with a global surrogate, the simpler single agent is more efficient and successful than the multiple agents. For the more complicated test function, in which local surrogates were slightly more accurate, the multiple agents outperformed the single agent. These

results lead us to believe that the success of the current agent algorithm is dependent on local surrogates being more accurate than a global surrogate.

This method aims too exploit the surrogate predictions by purely minimizing the function rather than exploring the design space as evidenced by the comparison of the percentage of iterations that put points near the optima. There is a focus on using surrogate predictions to aid multiple cheap local searches throughout the design space. This is an important differentiation between this algorithm and many global optimization algorithms that aim for and tout the balance of exploitation and exploration.

Continuing research can focus on using a global surrogate with the dynamic partitioning still in place. The reason for this is two-fold: (i) in the authors' experience, there are few situations in which local surrogates are significantly more accurate than a global surrogate, (ii) the complication of managing points between sub-regions to create surrogates is removed. Efficient Global Optimization[89] (EGO) is a popular global optimization algorithm that uses a global surrogate and adds points based on the present best solution (the present best data point). It is planned to modify the EGO algorithm for use with the dynamic design space partitioning, in which each sub-region has its own present best solution.

The proposed agent optimization method also has a great potential for parallel computing. As the number of computing nodes n increases, the calculation of the expensive objective and constraints functions scales with $1/n$ in terms of wall-clock time. But the speed at which problems can be solved then becomes limited by the time taken by the optimizer, i.e., the process of generating a new candidate solution. In the algorithm we have developed, the optimization task itself can be divided among the n nodes through agents. We plan to explore how agents can provide a useful paradigm for optimizing in parallel, distributed, asynchronous computing environments.

CHAPTER 6
FURTHER INVESTIGATION ON THE USE OF SURROGATE-BASED OPTIMIZATION TO LOCATE MULTIPLE CANDIDATE DESIGNS

The previous chapter presented a method to dynamically partition the design space to locate multiple candidate designs. The overall conclusion was that the success of the partitioning method depended on the degree of difficulty in approximating the problem with surrogates. The work in previous chapter led us to question if local surrogates were actually better than using a single global surrogate. Afterall, we did find that the error in the single agent's global surrogate was generally less than that of the multiple agents. As a result, we performed a study in which the design space was partitioned and global and local surrogates were fit to the design space and sub-regions. We measured the error at test points and concluded that using local surrogates were generally not less accurate than a single global surrogate, particularly when the number of design points was small. This study can be found in Appendix E.

In this chapter, we compare this method to a method that performs local optimization with a global surrogate that adds multiple points at a time and the Efficient Global Optimization algorithm. We observed the surprising result that partitioning of the design space may not hold as important of a role as spreading out many local searches in the design space. It was observed that existing global optimization algorithms have potential to be adapted to locate multiple candidate designs, but the key to efficiency lies in parallelization of optimization processes.

6.1 Motivation for Investigating Surrogate-Based Techniques

Locating multiple optima is often done with nature-inspired algorithms using niching methods (Beasley et al., 1993 [76]; Hocaoglu and Anderson, 1997 [77]). For example, Nagendra et al. [81] used a genetic algorithm to find several structural designs with comparable weight and identical load carrying capacity. However, when three of these designs were built and tested, their load carrying capacity was found to differ by 10%. Parsopoulos and Vrahas used particle swarm optimization [90]. Restarted local optimization methods with

clustering (Törn and Zilinkas [83], Törn and Viitanen [91]) have also been proposed for finding many local optima. These methods require a large number of function evaluations, which is prohibitively costly if the functions are expensive to evaluate.

To reduce the cost of optimization, surrogate models are often used (e.g. Jones et al., 1998 [89], Alexandrov et al., 1998 [92]) to approximate the output of the simulations. A surrogate (or metamodel) is an algebraic expression fit to a number of simulations. Traditionally, the locations where simulations are carried out were selected independently of the optimization, so that a surrogate fitting phase preceded the optimization phase. More recently, global optimization algorithms that combine surrogate fitting and optimization have gained popularity, most notably the Efficient Global Optimization (EGO) algorithm (Schonlau, 1997 [93], Jones et al., 1998 [89]). These use adaptive sequential sampling with points added at locations with high potential of improving the design.

The research in the previous chapter described a methodology that sought to extend adaptive sampling surrogate techniques to locate multiple optima. The proposed approach was based on the conjunction of two principles to identify many candidate optima: i) dynamic partitioning of the search space and ii) local surrogate approximations. In this chapter, we examine the effectiveness of this approach in locating multiple optima along with two methods: multiple starting points for local optimization and EGO, which is perhaps the currently favored surrogate-based global optimization algorithm. Additionally, we compare the use of global surrogate approximations in our previously developed approach in place of local surrogates.

The next section of this chapter briefly summarizes the general idea behind surrogate-based optimization to motivate the two approaches used as comparisons in this study, multiple starting points of multiple local optimizations and the EGO algorithm, and describes why they are interesting for this study. Section 6.3 compares these methods on two two-dimensional numerical examples, minimization of the Branin-Hoo and Sasena functions.

6.2 Surrogate-Based Optimization

As described in Sec. 5.3, a surrogate is a mathematical function that (i) approximates outputs of a studied model (e.g. the mass or the strength or the range of an aircraft as a function of its dimensions), (ii) is of low computation cost and (iii) aims at predicting new outputs [84]. The set of initial candidate solutions, or points, used to fit the surrogate is called the design of experiments (DOE). Well-known examples of surrogates are polynomial response surface, splines, neural networks, and kriging. Using the surrogate, a new point is added based on some sampling criterion, and the surrogate is updated with the new point. This process continues as dictated by some stopping criterion. The general procedure for a problem with inequality constraints described by the limit states g proceeds as in Algorithm 6. The choice of how to use the surrogate prediction to find the optimum x^* is considered in

Algorithm 6 Overall surrogate-based optimization

1: t = 1 (initial state)
2: **while** $t \leq t^{max}$ **do**
3: Build surrogates $\hat{f}$ and $\hat{g}$ from $(\mathbb{X}^t, \mathbb{F}^t, \mathbb{G}^t)$
4: Optimization to find $\hat{x}^*$ (see Algorithm 3)
5: Calculate $f(\hat{x}^*)$ and $g(\hat{x}^*)$
6: Update database $(\mathbb{X}^{t+1}, \mathbb{F}^{t+1}, \mathbb{G}^{t+1}) \cup (\hat{x}^*, f(\hat{x}^*), g(\hat{x}^*))$
7: $t = t + 1$
8: **end while**

the next two sub-sections. There is the choice of simply solving original optimization problem (i.e, minimizing $\hat{f}$) by solving Eq.(5–2), but there are many popular in-fill sampling criteria that have been developed. The following two sub-sections expand on two options to find the optimum x^* .

$$\begin{aligned} \underset{x \in \mathcal{S} \subset \mathcal{R}^n}{\text{minimize}} \quad & \hat{f}(x) \\ \text{subject to} \quad & \hat{g}(x) \leq 0 \end{aligned} \tag{5–2}$$

6.2.1 Multiple-Starting Points

In this research, we focus on local, gradient-based algorithms that remain efficient in high dimensions, but have the disadvantage of being highly dependent on the starting point.

The choice of the starting point or "initial guess" can affect the ability of a local algorithm to find the global optimum. Note that stochastic methods are also affected by the initial configurations (e.g., the initial population in genetic algorithms). An optimizer that uses gradients may not find the global optimum if its starting point is in the basin of attraction of a poorer local optimum. To overcome this, multiple starting points are often used, in order to take multiple trajectories to find a solution. Thus, the use of multiple starting points is good practice when using such algorithms. There is the possibility of obtaining as many solutions as starting points, though not all solutions may be unique as some starts may find the same solution. The choice of starting points is important, and typically comes from sampling methods (e.g., random sampling, grid sampling, Latin Hypercube sampling, etc.). There is also the option of halting the optimization for poor trajectories.

Using multiple starting points is a relatively simple approach that can become prohibitively costly if the objective function or constraints is expensive. In problems where the cost of fitting and evaluating a surrogate is much less than the cost of evaluating the true objective function or constraints, using multiple starting points in conjunction with surrogates is a viable approach to find multiple optima. Thus, we can investigate the use of multiple starting points to find multiple optima by solving Eq.(5–2). In an iterative optimization scheme, the single best solution of the starts or the multiple points resulting from multiple starting points can added per iteration. Some random sampling is needed to prevent premature convergence. This research investigates both surrogate and multi-start approaches.

6.2.2 Efficient Global Optimization

The Efficient Global Optimization (EGO) algorithm [89] is a sequential sampling global optimization method. It starts by fitting a surrogate that comes with a prediction uncertainty. After fitting the surrogate, the algorithm iteratively adds points to the data set in an effort to improve upon the present best sample. In each cycle, the next point to be sampled is the one that maximizes the expected improvement, $E[I(x)]$. Though another variant of the EGO algorithm uses maximizes the probability of improvement on a targeted solution (EGO-AT

[51]), this work focuses on $E[I(x)]$. $E[I(x)]$ is a measure of how much improvement upon the present best sample we expect to achieve if we add a point. Rather than only searching for the optimum predicted by the surrogate, EGO will also favor points where surrogate predictions have high uncertainty. Therefore, EGO is able to balance exploitation of areas with small objective function values and exploration of areas with high uncertainty. For further details on the EGO algorithm, the reader may seek out one of the many papers on EGO, notably [89, 93].

Since EGO tries to improve upon the present best solution, it may not be possible for it to locate multiple optima if the values of the optima are very different or when some optima are very poor. For example, if a local optimum of a function is already found, the expected improvement may not be large enough to put a point in an area that contains another optimum with a poorer objective function value. For this reason, for locating multiple optima we restrict the comparisons of the EGO method to optima that are close in objective function value. Additionally, EGO is capable of adding more than one point per iteration [50, 94], but this research only considers the use of EGO in adding a single point per iteration.

6.3 Numerical Examples

This section compares the success and efficiency of the methods presented in this chapter on locating multiple candidate designs for two numerical examples. Five methods are compared: Two multi-agent methods that use dynamic partitioning but different surrogate setups, two single agent methods that add one or three points per iteration, and EGO. The methods considered are described in Table 6-1. The first case listed in Table 6-1 uses the dynamic partitioning described in Ch. 5, but shares a global surrogate among the agents rather than fitting a local surrogate to each agent. Using a global surrogate removes the complication of exchanging points between sub-regions in order to avoid ill-conditioning when fitting a local surrogates. Additionally, it may be more accurate than several local surrogates as shown in the previous chapter. The method that uses local surrogates with partitioning is still studied and listed as the second method in Table 6-1.

Table 6-1. Description of methods

Method	Description
Agents and Partitioning: Global (Sec. 5.4)	Uses multi-agents with dynamic partitioning. Agents use the same global surrogate. As many points as agents are added per iteration.
Agents and Partitioning: Local (Sec. 5.4)	Uses multi-agents with dynamic partitioning. Agent uses local surrogate for its sub-region. As many points as agents are added per iteration.
Single (Sec. 6.2.1)	Single global surrogate agent adding one point per iteration. Multiple starts are used and the best point in terms of feasibility and objective function value is chosen. Exploration occurs when a start gives a solution too near an already existing point. Exploration adds a point that maximizes the minimum distance from existing points.
Single: Multiple Points Per Iteration (MPPI) (Sec. 6.2.1)	Single global surrogate adding 3 points per iteration by 3 start points for local optimization. Exploration occurs when a start gives a solution too near to an already existing point. Exploration adds a point that maximizes the minimum distance from existing points.
EGO (Sec. 6.2.2)	Global surrogate using EGO algorithm to add one point per iteration

In all cases, the number of function evaluations was fixed at 100, including those required for the initial design of experiments, for both examples. The number of points added for the Single:MPPI case was set to three because it was observed that this was the mean number of points added in the multi-agent cases for the same examples. Thus, we fixed the number of points per iteration to three to provide a fairer comparison between the two methods.

As different methods listed in Table 6-1 add a different number of points per iteration (i.e., the Single:MPPI method adds three points per iteration, multi-agent method adds as many points as agents, and Single and EGO cases only add one point per iteration), we examine two values when comparing efficiency: number of function evaluations and number of iterations. The advantage of adding multiple points per iteration as in the Single:MPPI and multi-agent methods comes from parallelization between the processes that add the multiple points. Thus, comparing these methods to ones that add only a single point per iteration should be done based on the number of iterations rather than function evaluations. In the

results presented for the two examples in this section, we present both values. Note that for the Single Agent and EGO cases the iterations and function evaluations are equal as both only add a single point per cycle.

6.3.1 Experimental Setup

For the example considered in this study, there are no nonlinear constraints, so only the objective function is approximated by surrogates.. The three possible surrogates are kriging surrogates with quadratic, linear, or constant trend function. From this set, each agent chose the best surrogate based on $PRESS_{RMS}$. The set of surrogates and the minimum number of points used to fit each surrogate is 1.5 x the number of coefficients of a quadratic response surface. If the minimum number of points are not available when fitting local surrogates to the sub-regions, points are borrowed from neighboring sub-regions in the order of increasing distance to the agent center, and, if the requirement is still not met, then all available points are used.

For the agent cases with partitioning, the parameters are provided in Table 6-2. For

Table 6-2. Multi-agent parameters for example problems

Parameter	Value
Max # of function evaluations	100
Max # of agents	6
Initial/Min # of agents	1
Min distance between agent centers	10% of max possible distance in space
Min distance between points	0.2% of max possible distance in space
Min average silhouette	0.25
Min # of points in each agent after creation	4
Stagnation threshold	3
Number of starting points for local optimization	10

distances, we consider the distance in the normalized space as a fraction of the maximum possible distance between two points in the design space (e.g., for two-dimensional problems, we normalized by $\sqrt{2}$). For example, we use this distance when considering the minimum distance between centers and the minimum distance between data points as given in Table 6-2.

The initial size of the DOE for both example problems was 12, with the points sampled by Latin Hypercube Sampling. In each case given in Table 6-1, the results shown are the median of 50 repetitions (i.e, 50 different initial DOEs). The local optimization problems were solved with a sequential quadratic programming (SQP) algorithm [88]. DOEs are obtained using Latin Hypercube sampling and the *maximin* criterion for five iterations.

6.3.2 Branin-Hoo Test Function

The first example is the minimization of the Branin-Hoo test function, a common benchmark test function used in surrogate-based global optimization. It is given in Eq.(6–1).

$$f(x) = \left(x_2 - \frac{5.1}{4\pi^2}x_1^2 + \frac{5}{\pi}x_1 - 6\right) + 10\left(1 - \frac{1}{8\pi}\right)cos(x_1) + 8 \leq 0 \tag{6–1}$$

The domain of the function is $-5 \leq x_1 \leq 10$ and $0 \leq x_1 \leq 15$. There are three global optima of the Branin-Hoo function, for which $f = 0.40$. A contour plot of the Branin-Hoo function is shown in Fig. 6-1.

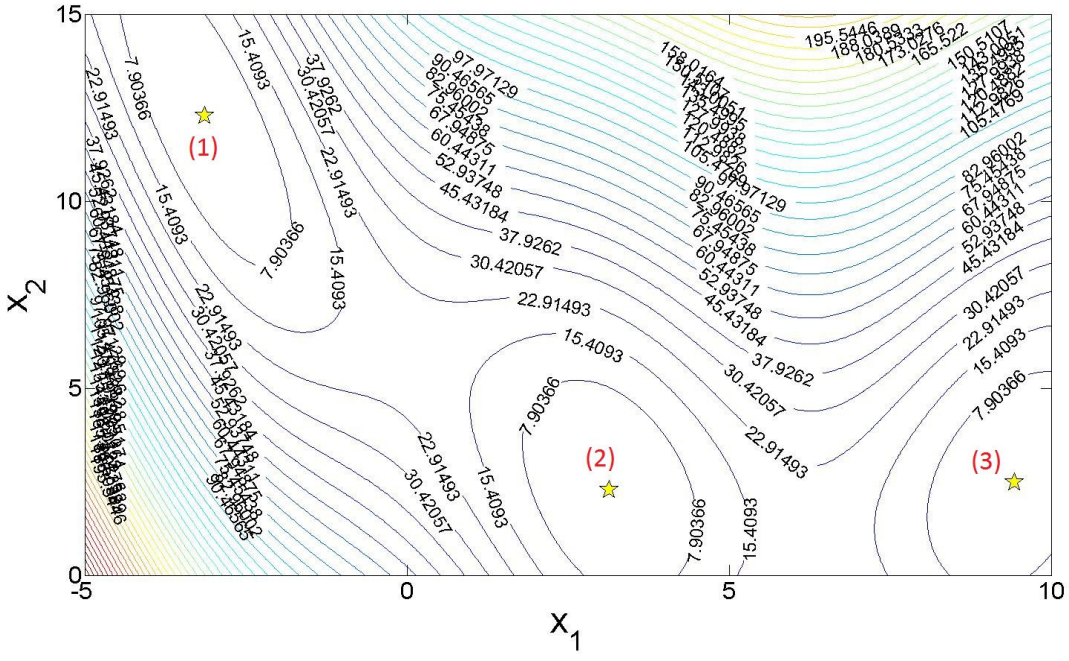

Figure 6-1. Contour plot of Branin-Hoo function showing three optima. For all optima, $f = 0.40$.

For 50 repetitions, the percentage of repetitions that successfully located a solution a 1% distance from the optimum is shown in Fig. 6-2, where the number of function evaluations shown does not include the evaluations required for the inital DOE of 12 points. This distance is the Euclidean distance normalized by the maximum possible distance between points in the design space (here, $\sqrt{2}$).

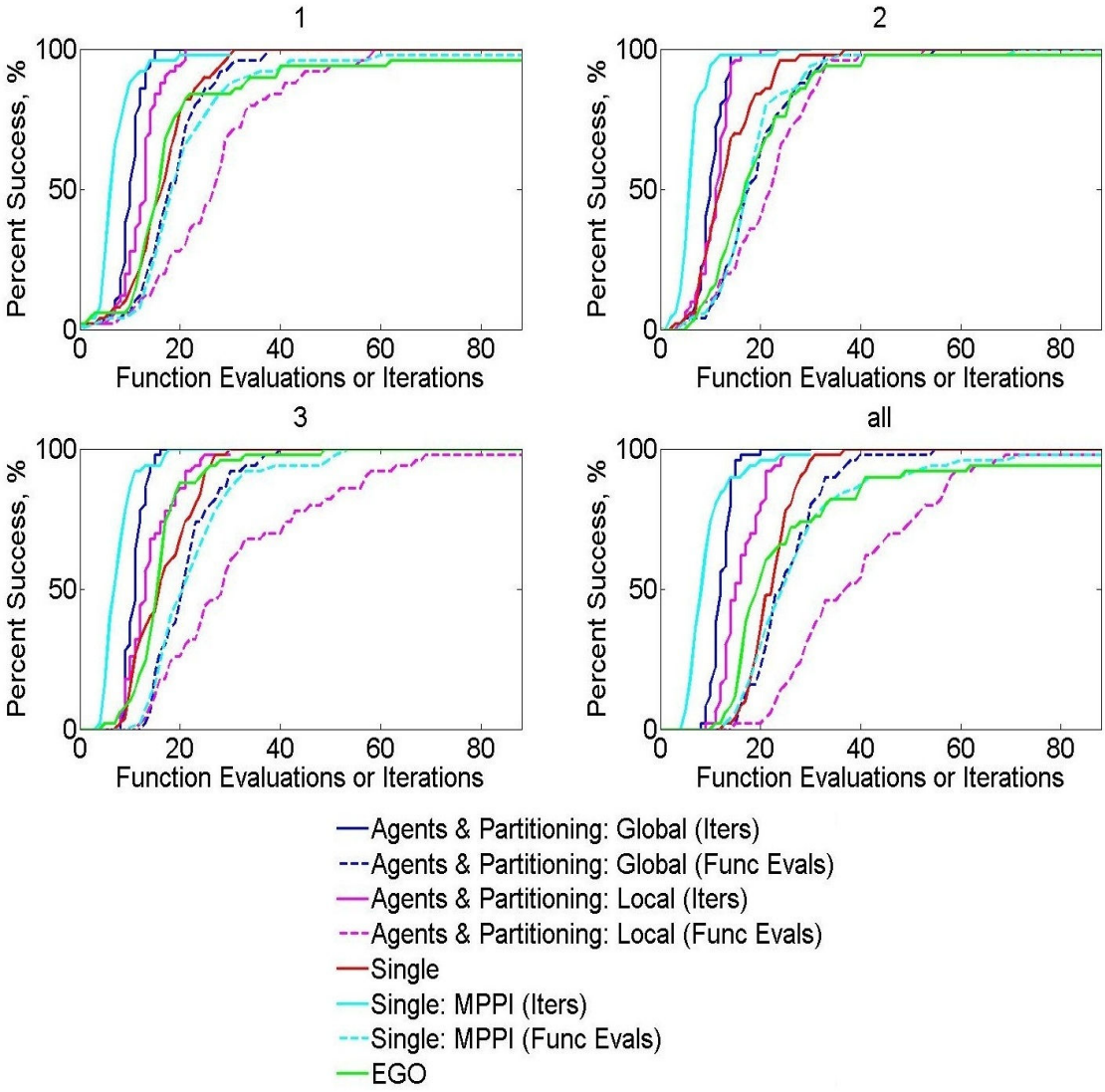

Figure 6-2. For the Branin-Hoo example, the percentage of 50 repetitions that found a solution within 1% distance from each optimum. For the cases that multiple points per iteration (agents and Single:MPPI) the value in terms of iterations is given by the solid lines and dashed lines for function evaluations.

First, if we make the comparison in terms of iterations, we observed that the Single:MPPI method is quickly successful in 80% of the repetitions. However, to reach percentages greater than 90%, the multi-agent method with the global surrogate located all optima with the fewest iterations. In terms of the number of iterations, the general trend was that the multi-agent method with a global surrogate reached 100% success with the fewest iterations followed by either the multi-agent method with local surrogates or Single:MPPI, then the single agent adding one point per iteration, and finally EGO. However, it should be noted that EGO actually found solutions near to the optima with a small number of function evaluations, but required more function evaluations to put a point within 1% of all optima as it was driven to search other regions with higher expected improvement due to larger uncertainty in the surrogate.

When considering the number of function evaluations, which does not account for the parallelization in the addition of multiple points per iteration, the single agent is the most efficient while the multi-agent method with local surrogates is the least efficient with the other methods falling in between.

Figure 6-3 displays the median objective function value with iterations and function evaluations for the solution nearest to each optimum. We observed that the Single:MPPI method had a median f value closest to the global optimum of $f = 0.39$ with the fewest iterations, and even the fewest function evaluations as compared to the other cases. In fact, the Single:MPPI method considering function evaluations was even more efficient than agents in terms of iterations. Otherwise, we observed much of the same trends between the one-point-per iteration methods and the agent methods.

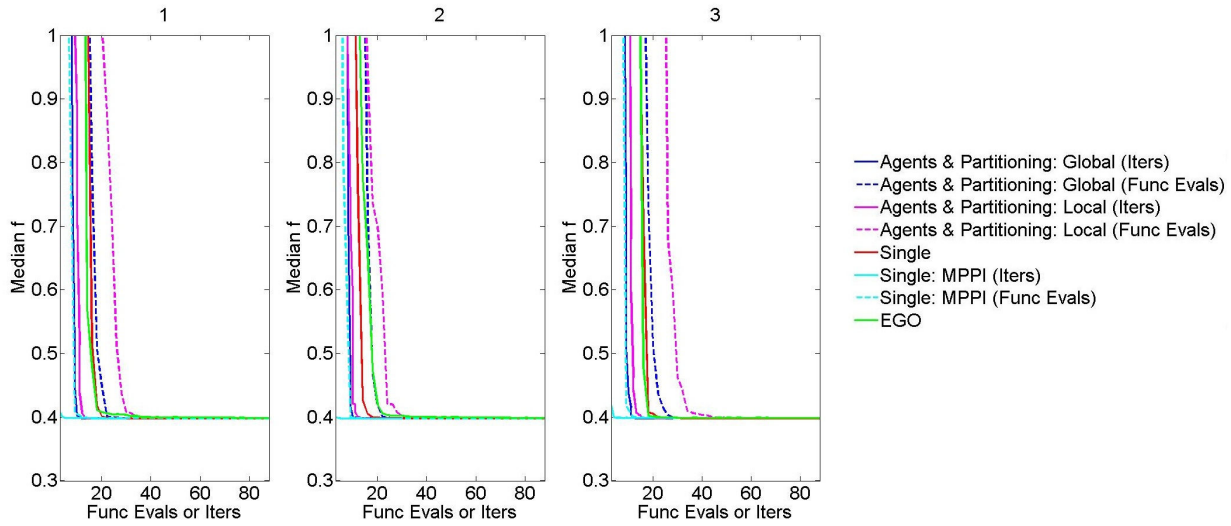

Figure 6-3. For the Branin-Hoo example, the median objective function of the solution nearest to each optimum. For the cases that multiple points per iteration (agents and Single:MPPI) the value in terms of iterations is given by the solid lines and dashed lines for function evaluations.

Figure 6-4 displays the placement of points in the design space after 100 total function evaluations for each method for a single repetition. It is observed that the single agent method put many points around the optima and only few points in the rest of the design space in exploration. In contrast, the Single:MPPI method both clustered points around the optima and filled the design space. The EGO method did not put nearly as many points around the optima and put many points in exploration in the design space, which is consistent with its goal of searching in areas with promising improvement.

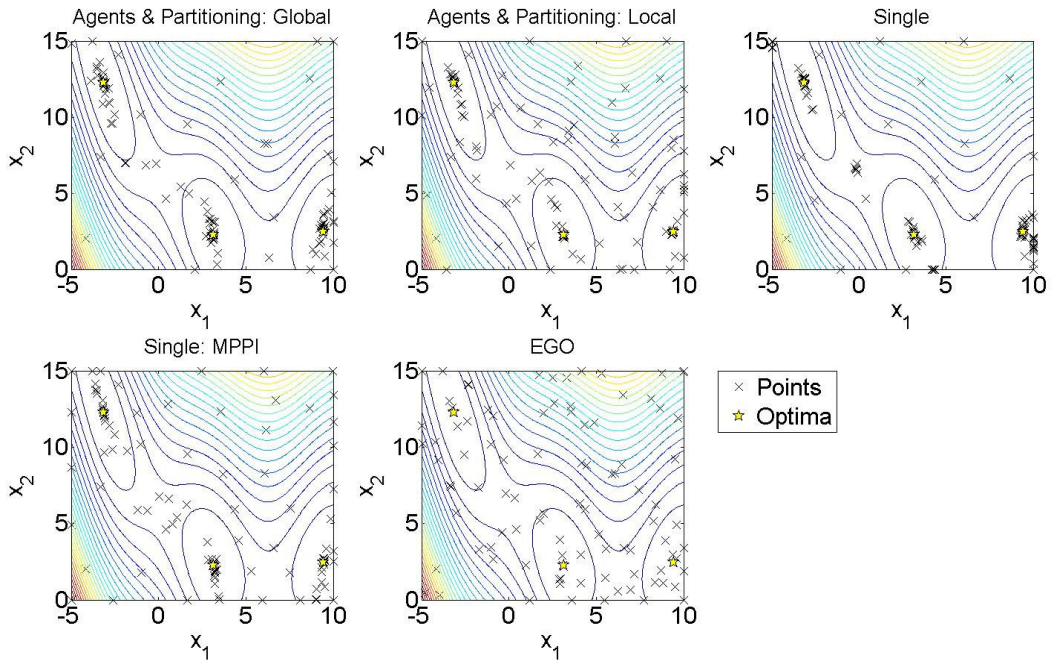

Figure 6-4. For the Branin-Hoo example, the plot of the points found by different methods for one repetition

The placement of points for the multi-agent cases was quite different when using global and local surrogates. While both put many points around each optimum, local surrogates resulted in many points away from the optima. This was partially due to the error in the surrogate, which predicted good objective function values away from the optima. To measure the error, we calculated the error at 1000 test points by e_{rms}. The e_{rms} normalized by the estimated range of the Branin-Hoo function is provided in Fig. 6-5.

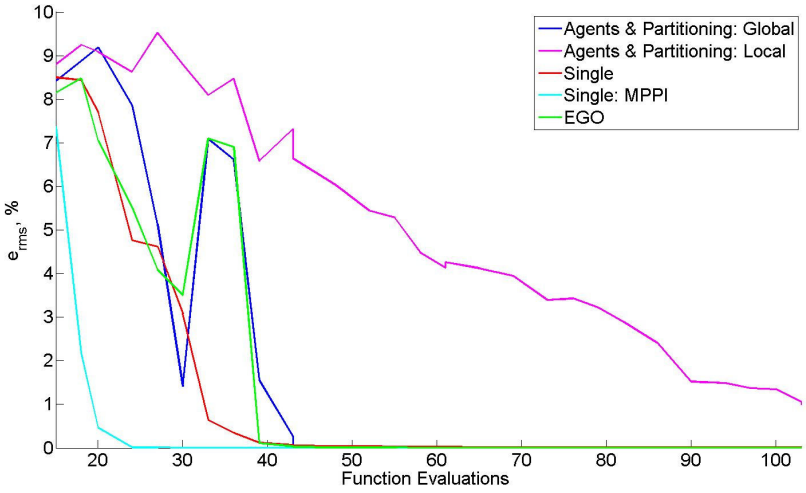

Figure 6-5. For the Branin-Hoo example, the error at 1000 test points with e_{rms} as the percentage of the estimated range of the function

It was observed that local surrogates were the least accurate, while the single global surrogate in the Single:MPPI method had less than 1% error after 20 function evaluations.

After observing that agent method using the global surrogate was only slightly less efficient than using a single agent adding 3 points per iteration, we examined the case with a constant 3 agents (3 sub-regions) and compared it to the Single:MPPI method adding three points per iteration. This simulates a case when three computing nodes are available, and all resources are used by assigning one agent to one node. Recall, that we previously set the initial number of agents at one, and let the number of agents evolve over time while setting the maximum number of agents at six. Figure 6-6 displays the percentage of 50 repetitions that located a solution with 1% distance from each optimum with iterations and function evaluations.

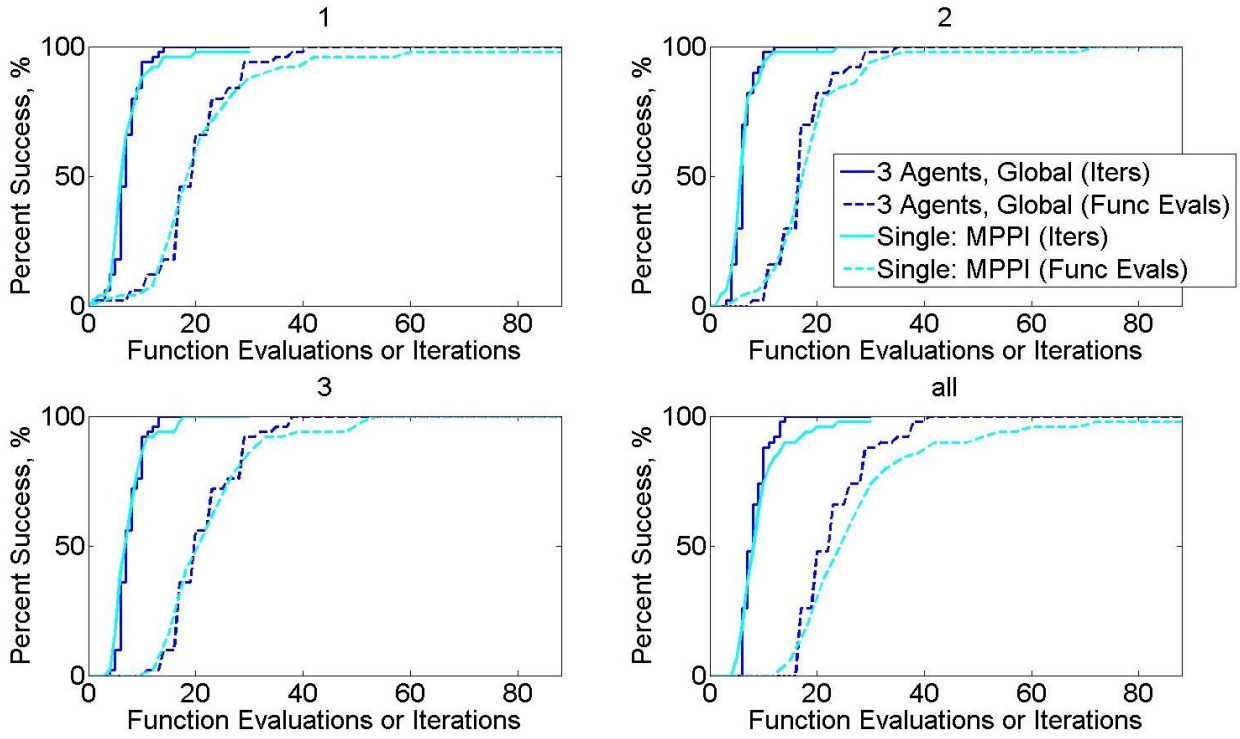

Figure 6-6. For the Branin-Hoo example, a comparison between the percentage of 50 repetitions that found a solution within 1% of the each optimum for the a constant 3 agents with a global surrogate and the Single: MPPI approach. Note that both methods add three points per iteration.

It was observed that the rate at which 100% success was achieved was quite similar between the two cases, with the agent method slightly more efficient. Therefore, efficiency may be increased by maximizing the use of computational resources by setting a constant number of agents rather than letting the number of agents evolve over time. However, it should be noted that Single:MPPI only allows three starting points in the design space, whereas the three agents each have ten starting points in the design space, for a total of 30 starting points. Thus, it is not entirely unexpected that the three agents achieve success at a slightly higher rate as they choose from 10 points to find the best point per iteration as compared to one. This shows that spreading out a large number of local searches in the design space, which is done by adding multiple points per iteration with the single global surrogate, may simply be as effective as partitioning of the design space.

6.3.3 Sasena Test Function

The second example problem, is the minimization of the Sasena function, which was used by Sasena under the name “mystery” function due to its unknown origin[95].

$$f(x) = 2 + 0.01(x_2 - x_1^2)^2 + (1 - x_1)^2 + 2(2 - x_2)^2 + 7sin(0.5x_1)sin(0.7x_1x_2) \tag{6–2}$$

The domain of the function is $0 \leq x_1, x_2 \leq 5$. A contour plot of the Sasena function is shown in Fig. 6-7. There are four optima, as shown in the figure, but the values of optima 3 ($f = 12.7$) and 4 ($f = 33.2$) are 40% and 90% from the global optimum ($f = -1.46$) in terms of the range of the function (38.6). Optimum 2 ($f = 2.87$), which has 11% difference from the global optimum is the only competitive optimum. Therefore, it is expected that the methods compared here are only effective at locating optimum 1 and 2.

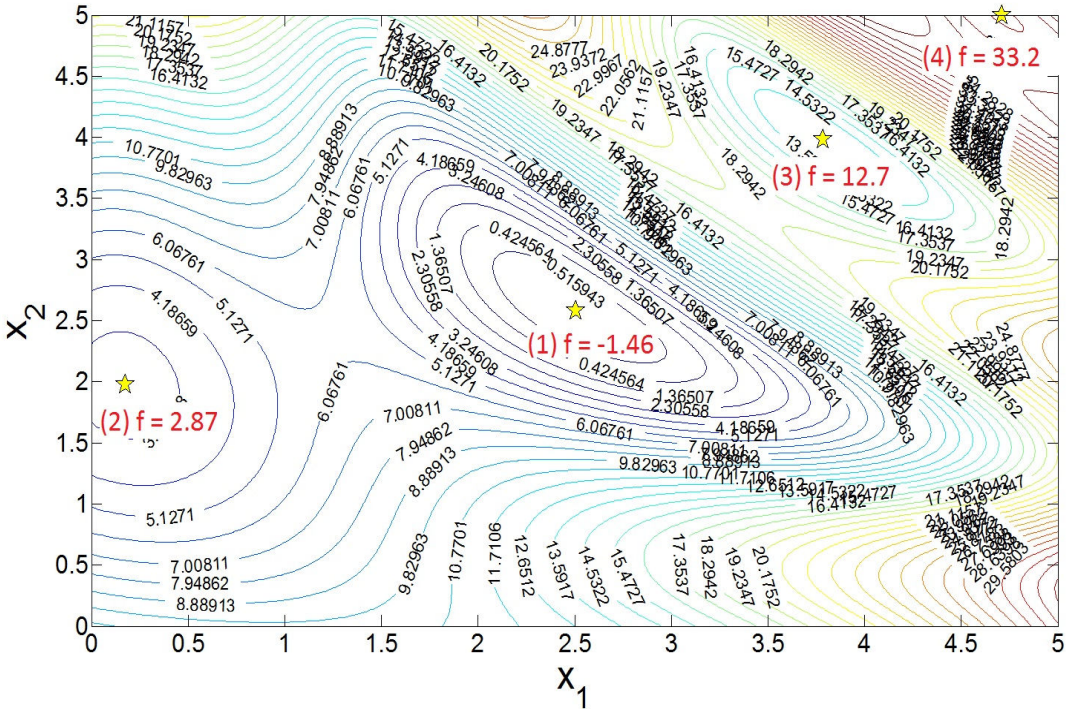

Figure 6-7. Contour plot of Sasena function showing four optima

In addition to its poor objective function value, optimum 4 has a small basin of attraction. In cases where the model that is being optimized has error, such small regions are may be wiped out by errors so a design in this region could be vulnerable.

For 50 repetitions, the percentage of repetitions that successfully located a solution a 1% distance from the optimum is shown in Fig. 6-8. We observed very little success at locating all optima by all methods, which was not unexpected as optima 3 and 4 are poor in comparison to the top two optima.

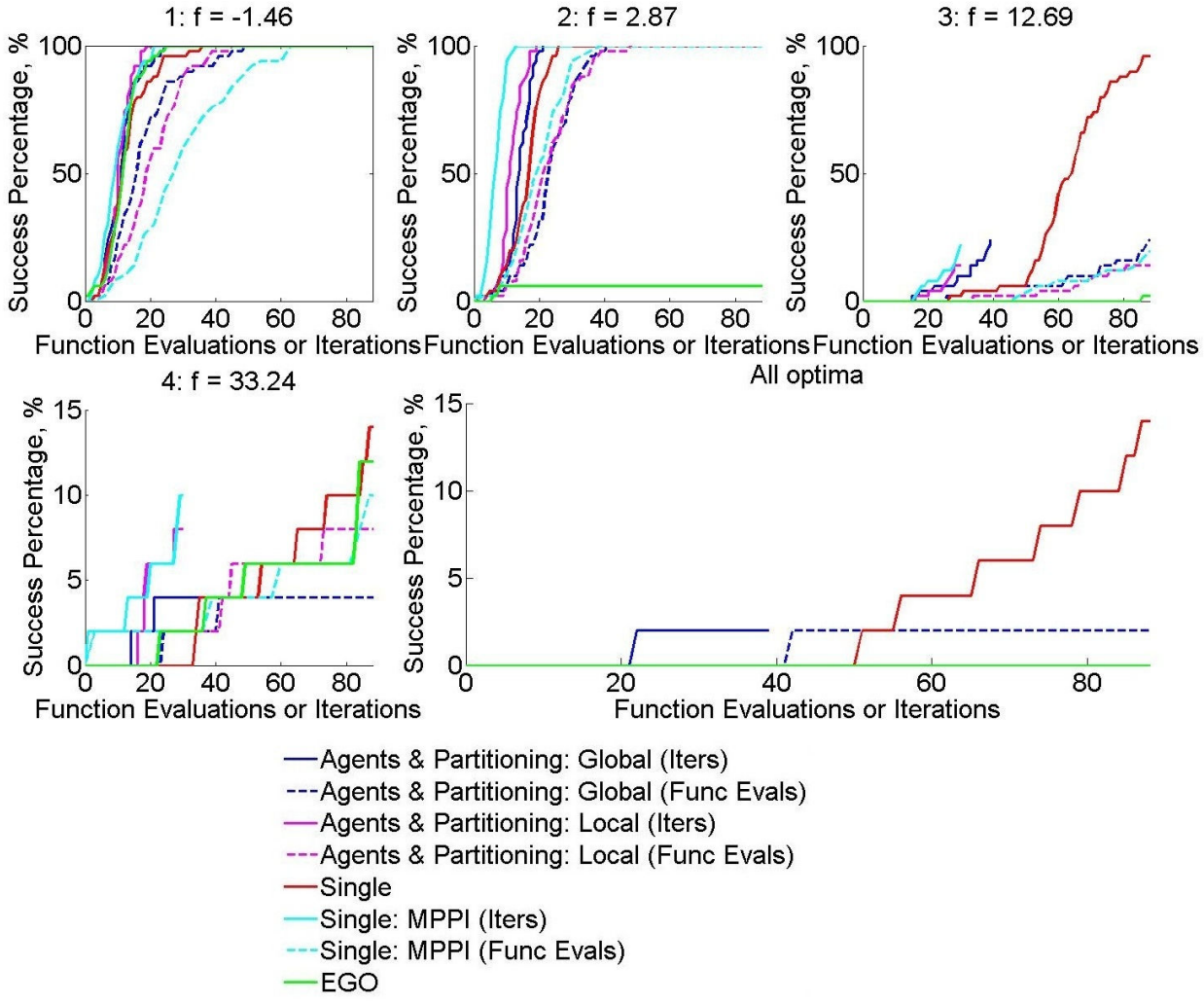

Figure 6-8. For the Sasena example, the percentage of 50 repetitions that found a solution within 1% distance from each optimum

When the comparison is made in terms of number of iterations, the methods that call for parallelization of the optimization processes (i.e, the multi-agent methods and Single:MPPI) outperform the one-point-per-iteration single agent and EGO algorithm. The Single:MPPI method again achieves a high percentage of successes with only a few iterations for optima 1 and 2, but the rate of success for both multi-agent cases is comparable for the global optimum. Another thing to note is the comparable performance of the multi-agent method with local surrogates compared to the global surrogate, which was not observed in the Branin-Hoo example.

It was also observed that EGO was efficient in locating the global optimum, but only had under 10% success in locating optimum 2. Based on this example, the current implementation of EGO has less potential to be successful in locating multiple optima when the optima are not almost equal.

When comparing the efficiency in terms of number of function evaluations, the one-point-per-iteration single agent is the most efficient. In fact, the single agent is able to locate optimum 3 in 90% of the repetitions. This is because the single agent locates optima 1 and 2 in early iterations, and is able to put points in the other parts of the space to locate optimum 3.

Figure 6-9 displays the median objective function value with iterations and function evaluations for the solution nearest to each optimum. We observed that the Single:MPPI method had a median f value closest to optima 1, 2, and 3 with the fewest iterations, and in most cases, the fewest function evaluations. Additionally, it was observed that for optimum 3, the median f for the Single:MPPI method is quite close to the true value, which was not clear when examining the success percentage. For optimum 4, it was observed that the nearest solution for all cases except Single:MPPI had a median f of 35.9, which corresponds to a space-filling point at the corner of the design space at $(5, 5)$.

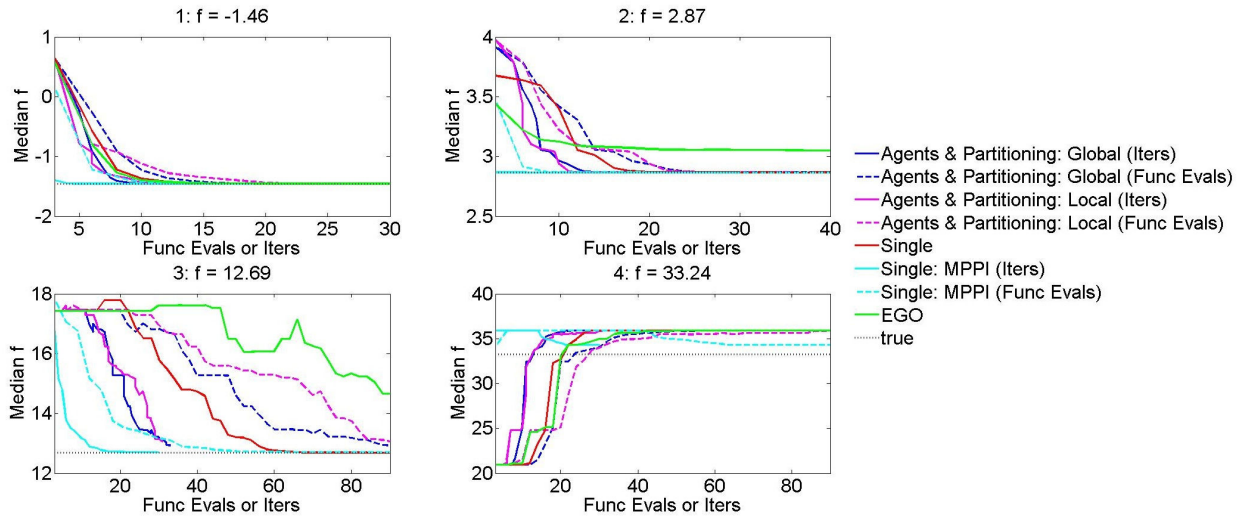

Figure 6-9. For the Sasena example, the median objective function of the solution nearest to each optimum. For the cases that multiple points per iteration (agents and Single:MPPI) the value in terms of iterations is given by the solid lines and dashed lines for function evaluations.

The error of the surrogate approximations at 1000 test points is shown in Fig. 6-10. As in the Branin-Hoo example, it is observed that the single surrogate with multiple points per iterations was the most accurate and the local surrogates from the multi-agent system were the least accurate.

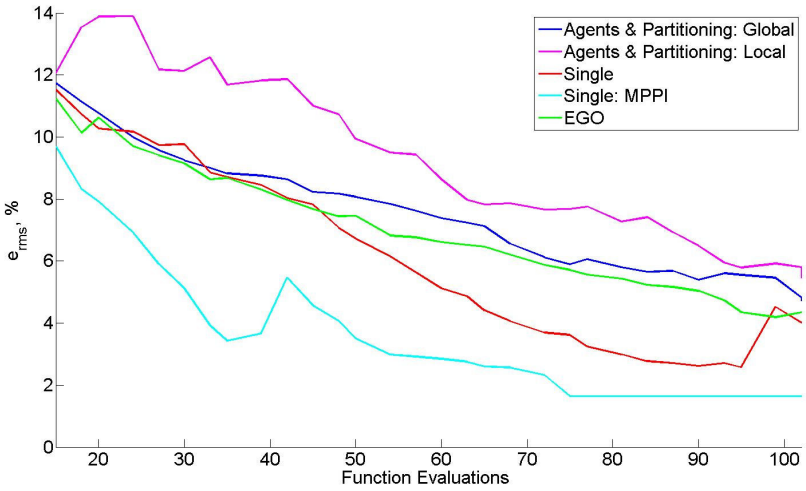

Figure 6-10. For the Sasena example, the error at 1000 test points with e_{rms} as the percentage of the estimated range of the function

Finally, we compared the success in locating a solution within 1% distance from each optimum using a constant 3 agents with a global surrogate and the Single:MPPI method. In both cases, three points are added per iteration. The results are shown in Fig. 6-11.

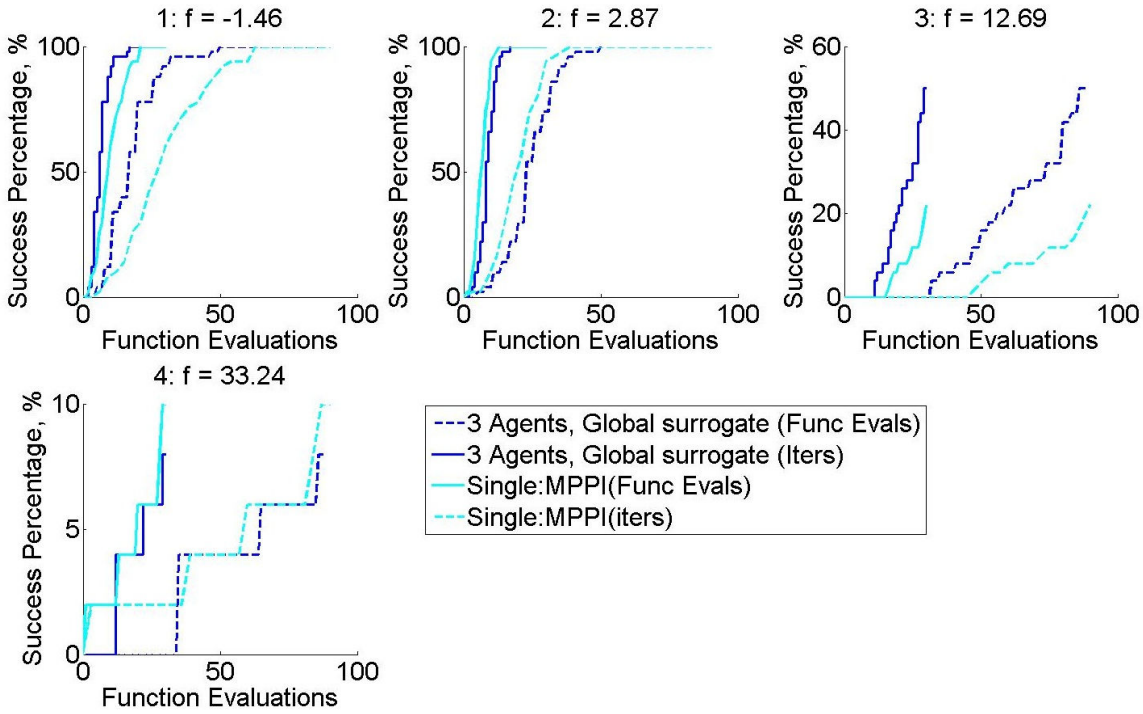

Figure 6-11. For the Sasena example, a comparison between the percentage of 50 repetitions that found a solution within 1% of the each optimum for the a constant 3 agents with a global surrogate and the Single: MPPI approach. Note that both methods add three points per iteration.

For the optimum 1, it was observed that the multi-agent method was slightly more efficient in achieving 100% success, but for optimum 2, the Single:MPPI method was only slightly more efficient. For optimum 3, the agent method had a slightly higher success percentage, while the success percentage was below 10% for both methods for optimum 4. As in the Branin-Hoo example, this showed that efficiency of the agent method may be increased by maximizing the use of computational resources by setting a constant number of agents. More interestingly, we observed again that spreading out local searches was nearly as successful and efficient as using agents and partitioning.

6.4 Discussion and Summary

This chapter provided a comparison of the success and efficiency in locating multiple optima by different surrogate-based optimization methods. Our previously developed multi-agent method that dynamically partitions the design space was compared against the EGO algorithm and a simple method that uses multiple starts in the design space to either add one or several points in an iteration. It was observed that EGO has the potential to locate multiple optima when optima functions values are similar, while the other methods presented here have this ability for optima that are within 11% of the range of the function. In practice, this is an ideal scenario as one would not want to waste resources on searching for poor optima.

The most efficient methods of those studied here aimed to take advantage of parallel computing for optimization. The use of multiple starting points for local optimization and adding multiple points per cycle proved to be a simple yet efficient method that warrants further research. The multi-agent approach, which involves optimization in several dynamically changing sub-regions in parallel, was also shown to be efficient in locating competitive optima. This shows that the benefit of partitioning the design space is that it helps spread local searches throughout the design space, and also increases the potential for parallelization.

We observed that the error in local surrogate approximations by the multiple agents was larger compared to a global surrogate. Additionally, we did not observe that local surrogates outperformed the global surrogate in either test problem, which supports the study in Appendix E that compared the accuracy of global to local surrogates for several test functions. For these reasons, it may be possible to only use a global surrogate, which removes the complication of exchanging points between agents to fit local surrogates.

In the future, a more in-depth look at the advantages of using multiple points per iteration can be studied. There is the possibility to explore asynchronous agents that partition the starting points for local optimization in the space and update the global surrogate as new points are added.

CHAPTER 7
CONCLUSIONS

The initial stages of design include the formulation of the optimization problem, including objective functions and constraints, and often include building a computational model with which to perform the initial design optimization. However, there is uncertainty in the process, which stems from the inability to perfectly formulate the optimization problem, inherent uncertainties in the design, and the uncertainties in the computational model. Tests and redesign are often performed on candidate designs, which allows for the identification of dangerous designs that can be redesigned and also provides measures by which to calibrate computational models. This research considers two areas of the design of engineering systems: 1) the trade-off of the effect of a test and post-test redesign on reliability and cost and 2) the search for multiple candidate designs as insurance against unforeseen faults in some designs.

The main contributions of this research are as follows:

1. A methodology to quantify the effect of a single future test and redesign on performance and cost
2. An investigation on how to trade off performance and development costs by including the effect of a single future test and redesign, and additionally how this allows companies probabilistically set design and re-design rules
3. A dynamic partitioning method of the design space that combines surrogates and local search to locate multiple candidate designs

First, a methodology to quantify the effect of a single future test and redesign on performance and cost was presented for fixed design and redesign rules. This method was based on sampling computational and experimental errors to simulate alternative future test outcomes, for which the decision to design or redesign was made. Two methods of calibration and redesign were presented. In one method, a simple correction factor based on the ratio of the simulated experimental measurement to the predicted value from the computational model was used in calibration, and redesign was performed deterministically to restore the initial level of safety of the design as dictated by a required safety margin. The

second method used Bayesian updating to update the initial computational error distribution and redesigned to meet a targeted reliability level given the updated error distribution. It was observed these methods provided estimates of the distribution of the probability of failure and performance of a design after test and redesign.

As an extension of the previous research, it was shown that the probabilistic quantification of the effect of the future test and redesign could be used to trade off performance and development costs by setting design and redesign rules. This research considered deterministic design and redesign rules, which are representative of current design practice used presently in industry. In this study, it was shown that the optimal trade-off called for initially conservative designs with large safety margins, which were made less conservative but with increased performance with increasing redesign (development) costs. This result was compared to the opposite approach in which a minimum required safety margin is given, which reflects the practice of regulatory agencies providing minimal required safety margins and factors.

The third area of research focused on locating multiple candidate designs by a combination of dynamic design space partitioning and surrogate-based optimization by mutliple local searches in sub-regions. This research focused on how to partition the design space such that the center of each region was located on a local optimum, while creating regions to explore the design space and merging regions that converged to the same area. The coordination between regions for surrogate-fitting, optimization, and exchange of design points was inspired by multi-agent approaches seen in distributed optimization algorithms that take advantage of the decomposition of the optimization formulation. This research mainly explored the use of local and global surrogates, where a local surrogate was used in each region of the design space in order to provide a more accurate approximation of the local behavior. This method was compared to a relatively simple approach in which a single surrogate using multiple starting points for local optimization over the entire design space. It was observed that the success of the partitioning method was primarily due to the use

of multiple starting points for local searches in the space. In effect, this led the multi-agent method to exploit regions of predicted low function value and only explore sparsely populated regions of the design space when this was not possible. Additionally, it was found that the success and efficiency of the partitioning with local versus global surrogates method may be dependent on the degree of difficulty in approximating the behavior with surrogates. For several test problems, it was found that using local surrogates was not as advantageous as a single global surrogate. It was also observed that there may be large gains in efficiency if the optimization in the regions is parallelized.

7.1 Perspectives

Based on the research presented in this dissertation, future research includes three tasks: 1) efficient identification of individual local optima, 2) establishing the range of acceptable designs based on the vulnerability of the best optima 3) distributed implementation of the methods.

7.1.1 Efficient Identification of Individual Local Optima

While the research in Ch. 5 have shown that locating multiple optima with surrogates is a promising direction of research, there are remaining formidable challenges that can be addressed.

7.1.1.1 Isolating basins of attraction

The goal is to isolate and characterize the basins of attraction of each local optimum. In past implementations, only the performance of design points was considered to center the agents. Yet, one sub-region may span two or more basins of attraction, such that a local optimum may be missed because the optimization repeatedly finds the optimum with the lower objective function value. There is a need to develop an efficient method to detect that a sub-region contains more than one acceptable optimum.

Proposed approach. Since the center of the sub-region is at the best point in the sub-region in terms of the objective function value (and feasibility in constrained problems), the poorer other optima are not explicitly identified. The proposed improvement is to tag

the potential local optima that are found using multi-start local methods on the surrogates according to whether or not they satisfy optimality conditions.There should also be a distinction between optima inside a sub-region and optima at the boundary of a sub-region, as the boundaries between sub-regions are artifacts of the method but not real design constraints. For example, if there are three optima in two sub-regions, two centers may be located at the two centers, but one basin of attraction may span both sub-regions. Recognizing the position of the points at the boundary along with tagging the potential optima may aid in the creation of sub-regions that will lead to the isolation of basins of attraction.

7.1.1.2 Suspending or allocating few resources to unpromising sub-regions

Some sub-regions may appear to have local optima that are too poor to be worthwhile. It is important to not write-off these regions completely as they may contain a good optimum in a very narrow basin of attraction. However, search in the sub-region may be suspended or fewer expensive function evaluations may be allocated to this region until more promising sub-regions are explored. Developing such a criterion is an important step to make this type of method more efficient.

Proposed approach. A common stopping criterion found in global optimization is based on the convergence of the objective function value [96, 97]. For this research, it is proposed that the criterion to suspend search in a sub-region or allocate fewer resources to the region is based on objective function value, feasibility, size of the domain, and its vulnerability to modeling errors. Such a criterion would differentiate between relatively small regions with poor objective function values in which search may be suspended, and large regions with small function values which may still benefit from further exploration to identify more optima. In the DIRECT method, Jones et al. [98] allocated resources in the regions of the design space that represented the best compromises, according to Pareto dominance, between the objective function and the size of the unexplored neighborhood. It is proposed to extend such a multi-criterion rationale in guiding the search considering i) the performance of the designs

and ii) the density of the starting points in the agent sub-regions, and (iii) vulnerability indices as the criteria for allocating computing resources. With such an approach, narrow basins of attraction will be found early if they are in a region of good objective functions, and vice versa, which matches the practical interest they may have (an optimum in a narrow valley surrounded by poor performance designs is likely to be too unstable for practical purposes).

7.1.2 Vulnerability Analysis and Range of Acceptable Objective Functions

Chapters 3 and 4 presented a methodology that sought to model the effect of errors on the eventual mass of a design by simulating futures where the errors force redesign based on bounds on modeling errors. This was done assuming that the errors are small to moderate and future tests that will reveal them to require only re-calibration of the analysis. The research demonstrated that a design can significantly change when considering errors in combination with tests and redesign to check for and compensate for these errors. By considering the effect of errors and simulating possible futures, the vulnerability of a design to be affected by errors can be measured by the probability of redesign (the probability that the design does not meet requirements), while performance measures, such as mass, give an indication of the extent of the changes to the design that have to be made to compensate for the errors.

Additional research in this area has extended this methodology to multiple failure modes [68] and also sought to model the effect of unexpected large errors [99]. This work can be extended to allow the comparison of multiple designs and to estimate the probability of islands of feasibility being wiped out.

Proposed approach that takes advantage of modeling of the effect of future tests and redesign. The present approach is based on Monte Carlo simulations of multiple possible futures associated with different error magnitudes. The associated computational cost is high, and therefore not feasible to be incorporated inside a global optimization algorithm. We propose to develop approximate estimates of the mean objective function increment after future redesign as well as its standard deviation. This will be based on a

simple re-calibration approach that we have explored in Ch. 3. It is also proposed to develop estimates of the probability that an island of feasibility associated with a given local optimum will completely disappear. This can happen when the island is narrow due to small errors that are within the expected range anticipated by the designer. For example, for the example presented in Ch. 5, an error of 12 K in the temperature model of the ITPS will wipe out Region 2 of Figure 3 due to thermal failure. However, feasible regions may also disappear due to unexpected appearance of overlooked failure modes or objective functions. It is proposed to allow designers to assign such probabilities based on the closeness of the design to their past experience. Designs that appear to be mere refinements of previous experience may be assigned low probability while designs that look very different may be assigned higher probabilities.

APPENDIX A
COMPARISON OF BAYESIAN FORMULATIONS

In a rigorous formulation of the likelihood function, we would calculate the conditional probability of obtaining the measured temperature when the true temperature of the test article is T, as shown in Eq.(A–1)

$$l_{test}(T) = \begin{cases} \frac{1}{0.14T} & \text{if } \left|\frac{T-T_{meas}}{T}\right| \leq 0.07; \\ 0 & \text{otherwise.} \end{cases} \tag{A–1}$$

In the illustrative example in Section 3.3.2.1, we simplified this formulation so that we calculated the conditional probability of obtaining T given T_{meas}, as shown in Eq.(3–16). In Fig.A-1, we compare the two likelihood functions and the resulting updated distribution of $f^{upd}_{test,Ptrue}$ for the case in the example.

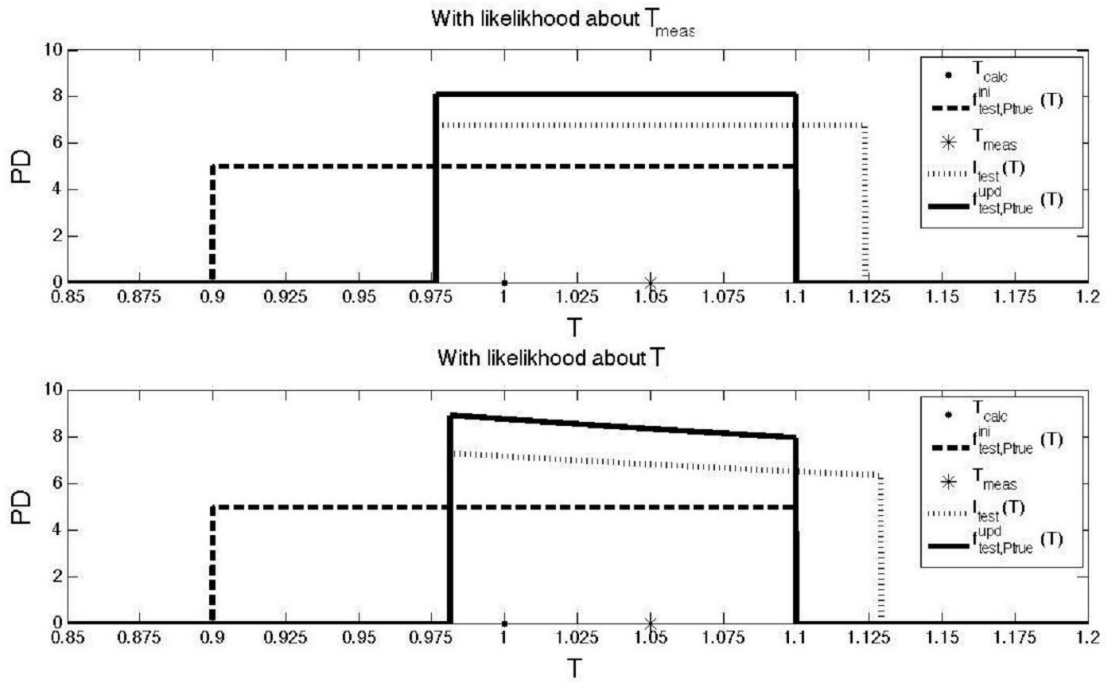

Figure A-1. Illustrative example of Bayesian updating using the likelihood about T_{meas} (top), and the likelihood about T (bottom)

The figures show only a small difference in the bounds of the updated temperature distribution and the values of the pdf. A comparison is shown in Table A-1.

Table A-1. Comparison of $f^{upd}_{test,Ptrue}$ with different formulations of the likelihood function

Comparison	$l_{test}(T)$ about T_{meas}	$l_{test}(T)$ about T
Bounds where updated distribution is nonzero	[0.9765, 1.1]	[0.9813, 1.1]
Max $f^{upd}_{test,Ptrue}$ and location	8.1 on [0.9765, 1.1]	8.9 at T = 0.9813

APPENDIX B
EXTRAPOLATION ERROR

In this research, it was assumed the variation in the magnitude of the extrapolation error e_{extrap} was linear with the distance of the design from the test design. The choice of this extrapolation error is very much up to the analyst, as it is a measure in the variation of the errors from the updated Bayesian estimate away from the test design. Here, we examine the effect of an assumption that the extrapolation error is quadratic, as expressed in Eq.(B–1).

$$e_{extrap} = (e_{extrap})_{max} \left(\frac{||d - d_{test}||}{\Delta d_{lim}} \right)^2 \tag{B–1}$$

For the example problem in Section 3.5, we estimated e_{extrap} to be 2% when d is changed by $\pm 10\%$ from d_{test}. With the quadratic extrapolation error, this is expressed as in Eq.(B–2). Because of this requirement, the magnitude of the quadratic extrapolation error is smaller for designs at a distance less that $\pm 10\%$ away from the test design but larger at greater distances compared to the linear variation. We present this comparison in Fig.(B-1). Examining the same 10000 possible outcomes of the future test with probabilistic redesign ($p_{f,target} = 0.01\%$), the results in Table B-1 were obtained.

$$e_{extrap} = 0.02 \left(\frac{||d - d_{test}||}{0.1||d_{test}||} \right)^2 \tag{B–2}$$

The results show that there is improved agreement between the true and analyst estimated probabilities of failure, as well as a slightly decreased mass and variation in the mass, with the quadratic variation in extrapolation error. Since the extrapolation error is smaller at a distance less than $\pm 10\%$ away from the test design, the agreement between the true and analyst-estimated probabilities of failure is better with the quadratic extrapolation error. However, the agreement still suffers due to the large magnitude of the extrapolation error at distances greater than $\pm 10\%$.

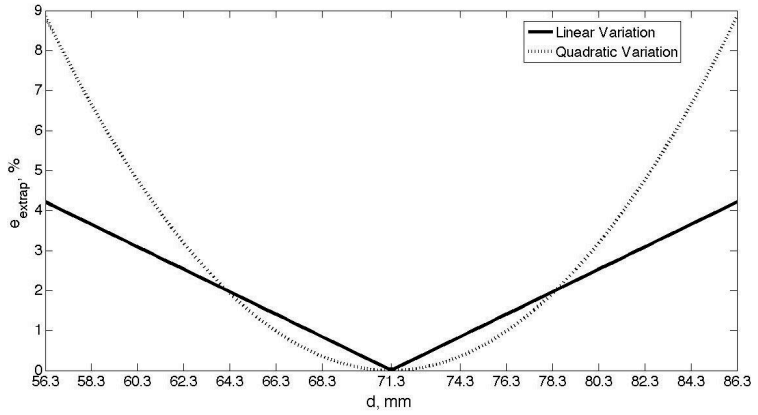

Figure B-1. Comparison of the e_{extrap} with linear and quadratic variation with the distance of the design from the test design (test design is $d = 71.3$ mm)

Table B-1. Calibration by the Bayesian updating approach with probability of failure based redesign ($p_{f,target} = 0.01\%$), quadratic extrapolation error, and no bounds on redesign d_S

Variation in e_{extrap} with d_s	Parameter	Original	Mean	Standard Deviation	Minimum	Maximum
Linear	d_S (mm)	71.3	65.3	8.9	47.5	77.7
	mass (kg/m^2)	35.1	33.7	2.1	29.5	36.5
	$p_{f,true}$ (%)	0.12	0.003	0.016	0	0.100
	$p_{f,analyst-corr}$ (%)	0.12	0.007	0.004	0	0.015
Quadratic	d_S (mm)	71.3	66.4	7.3	54.4	77.1
	mass (kg/m^2)	35.1	33.9	1.7	31.1	36.4
	$p_{f,true}$ (%)	0.12	0.004	0.019	0	0.100
	$p_{f,analyst-corr}$ (%)	0.12	0.007	0.004	0	0.015

APPENDIX C
SIMULATING A TEST RESULT AND CORRECTION FACTOR θ

As described in Sec. 4.3, a test is performed to verify a design, and the test is performed on a test article denoted by d_{test} and r_{test} to find the experimentally measured temperature ΔT_{meas}. For this design, we can calculate $\Delta T_{calc}(d_{test}, r_{test})$. We can relate both the measured and calculated temperatures to the true temperature of the test article by the true experimental and computational errors as

$$T_{test,true} = T_0 + \Delta T_{meas}(d_{test}, r_{test})(1 - e_{x,true}) = T_0 + \Delta T_{calc}(d_{test}, r_{test})(1 - e_{c,true}) \tag{C–1}$$

Rearranging this equation, we arrive at the correction factor $\theta = \frac{1-e_{c,true}}{1-e_{x,true}}$.

In this section, it is shown that the mass before and after redesign can be found using a surrogate that is a function of safety margin and difference between the allowable temperature T_{allow} and initial temperature T_0. A surrogate of of the probability of failure that is a function of the same two variables and the computational error e_c can be made as well.

As shown in Eq.(4–2), the initial design satisfies

$$T_0 + \Delta T_{calc}(d, r) + S_1 = T_{allow} \tag{C–2}$$

Rearranged so that $\Delta T_{calc}(d, r)$ is on the left hand side, this becomes

$$\Delta T_{calc}(d, r) = (T_{allow} - T_0) - S_1 \tag{C–3}$$

By Eq.(4–5)the redesign should satisfy

$$T_0 + \theta \Delta T_{calc}(d, r) + S_4 = T_{allow} \tag{C–4}$$

which rearranged so that $\Delta T_{calc}(d, r)$ is on the left hand side is

$$\Delta T_{calc}(d, r) = (T_{allow} - T_0)/\theta - S_4/\theta \tag{C–5}$$

By Eqs.(C–3) and (C–5), the two are equivalent if $(T_{allow} - T_0) = [(T_{allow} - T_0)/\theta]_{afterredesign}$ and $S_1 = S_4/\theta$. Therefore, ΔT_{calc}, along with its corresponding mass and probability of failure, is a function of $(T_{allow} - T_0)$ and S, where the values with and without redesign are related through θ. This allows the mass to be calculated simply using surrogates with the inputs $(T_{allow} - T_0)$ and S. A surrogate to obtain the probability of failure can also be obtained by including the computational error e_c as an input.

Note that $\Delta T_{calc}(d, r)$ does not need to be calculated because, for a given $(T_{allow} - T_0)$ and S_1, we can find $\Delta T_{calc}(d, r)$ by

$$(T_{allow} - T_0) - S_1 = \Delta T_{calc}(d, r) \tag{C–6}$$

When the correction is applied, then we evaluate if redesign is necessary by

$$\begin{aligned} &\text{Redesign if: } (T_{allow} - T_0) - \theta[(T_{allow} - T_0) - S_1] \leq S_2 \\ &\text{or } (T_{allow} - T_0) - \theta[(T_{allow} - T_0) - S_1] \geq S_3 \end{aligned} \tag{C–7}$$

which simplifies to

$$\begin{aligned} &\text{Redesign if: } (T_{allow} - T_0)(1 - \theta) + \theta S_1 \leq S_2 \\ &\text{or } (T_{allow} - T_0)(1 - \theta) + \theta S_1 \geq S_3 \end{aligned} \tag{C–8}$$

Kriging surrogates (quadratic trend function with a Gaussian correlation model) were used for the surrogates of the mass and reliability index. The accuracy of the surrogates was measured by the $PRESS_{RMS}$, a leave-one-out cross validation error measure, and the e_{RMS} at 50 test points. A summary of the surrogates is provdied in Table C-1.

Table C-1. Summary of surrogates

Surrogate	Inputs	# of Points for Fitting	$PRESS_{RMS}$ [1](%)	Test e_{RMS} [2](%)
β	$(T_{allow} - T_0)$, S , e_c	40	11	7
m	$(T_{allow} - T_0)$, S	20	0.5	0.1

1 $PRESS_{RMS} = \sqrt{\frac{1}{p} e_{XV}^T e_{XV}}$, where p is the number of points used for fitting and e_{XV} is the vector of the difference between the true value and the surrogate prediction

2 $e_{RMS} = \sqrt{\frac{1}{q} e_{test}^T e_{test}}$, where q is the number of test points and e_{test} is a the vector of the difference between the true value and the surrogate prediction

APPENDIX D
EFFECT OF ADDITIONAL UNCERTAINTIES

In Ch. 4 we formulated the probability of failure is calculated with the limit state g as

$$g_{true} = T_{allow} - T_{true}(d, r, v_0) \tag{4–7}$$

where

$$T_{true}(d, r, v_0) = T_0(1 - v_0) + (1 - e_{c,true})\Delta T_{calc}(d, r) \tag{4–6}$$

Given the uncertainties in v_0, ΔT_{calc}, e_c, and T_{allow}, we can calculate the variance of the limit state as

$$\sigma^2_{g,current} = T_0^2\sigma^2_{v_0} + \sigma^2_{\Delta T_{calc}} + \Delta T^2_{calc}\sigma^2_{e_c} + \sigma^2_{\Delta T_{calc}}e_c^2 + \sigma^2_{e_c}\sigma^2_{\Delta T_{calc}} + \sigma^2_{T_{allow}} \tag{D–1}$$

We use the subscript “current” to denote this as the limit state that is used in Ch. 4.

In Ch. 3 and in [100], the limit state was formulated as

$$g_{previous} = T^{det}_{allow} - T_{calc}(d, r)(1 - e_c) \tag{D–2}$$

for which the variance is

$$\sigma_{g_{previous}} = \sigma^2_{T_{calc}} + T^2_{calc}\sigma^2_{e_c} + \sigma^2_{T_{calc}}e_c^2 + \sigma^2_{e_c}\sigma^2_{T_{calc}} \tag{D–3}$$

In Ch. 4, we included the additional uncertainties in the initial temperature, calculated change and temperature, and allowable temperature to form a more realistic problem.

Let us consider two cases where redesign the combination of the test and redesign reduces the standard deviation of e_c for the design listed in Table D-1. The values of the uncertain variables are given in Table 3-1, for which the variables involved in the calculation of T_{calc} and ΔT_{calc} result in a standard deviation of 12.4 K in these values.

Using Eqs.(D–3) and (D–1), we calculate the standard deviation of the limit state g as shown int Table D-2. It was observed that the additional uncertainties, particularly the uncertainty in T_{allow}, reduced the effect of the test and redesign’s reduction of σ_{e_c} on the reduction of the standard deviation of the limit state. The reductions were more than two

Table D-1. Values of the uncertain variables in the limit states.

Distribution	Before Redesign	After Redesign Case 1	After Redesign Case 2
T_0		300 (deterministic)	
T_{calc}		N(550,12.4^2)	
ΔT_{calc}		N(250,12.4^2)	
T_{allow}		LN(660,16^2)	
e_c	N(0,0.069^2)[1]	N(0,0.0621^2)[2]	N(0,0.035^2)[3]

1 This is the standard deviation of the normal distribution that is equivalent to the uniform distribution of e_c between ± 0.12 (i.e., $\frac{0.12}{\sqrt{3}}$).
2 In case 1, redesign causes a 10% reduction in standard deviation of e_c.
3 In case 2, redesign causes a 50% reduction in standard deviation of e_c.

Table D-2. Standard deviation of the limit states before and after redesign. Note that the nominal value of e_c is 0.

Distribution	Before Redesign	After Redesign Case 1 (% change)	After Redesign Case 2 (% change)
$\sigma_{g_{previous}}$	39.9	36.4 (-9%)	22.7 (-43%)
$\sigma_{g_{current}}$	26.8	25.7 (-4%)	22.2 (-17%)

times larger using the previous formulation, which accounts for the differences in mean and 95th percentile of the probability of failure we observed in Ch. 4 and the work in the Ch. 3.

APPENDIX E
GLOBAL VS LOCAL SURROGATES

In this appendix, the accuracy of a single global surrogate over the design region is compared to several local surrogates fit in sub-regions. In this study we examine five two-dimensional functions and one six-dimensional function. Four of the two-dimensional functions were taken from a study by Xiong et al. [101], in which some functions were examined because they had visible non-stationary behavior (varying levels of smoothness or bumpiness in the space) such that the stationary assumption of a stationary covariance structure that underlies kriging does not hold. The six functions studied are listed below, where the functions that come from the study [101] are labeled.

1. Branin-Hoo:

$$f(x) = \left(x_2 - \frac{5.1}{4\pi^2}x_1^2 + \frac{5}{\pi}x_1 - 6\right) + 10\left(1 - \frac{1}{8\pi}\right)cos(x_1) + 8 \leq 0 \quad x_1\epsilon[-5, 10],\ x_2\epsilon[0, 15] \tag{6–1}$$

2. Sasena ("mystery function" in [101]):

$$f(x) = \underset{x_1,x_2\epsilon[0,1]}{} 2 + 0.01(x_2 - x_1^2)^2 + (1 - x_1)^2 + 2(2 - x_2)^2 + 7sin(0.5x_1)sin(0.7x_1x_2) \tag{6–2}$$

3. Function 3 [101]:

$$f(x) = sin(\frac{1}{x_1x_2}),\ x_1,x_2\epsilon[0.3, 1] \tag{E–1}$$

4. Function 4 [101]:

$$f(x) = x_1exp(-x_1^2 - x_2^2),\ x_1,x_2\epsilon[-2.5, 2.5] \tag{E–2}$$

5. Function 5 [101]:

$$f(x) = cos(6(x_1 - 0.5)) + 3.1|x_1 - 0.7| + 2(x_1 - 0.5) + \cdots 7sin(\frac{1}{|x_1 - 0.5| + 0.31}) + 0.5x_2\ x_1,x_2\epsilon[0, 1] \tag{E–3}$$

6. Hartman 6:

$$f(x) = -\sum_{i=1}^{q} a_iexp\left(-\sum_{j=1}^{m} b_{ij}(x_j - d_{ij})^2\right) \quad x_i\epsilon[0, 1] \tag{E–4}$$

In this instance of Hartman 6, $q = 4$ and $a = \begin{bmatrix}1.0 & 1.2 & 3.0 & 3.2\end{bmatrix}$ where

$$B = \begin{bmatrix} 10.0 & 3.0 & 17.0 & 3.5 & 1.7 & 8.0 \\ 0.05 & 10.0 & 17.0 & 0.1 & 8.0 & 14.0 \\ 3.0 & 3.5 & 1.7 & 10.0 & 17.0 & 8.0 \\ 17.0 & 8.0 & 0.05 & 10.0 & 1.0 & 14.0 \end{bmatrix}$$

$$D = \begin{bmatrix} 0.1312 & 0.1696 & 0.5569 & 0.0124 & 0.8283 & 0.5886 \\ 0.2329 & 0.4135 & 0.8307 & 0.3736 & 0.1004 & 0.9991 \\ 0.2348 & 0.1451 & 0.3522 & 0.2883 & 0.3047 & 0.3047 \\ 0.4047 & 0.8828 & 0.8732 & 0.5743 & 0.1091 & 0.0381 \end{bmatrix}$$

The test procedure can be described as follows:

1. Generate a DOE using LHS
2. Fit a global surrogate
3. Fit local surrogates: Partition the design space into n regions by choosing c random centers from the DOE and partition the space based on the distance of a point to the nearest center. Fit a surrogate in each region. Repeat for 10 random sets of centers.
4. Calculate error at 500 test points and then calculate e_{RMS} for global and local surrogates

This process is repeated for 50 DOEs for the size of 12, 22, 31, 41, and 50 points for the two-dimensional functions and 56, 80, 103, 127, and 150 for Hartman 6.

Due to the randomness in choosing centers, it is possible that some sub-regions may be small and hold only a small number of points. In order to avoid ill-conditioning in these cases, the nearest points from neighboring sub-regions used to build the surrogate. For both the quadratic response surface and kriging, the minimum number of points used to fit a surrogate was 12 for the two-dimensional problems and 56 for the six-dimensional problem.

Figure E-1 shows the test error at 500 test points, measured by the root mean square of the error, and normalized by the mean of the available data. Overall, it was observed that the kriging surrogate was more accurate than the quadratic response surface. It was observed that a global kriging surrogate was clearly more accurate for the Sasena function and function 4. For the other test problems, there was only a small observable distance in accuracy between global and local kriging, with global kriging seemingly slightly more accurate. At large DOEs, there is less of a difference in accuracy between global and local surrogates.

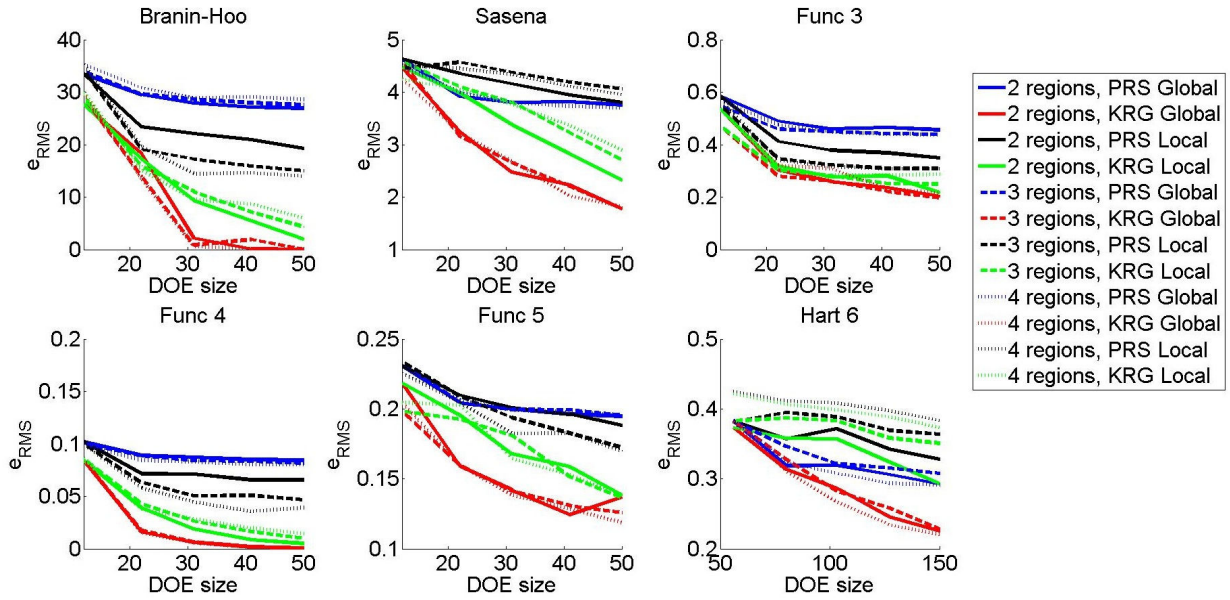

Figure E-1. For 4 equal sized regions, a comparison of the test error for global and local kriging surrogates.

From this study, we can conclude that several local surrogates generally do not carry an advantage over local surrogates. However, in this study, the sub-regions did not result from a partitioning scheme that considered function value; they were the results of randomly placed centers in the design space. It is not clear if dividing the design space into partitions that captured local behavior would improve the accuracy of the surrogate.

Additionally, knowing how to smartly split the design space would require an accurate estimation of the global behavior, which would come from an accurate global surrogate. In terms of optimization, accurate global surrogates could lead to a switch from optimization with a surrogate to local optimization with the true function in interesting regions rather than forming a local surrogate at the interesting region and continuing optimization with a surrogate.

REFERENCES

[1] Oberkampf, W. L., Deland, S. M., Rutherford, B. M., Diegert, K. V., and Alvin, K. F., "Error and Uncertainty in Modeling and Simulation," *Reliability Engineering and System Safety*, Vol. 75, 2002, pp. 333–357.

[2] Acar, E., Haftka, R. T., and Kim, N. H., "Effects of Structural Tests on Aircraft Safety," *AIAA Journal*, Vol. 48, No. 10, 2010, pp. 2235–2248.

[3] Melchers, R. E., *Structural Reliability Analysis and Prediction*, New York: Wiley, 1999.

[4] Fujimoto, Y., C., K. S., Hamada, K., and Huang, F., "Inspection Planning Using Genetic Algorithm for Fatigue Deteriorating Structures," *International Offshore and Polar Engineering Conference, Vol.4*, International Society of Offshore and Polar Engineers, Golden, CO, 1998, pp. 99–109.

[5] Toyoda-Makino, M., "Cost-based Optimal History Dependent Strategy for Random Fatigue Cracks Growth," *Probabilistic Engineering Mechanics*, Vol. 14, No. 4, Oct. 1999, pp. 339–347.

[6] Garbatov, Y. and Soares, C. G., "Cost and Reliability Based Strategies for Fatigue Maintenance Planning of Floating Structures," *Reliability Engineering and Systems Safety*, Vol. 73, No. 3, 2001, pp. 293–301.

[7] Kale, A., Haftka, R. T., and Sankar, B. V., "Efficient Reliability-Based Design and Inspection of Panels Against Fatigue," *Journal of Aircraft*, Vol. 45, No. 1, 2008, pp. 86–96.

[8] Sankararaman, S., McLemore, K., Liang, C., Bradford, S. C., and Peterson, L., "Test resource allocation for uncertainty quantification of multi-level and coupled systems," *52nd AIAA/ASME/ASCE/AHS/ASC Structures, Structural Dynamics, and Materials Conference*, Denver, CO, 2011.

[9] Voutchkov, I. and Keane, A. J., "Multiobjective optimization using surrogates," *7th International Conference on Adaptive Computing in Design and Manufacture*, Bristol, UK, 2006, pp. 167–175.

[10] Samad, A., Kim, K., Goel, T., Haftka, R. T., and Shyy, W., "Multiple surrogate modeling for axial compressor blade shape optimization," *Journal of Propulsion and Power*, Vol. 25, No. 2, 2008, pp. 302–310.

[11] Viana, F. A. C. and Haftka, R. T., "Using multiple surrogates for metamodeling," *7th ASMO-UK/ISSMO International Conference on Engineering Design Optimization*, Bath, UK, 2008.

[12] Glaz, B., Goel, T., Liu, L., Friedmann, P., and Haftka, R. T., "Multiple-surrogate approach to helicopter rotor blade vibration reduction," *AIAA Journal*, Vol. 47, No. 1, 2009, pp. 271–282.

[13] Viana, F. A. C. and Haftka, R. T., "Surrogate-based optimization with parallel simulations using probability of improvement," *13th AIAA/ISSMO Multidisciplinary Analysis and Optimization Conference*, Fort Worth, TX, 2010.

[14] Modi, P. J., Shen, W., Tambe, M., and Yokoo, M., "ADOPT: Asynchronous Distributed Constraint Optimization with Quality Guarantees," *Artificial Intelligence*, Vol. 161, No. 2, 2005, pp. 149–180.

[15] Holmgren, J., Persson, J. A., and Davidsson, P., "Agent Based Decomposition of Optimization Problems," *First International Workshop on Optimization in Multi-Agent Systems*, 2008.

[16] Welcomme, J.-B., Gleizes, M.-P., and Glize, P., "Résolution de problèmes multidisciplinaires multi-objectifs par systèmes multi-agents adaptifs: Application à la conception préliminaire avion," *Journées Francophones sur les Systèmes Multi-Agents (JFSMA 2007)*, Carcassonne, 2007, pp. 1–15.

[17] Picard, G. and Glize, P., "Model and analysis of local decision based on cooperative self-organization for problem solving," *Multiagent and Grid Systems*, Vol. 2, No. 3, 2006, pp. 253–265.

[18] Tu, J., Choi, K. K., and Park, Y. H., "A New Study on Reliability Based Design Optimization," *Journal of Mechanical Design*, Vol. 121, No. 4, 1999, pp. 557–564.

[19] Y.-T., W., "Computational Methods for Efficient Structural Reliability and Reliability Sensitivity Analysis," *AIAA Journal*, Vol. 32, No. 8, 1994, pp. 1717–1723.

[20] Grandhi, R. V. and Wang, L. P., "Reliability-Based Structural Optimization Using Improved Two-Point Adaptive Nonlinear Approximations," *Finite Element Analysis and Design*, Vol. 29, No. 1, 1998, pp. 35–48.

[21] Qu, X. and Haftka, R. T., "Reliability-based Design Optimization Using Probabilistic Sufficiency Factor," *Structural and Mutlidisciplinary Optimization*, Vol. 27, No. 5, 2004, pp. 314–325.

[22] Liang, J., Mourelatos, J. P., and Nikolaidis, E., "A Single-Loop Approach for System Reliability-Based Design Optimization," *Journal of Mechanical Design*, Vol. 129, No. 12, 2007, pp. 1215–1224.

[23] Ba-abbad, M. A., Nikolaidis, E., and Kapania, R. K., "New Approach for System Reliability-Based Design Optimization," *AIAA Journal*, Vol. 44, No. 5, 2006, pp. 1087–1096.

[24] Wu, Y.-T., Shin, Y., Sues, R., and Cesare, M., "Safety-Factor Based Approach for Probabilistic-Based Design Optimization," *42nd AIAA/ASME/ ASCE/AHS/ASC Structures, Structural Dynamics and Materials Conference*, Seattle, WA, 2001.

[25] Castillo, E., Minguez, R., Teran, A. R., Fernandez-Canteli, A., Minguez, and R. Teran, A. R., "Design and sensitivity analysis using the probability-safety-factor method. An application to retaining walls," *Structural Safety*, Vol. 26, No. 2, 2004, pp. 159–179.

[26] Du, X. and Chen, W., "Sequential Optimization and Reliability Assessment Method for Efficient Probabilistic Design," *Journal of Mechanical Design*, Vol. 126, No. 2, 2004, pp. 225–233.

[27] Rosenblatt, M., "Remarks on a Multivariate Transformation," *The Annals of Mathematical Statistics*, Vol. 23, No. 3, 1952, pp. 470–472.

[28] Smarslok, B. P., Haftka, R. T., Carraro, L., and Ginsbourger, D., "Improving accuracy of failure probability estimates with separable Monte Carlo," *International Journal of Reliability and Safety*, Vol. 4, No. 4, 2010, pp. 393–414.

[29] Kale, A. and Haftka, R. T., "Tradeoff of Weight and Inspection Cost in Reliability-Based Structural Optimization," *Journal of Aircraft*, Vol. 45, No. 1, 2008, pp. 77–85.

[30] Acar, E., Haftka, R. T., Kim, N. H., and Buchi, D., "Including the Effects of Future Tests in Aircraft Structural Design," *8th World Congress for Structural and Multidisciplinary Optimization*, Lisbon, Portugal, June 2009.

[31] Meyers, R. H. and Montgomery, D. C., *Response surface methodology: process and product optimization using design experiments*, John Wiley and Sons, 1995.

[32] Meyers, R. H., *Classical and modern regression with applications*, Duxbury Press, 2000.

[33] Kleijnen, J. P. C., "Kriging metamodeling and simulation: a review," *European Journal of Operational Research*, Vol. 192, No. 3, 2009, pp. 707–716.

[34] Simpson, T. W., Mauery, T. M., Korte, J. J., and Mistree, F., "Kriging models for global approximation in simulation-based multidisciplinary design optimization," *AIAA Journal*, Vol. 39, No. 12, 2001, pp. 2233–2241.

[35] Stein, M. L., *Interpolation of Spatial Data: some theory for kriging*, Springer Verlag, 1999.

[36] Smola, A. J. and Schölkopf, B., "A tutorial on support vector regression," *Statistics and computing*, Vol. 14, No. 3, 2004, pp. 199–222.

[37] Park, J. and Sandberg, I. W., "Universal approximation using radial-basis-function networks," *Neural Computation*, Vol. 3, No. 2, 1991, pp. 246–257.

[38] Smith, M., *Neural Networks for Statistical Modeling*, Von Nostrand Reinhold, 1993.

[39] Viana, F. A. C., *Multiple Surrogates for Prediction and Optimization*, Ph.D. thesis, University of Florida, 2011.

[40] Jin, R., Du, X., and Chen, W., "The use of metamodeling techniques for optimization under uncertainty," *Structural and Multidisciplinary Optimization*, Vol. 25, No. 2, 2003, pp. 99–116.

[41] Queipo, N. V., Haftka, R. T., Shyy, W., and Goel, T., "Surrogate-based analysis and optimization," *Progress in Aerospace Sciences*, Vol. 41, No. 1, 2005, pp. 1–28.

[42] Sacks, J., Welch, W. J., J., M. T., and Wynn, H. P., "Design and analysis of computer experiments," *Statistical Science*, Vol. 4, No. 4, 1989, pp. 409–435.

[43] Simpson, T. W., Peplinski, J. D., Koch, P. N., and Allen, J. K., "Metamodels for computer based engineering design: survey and recommendations," *Engineering with Computers*, Vol. 17, No. 2, 2001, pp. 129–150.

[44] Zerpa, L. E., Queipo, N. V., Pintos, S., and Salager, J.-L., "An optimization methodology of alkaline-surfactant-polymer flooding processes using field scale numerical simulation and multiple surrogates," *Journal of Petroleum Science and Engineering*, Vol. 47, No. 3–4, 2005, pp. 197–208.

[45] Goel, T., Haftka, R. T., Shyy, W., and Queipo, N. V., "Ensemble of Surrogates," *Structural and Multidisciplinary Optimization*, Vol. 33, No. 3, 2007, pp. 199–216.

[46] Acar, E. and Rais-Rohani, M., "Ensemble of metamodels with optimized weight factors," *Structural and Multidisciplinary Optimization*, Vol. 37, No. 3, 2010, pp. 279–294.

[47] Acar, E., "Various approaches for constructing an ensemble of metamodels using local measures," *Structural and Multidisciplinary Optimization*, Vol. 42, No. 6, 2010, pp. 879–896.

[48] Ginsbourger, D., Le Riche, R., and Carraro, L., "Computational Intelligence in Expensive Optimization Problems," chap. Kriging is, Springer series in Evolutionary Learning and Optimization, 2010, pp. 131–162.

[49] Queipo, N. V., Verde, A., Pintos, S., and Haftka, R. T., "Assessing the value of another cycle in Gaussian process surrogate-based optimization," *Structural and Multidisciplinary Optimization*, Vol. 39, No. 5, 2009, pp. 1–17.

[50] Viana, F. A. C., Haftka, R. T., and Watson, L. T., "Why not run the efficient global optimization algorithm with multiple surrogates?" *51th AIAA/ASME/ASCE/AHS/ASC Structures, Structural Dynamics, and Materials Conference*, Orlando, FL,USA, 2010.

[51] Chaudhuri, A., Haftka, R., and Viana, F., "Efficient Global Optimization with Adaptive Target for Probability of Targeted Improvement," *8th AIAA Multidisciplinary Design Optimization Specialist Conference*, American Institute of Aeronautics and Astronautics, Honolulu, HI, April 2012, pp. 1–13.

[52] Kumar, S., Villanueva, D., Haftka, R. T., and Sankar, B. V., "Probabilistic Optimization of an Integrated Thermal Protection System," *12th AIAA/ISSMO Multidisciplinary Analysis and Optimization Conference*, Victoria, BC, 2008.

[53] Villanueva, D., Sharma, A., Haftka, R. T., and Sankar, B. V., "Risk Allocation by Optimization of an Integrated Thermal Protection System," *8th World Congress for Structural and Multidisciplinary Optimization*, Lisbon, Portugal, 2009.

[54] Villanueva, D., Haftka, R. T., and Sankar, B. V., "Including Future Tests in the Design and Optimization of an Integrated Thermal Protection System," *12th AIAA Non-Deterministic Approaches Conference*, Orlando, FL, 2010.

[55] Villanueva, D., Haftka, R. T., and Sankar, B. V., "Probabilistic Optimization of an Integrated Thermal Protection System Including the Effect of Future Tests," *2nd International Conference on Engineering Optimization*, Lisbon, Portugal, 2010.

[56] Villanueva, D., Le Riche, R., Picard, P., and Haftka, R. T., "A Multi-Agent System Approach To Reliability Based Design Optimization Including Future Tests," *12e Congr{è}s de la Soci{é}t{é} Francaise de Recherche Op{é}rationnelle et d'Aide {à} la Decision (ROADEF'11)*, Saint-Etienne, France, 2011.

[57] Villanueva, D., Le Riche, R., Picard, G., Haftka, R. T., and Sankar, B. V., "Decomposition of System Level Reliability-Based Design Optimization to Reduce the Number of Simulations," *ASME 2011 International Design Engineering Technical Conferences and Computers and Information in Engineering Conference*, Washington, DC, USA, 2011.

[58] Freeman, D. C., Talay, T. A., and Austin, R. E., "Reusable Launch Vehicle Technology Program," *Acta Astronautica*, Vol. 41, No. 11, 1997, pp. 777–790.

[59] Blosser, M. L., "Development of Advance Metallic, Thermal-Protection-System Prototype Hardware," *Journal of Spacecraft and Rockets*, Vol. 41, No. 2, 2004, pp. 183–194.

[60] Poteet, C. C., Abu-Khajeel, H., and Hsu, S.-Y., "Preliminary thermal-mechanical sizing of a metallic thermal protection system," *Journal of Spacecraft and Rockets*, Vol. 41, No. 2, 2004, pp. 173–182.

[61] Bapanapalli, S. K., *Design of an Integrated Thermal Protection System for Future Space Vehicles*, Ph.D. thesis, University of Florida, 2007.

[62] Gogu, C., Haftka, R. T., Bapanapalli, S. K., and Sankar, B. V., "Dimensionality Reduction Approach for Response Surface Approximations: Application to Thermal Design," *AIAA Journal*, Vol. 47, No. 7, 2009, pp. 1700–1708.

[63] Sharma, A., *Multi-fidelity design of an integral thermal protection system for future space vehicle during re-entry*, Ph.D. thesis, University of Florida, 2010.

[64] Viana, F. A. C., "SURROGATES Toolbox User's Guide, Version 2.1," 2010.

[65] Golden, P., Millwater, H., Dubinsky, C., and Singh, G., "Experimental Resource Allocation for Statistical Simulation of Fretting Fatigue Problem (Preprint)," Tech. rep., DTIC Document, 2012.

[66] Venter, G. and Scotti, S. J., "Accounting for Proof Test Data in a Reliability-Based Design Optimization Framework," *AIAA Journal*, Vol. 50, No. 10, 2012, pp. 2159–2167.

[67] Durga Rao, K., Kushwaha, H., Verma, A., and Srividya, A., "Quantification of epistemic and aleatory uncertainties in level-1 probabilistic safety assessment studies," *Reliability Engineering & System Safety*, Vol. 92, No. 7, July 2007, pp. 947–956.

[68] Matsumura, T., Haftka, R. T., and Sankar, B. V., "Reliability Estimation Including Redesign Following Future Test for an Integrated Thermal Protection System," *9th World Congress on Structural and Multidisciplinary Optimization*, Shizuoka, Japan, 2011.

[69] Birge, J. R. and Louveaux, F., *Introduction to Stochastic Programming*, Springer Series in Operations Research and Financial Engineering, Springer New York, New York, NY, 2011.

[70] Liu, M. L. and Sahinidis, N. V., "Optimization in Process Planning under Uncertainty," *Industrial & Engineering Chemistry Research*, Vol. 5885, No. 95, 1996, pp. 4154–4165.

[71] Gupta, A. and Maranas, C. D., "A Two-Stage Modeling and Solution Framework for Multisite Midterm Planning under Demand Uncertainty," *Industrial & Engineering Chemistry Research*, Vol. 39, No. 10, Oct. 2000, pp. 3799–3813.

[72] "Guide to Verifying Safety-Critical Structures for Reusable Launch and Reentry Vehicles, Version 1," Tech. Rep. November, Federal Aviation Administration, Washington, DC, USA, 2005.

[73] Zhao, D. and Xue, D., "A multi-surrogate approximation method for metamodeling," *Engineering with Computers*, Vol. 27, No. 2, 2005, pp. 139–153.

[74] Wang, G. G. and Simpson, T. W., "Fuzzy Clustering Based Hierarchical Metamodeling for Design Space Reduction and Optimization," *Engineering Optimization*, Vol. 36, No. 3, 2004, pp. 313–335.

[75] Shoham, Y. and Leyton-Brown, K., *Multiagent Systems: Algorithmic, Game-Theoric, and Logical Foundations*, Cambridge University Press, 2009.

[76] Beasley, D., Bull, D. R., and Martin, R. R., "A sequential niche technique for multimodal function optimization," *Evolutionary computation*, Vol. 1, No. 2, 1993, pp. 101–125.

[77] Hocaoglu, C. and Sanderson, A. C., "Multimodal function optimization using minimal representation size clustering and its application to planning multipaths," *Evolutionary Computation*, Vol. 5, No. 1, 1997, pp. 81–104.

[78] Brits, R., Engelbrecht, A. P., and van den Bergh, F., "Locating multiple optima using particle swarm optimization," *Applied Mathematics and Computation*, Vol. 189, No. 2, 2007, pp. 1859–1883.

[79] Parsopoulos, K. E. and Vrahatis, M. N., *Artificial Neural Networks and Genetic Algorithms*, chap. Modificati, Springer, 2001, pp. 324–327.

[80] Li, X., "Adaptively Choosing Neighbourhood Bests Using Species in a Particle Swarm Optimizer for Multimodal Function Optimization," *Genetic and Evolutionary Computation (GECCO 2004)*, Vol. 3102 of *Lecture Notes in Computer Science*, 2004, pp. 105–116.

[81] Nagendra, S., Jestin, D., Gurdal, Z., Haftka, R. T., and Watson, L. T., "Improved genetic algorithm for the design of stiffened composite panels," *Computers & Structures*, Vol. 58, No. 3, 1996, pp. 543–555.

[82] Li, J. P., Balazas, M. E., Parks, G., and Clarkson, P. J., "A Species Conserving Genetic Algorithm for Multimodal Function Optimization," *Evolutionary Computation*, Vol. 10, No. 3, 2002, pp. 207–234.

[83] Torn, A. and Zilinskas, A., "Global Optimization," *Lecture Notes in Computer Science 350*, Springer Verlag, 1989.

[84] Kleijen, J., *Design and analysis of simulation experiments*, Springer, 2008.

[85] Aurenhammer, F., "Voronoi diagrams: a survey of a fundamental geometric data structure," *ACM Computing Surveys (CSUR)*, Vol. 23, No. 3, 1991, pp. 345–405.

[86] Hartigan, J. A. and Wong, M. A., "Algorithm AS 136: A K-Means Clustering Algorithm," *Journal of the Royal Statistical Society. Series C (Applied Statistics)*, Vol. 28, No. 1, 1979, pp. 100–108.

[87] Rousseeuw, P. J., "Silhouettes: a Graphical Aid to the Interpretation and Validation of Cluster Analysis," *Computational and Applied Mathematics*, Vol. 20, 1987, pp. 53–65.

[88] MATLAB, *version 7.9.0.529 (R2009b)*, chap. fmincon, The MathWorks Inc., Natick, Massachusetts, 2009.

[89] Jones, D. R., Schonlau, M., and Welch, W. J., "Efficient Global Optimization of Expensive Black-Box Functions," *Journal of Global Optimization*, Vol. 13, No. 4, 1998, pp. 455–492.

[90] Parsopoulos, K. E. and Vrahatis, M. N., "Modification of the Particle Swarm Optimizer for locating all the global minima," *Artificial Neural Networks and Genetic Algorithms*, 2001, pp. 324–327.

[91] Torn, A. and Viitanen, S., "Topographical global optimization using pre-sampled points," *Journal of Global Optimization*, Vol. 5, No. 3, Oct. 1994, pp. 267–276.

[92] Alexandrov, N. M., Dennis Jr, J. E., Lewis, R. M., and Torczon, V., "A trust-region framework for managing the use of approximation models in optimization," *Structural Optimization*, Vol. 15, No. 1, 1998, pp. 16–23.

[93] Schonlau, M., *Computer experiments and global optimization*, Ph.D. thesis, University of Waterloo.

[94] Janusevskis, J., Le Riche, R., Ginsbourger, D., and Girdziusas, R., "Expected improvements for the asynchronous parallel global optimization of expensive functions: Potentials and challenges," *Learning and Intelligent Optimization*, Springer, 2012, pp. 413–418.

[95] Sasena, M. J., *Flexibility and Efficiency Enhancements for Constrained Global Design Optimization with Kriging Approximations by*, Ph.D. thesis, University of Michigan, 2002.

[96] Zielinski, K. and Laur, R., "Stopping criteria for a constrained single-objective particle swarm optimization algorithm," *INFORMATICA-LJUBLJANA-*, Vol. 31, No. 1, 2007, pp. 51.

[97] Schwefel, H.-P. P., *Evolution and optimum seeking: the sixth generation*, John Wiley & Sons, Inc., 1993.

[98] Jones, D. R., Perttunen, C. D., and Stuckman, B. E., "Lipschitzian optimization without the Lipschitz constant," *Journal of Optimization Theory and Applications*, Vol. 14, No. 3, 2004, pp. 199–222.

[99] Matsumura, T., Haftka, R., and Kim, N., "The Contribution of Building Block Test to Discover Unexpected Failure Modes," *52th AIAA/ASME/ASCE/AHS/ASC Structures, Structural Dynamics, and Materials Conference*, American Institute of Aeronautics and Astronautics, 2011.

[100] Villanueva, D., Haftka, R. T., and Sankar, B. V., "Including the Effect of a Future Test and Redesign in Reliability Calculations," *AIAA Journal*, Vol. 49, No. 12, 2011, pp. 2760–2769.

[101] Xiong, Y., Chen, W., Apley, D., and Ding, X., "A non-stationary covariance-based Kriging method for metamodelling in engineering design," *International Journal for Numerical Methods in Engineering*, Vol. 71, No. 6, 2007, pp. 733–756.

BIOGRAPHICAL SKETCH

Diane Villanueva was born in Jacksonville, Florida in 1986. She graduated with a Bachelor of Science in Aerospace Engineering from the University of Florida in 2008. The same year, she joined the Structural and Multidisciplinary Optimization Group at the University of Florida. During the summer of 2009, she was a visiting researcher at NASA Langley Research Center in Hampton, Virginia. In 2010, she entered into a joint Ph.D. program with the Ecole des Mines de Saint-Etienne in France. She was awarded the Alumni Fellowship from the University of Florida and the Amelia Earhart Fellowship from Zonta International.

Her research interests include uncertainty analysis, non-deterministic methods, and distributed optimization techniques.

École Nationale Supérieure des Mines
de Saint-Étienne

NNT : 2013 EMSE 0687

Diane VILLANUEVA

RELIABILITY BASED DESIGN INCLUDING FUTURE TESTS AND MULTI-AGENT APPROACHES

Speciality : Engineering

Keywords : Reliability based design optimization, surrogates, tests, uncertainty

Abstract :

The initial stages of reliability-based design optimization involve the formulation of objective functions and constraints, and building a model to estimate the reliability of the design with quantified uncertainties. However, even experienced hands often overlook important objective functions and constraints that affect the design. In addition, uncertainty reduction measures, such as tests and redesign, are often not considered in reliability calculations during the initial stages. This research considers two areas that concern the design of engineering systems: 1) the trade-off of the effect of a test and post-test redesign on reliability and cost and 2) the search for multiple candidate designs as insurance against unforeseen faults in some designs.

In this research, a methodology was developed to estimate the effect of a single future test and post-test redesign on reliability and cost. The methodology uses assumed distributions of computational and experimental errors with re-design rules to simulate alternative future test and redesign outcomes to form a probabilistic estimate of the reliability and cost for a given design. Further, it was explored how modeling a future test and redesign provides a company an opportunity to balance development costs versus performance by simultaneously designing the design and the post-test redesign rules during the initial design stage.

The second area of this research considers the use of dynamic local surrogates, or surrogate-based agents, to locate multiple candidate designs. Surrogate-based global optimization algorithms often require search in multiple candidate regions of design space, expending most of the computation needed to define multiple alternate designs. Thus, focusing on solely locating the best design may be wasteful. We extended adaptive sampling surrogate techniques to locate multiple optima by building local surrogates in sub-regions of the design space to identify optima. The efficiency of this method was studied, and the method was compared to other surrogate-based optimization methods that aim to locate the global optimum using two two-dimensional test functions, a six-dimensional test function, and a five-dimensional engineering example.

École Nationale Supérieure des Mines
de Saint-Étienne

NNT : 2013 EMSE 0687

Diane VILLANUEVA

OPTIMISATION FIABILISTE : PRISE EN COMPTE DES TESTS FUTURS ET APPROCHE PAR SYSTÈMES MULTI-AGENT

Spécialité: sciences pour l'ingénieur

Mots clefs : optimisation fiabiliste, tests, incertitudes, systèmes multi-agent

Résumé :

Les premières étapes d'une conception fiabiliste impliquent la formulation de critères de performance et de contraintes de fiabilité d'une part, et le choix d'une représentation des incertitudes d'autre part. Force est de constater que, le plus souvent, des aspects de performance ou de fiabilité conditionnant la solution optimale ne seront pas connus ou seront négligés lors des premières phases de conception. De plus, les techniques de réduction des incertitudes telles que les tests additionnels et la reconception ne sont pas pris en compte dans les calculs de fiabilité initiaux.

Le travail exposé dans ce manuscrit aborde la conception optimale de systèmes sous deux angles : 1) le compromis entre performance et coût généré par les tests supplémentaires et les re-conceptions et, 2) l'identification de multiples solutions optimales (dont certaines locales) en tant que stratégie contre les erreurs initiales de conception.

Dans la première partie de notre travail, une méthodologie est proposée pour estimer l'effet sur la performance et le coût d'un produit d'un test supplémentaire et d'une éventuelle re-conception. Notre approche se base, d'une part, sur des distributions en probabilité des erreurs de calcul et des erreurs expérimentales et, d'autre part, sur une rêgle de reconception a priori. Ceci permet d'estimer a posteriori la probabilité et le coût d'un produit. Nous montrons comment, à travers le choix de politiques de prochain test et de re-conception, une entreprise est susceptible de contrôler le compromis entre performance et coût de développement.

Dans la seconde partie de notre travail, nous proposons une méthode pour l'estimation de plusieurs solutions candidates à un problème de conception où la fonction coût et/ou les contraintes sont coûteuses en calcul. Une approche pour aborder de tels problèmes est d'utiliser un métamodèle, ce qui nécessite des évaluations de points en diverses régions de l'espace de recherche. Il est alors dommage d'utiliser cette connaissance seulement pour estimer un optimum global. Nous proposons une nouvelle approche d'échantillonnage à partir de métamodèles pour trouver plusieurs optima locaux. Cette méthode procède par partitionnement adaptatif de l'espace de recherche et construction de métamodèles au sein de chaque partition. Notre méthode est testée et comparée à d'autres approches d'optimisation globale par métamodèles sur des exemples analytiques en dimensions 2 à 6, ainsi que sur la conception d'un bouclier thermique en 5 dimensions.